MEDICAL PHYSICS International

The Journal of the International Organization for Medical Physics

Volume 12, Number 1, June 2024

MEDICAL PHYSICS INTERNATIONAL

THE JOURNAL OF

THE INTERNATIONAL ORGANIZATION FOR MEDICAL PHYSICS

MEDICAL PHYSICS INTERNATIONAL
The Journal of the International Organization for Medical Physics

Aims and Coverage:

Medical Physics International (MPI) is the official IOMP journal. It provides a platform for medical physicists to share their experience, ideas and new information generated from their work of scientific, educational and professional nature. The e- journal is available free of charge to IOMP members. MPI- History Edition is dedicated to History of Medical Physics.

MPI web address: www.mpijournal.org

Published by: The International Organization for Medical Physics (IOMP); Web address: www.iomp.org ; Post address: IOMP c/o IPEM, 230 Tadcaster Road, York YO24 1ES, UK.

ISSN 2306 – 4609

CONTENTS

EDITORIAL

EDITORIAL FROM CO-EDITORS-IN-CHIEF

Francis Hasford[1], Sameer Tipnis[2]

[1] Radiological and Medical Sciences Research Institute, Ghana Atomic Energy Commission, Accra, Ghana.
[2] Department of Radiology and Radiological Sciences, Medical University of South Carolina, Charleston, USA.

Dear colleagues and friends,

In the second week of January 2024, the December 2023 issue of MPI (Vol. 11, No. 2) was published. The edition attracted lots of readership, with MPI website attracting 1,000+ readers daily upon release. The issue had 618 pages, which makes it the biggest volume so far produced. Included in the issue were the ICMP-2023 Book of Abstracts and theses abstracts of the ICTP Master of Medical Physics Programme.

Owing to huge volume of pages for MPI editions that feature book of abstracts, special issue (MPI-Proceedings) is being planned solely for publication of books of abstracts of future editions of the International Conference of Medical Physics (ICMP) and World Congresses (WCs). In this case, all books of abstracts of subsequent ICMP and WCs will be catalogued in one place. Ultimate vision is to develop MPI as an IOMP brand and gradually grow it by adding more journals as needed (e.g., MPI, MPI-History Edition, MPI-Experiences, MPI-Proceedings, etc.).

As Co-Editors-in-Chief (EiCs), we appreciate the support and contribution of everyone, including medical physics researchers, scholars, and experts who have contributed their valuable research articles to MPI and have been part of our success story this far. We continue to look forward to working with everyone to advance medical physics scientific knowledge through publication of high-quality impactful articles in the MPI. In ensuring quality standard articles are produced, we perform in-depth read and critique the received submissions, and then discuss the merits as well as drawbacks of the manuscripts before sending feedback for authors' revision. This assures a balance of perspectives.

This current edition of MPI (Vol. 12, No. 1) contains twelve articles in the thematic areas: Collaborating Organizations, Educational Topics, Professional Issues, Invited Research Papers, and How-To.

We encourage readers to submit more practical tip or "how-to" articles which can be used by fellow medical physicists around the globe. Kindly visit www.mpijournal.org/index.aspx for latest MPI publications and enjoy reading our exciting publications.

Francis Hasford, PhD.

Editor-in-Chief

Radiological and Medical Sciences Research Institute, Ghana Atomic Energy Commission, Accra, Ghana.

haspee@yahoo.co.uk

Sameer Tipnis, PhD.

Editor-in-Chief

Department of Radiology and Radiological Sciences, Medical University of South Carolina, Charleston, USA.

tipnis@musc.edu

COLLABORATING ORGANIZATIONS

THE CURRENT STATUS OF MEDICAL PHYSICS IN JAMAICA, RADIATION PROTECTION EDUCATION AND COMPLIANCE ACROSS RADIATION USER PROFESSIONALS

R. Shields[1]

[1] PRAD Radiation Partners Limited

Abstract— **Before 2015, the safe use of radiation had not been strongly enforced among radiation professionals in various sectors. However, by July 2015, the parliament of Jamaica, passed the Nuclear Safety and Radiation Protection Act (NSRPA) to formalize the use of all forms of radiation generators and radioactive materials. By September 2017, under this Act, an independent regulatory body was formulated to be the instrument for regulating the radiation landscape. This national radiation regulatory body is known as the Hazardous Substance Regulatory Authorities (HSRA). These two pivotal moments inadvertently made Jamaica the first English speaking Caricom Community (CARICOM) nation with radiation laws and an independent regulatory body.**

These events have propelled Jamaica's development through sectors such as radiation medicine, industry, and national security. However, 9 years later, there has still been resistance and slow assimilation of radiation compliance by some private radiation user professionals. To further elaborate, various gaps have been seen that compromise radiation safety in practices within dentistry to surgery.

This occurrence has revealed the need for further education and training for all professionals by certified radiation safety experts to improve the overall standards to an international reference level.

Keywords— **Jamaica, medical physics, radiation protection education, medical imaging, dentistry, interventional surgery, fluoroscopy.**

I. INTRODUCTION

Jamaica is a small island developing state (SIDs) of the Caribbean Community (CARICOM), with a population of 3 million people. Although a SID, Jamaica has not been unfamiliar with the use of nuclear science for peaceful purposes. Since 1984, Jamaica became the first English-speaking Caribbean country to host a 20KW research nuclear reactor, known as the SLOWPOKE - 2. This feature was supported by the European Union (EU) and the International Atomic Energy Agency (IAEA) and has paved the way for the future of nuclear science in Jamaica and the Caribbean. 40 years later, since the advent of this reactor, this has supported the progress of Jamaica through services related to academic research, personnel and environmental radiation monitoring, mineral exploration, environmental protection, climate change, agriculture water and food security, and nutrition and medicine.

Although the occurrence of a reactor highlighted the many values of nuclear science and scientific endeavour, there was a missing key element that would further unlock the potential of the atom for the Jamaican society. This has been a lack of radiation legislation and regulators. These shortcomings have restricted access for local entities to do business internationally to procure and import radioactive sources and other related services. The current international nuclear/radioactive materials supplier landscape demands a country have national nuclear regulations and laws to supply its goods and services. This is in keeping with the IAEA mandates to prevent the misuse of radioactive or nuclear materials to safeguard lives and the environment.

Over the period there has been a notable increase in the use of radiation-generating equipment and medical radioisotopes for the medical and dental sector, both privately and publicly. This increase is in response to the notable ongoing upward trends in Non - Communicable Diseases (NCDs), such as cancer and cardiovascular disease, and the purchasing power parity of both the service providers and consumers of these services. The same can be observed within the industrial and security sectors, as Jamaica increases industrialization via its manufacturing activities and ports that allow goods and people to flow through the country for business or leisure tourism.

II. MEDICAL PHYSICS AND RADIATION LEGISLATION

However, with all these beneficial uses, the safe use of radiation has not been strongly enforced among radiation professionals in various sectors. Radiation Safety officers (RSO) and education have been a limited and foreign concept. Exposure to radiation safety would have been either through the enrolment into a formal radiation-affiliated academic program at an introductory level or restricted to personnel who are privately employed and educated by an international supplier customer support team on the functionality and operation of equipment, devices, or materials.

Intermediate to advanced education and training is not widely exposed nor accessible and therefore there is a reflection of poor to barely acceptable radiation safety practices in some clinical practices. Furthermore, in a setting where radiation generators are present, all stakeholders within the operation would not be adequately aware of the dangers of radiation exposure vs the specialist who may be operating it. Stakeholders such as administration, sanitation staff, medical/ dental ancillary staff, and the temporarily visiting general public are at risk. This also can be extended to highly educated professionals such as clinical members of

a surgical team, dental hygienists, veterinary assistants, or engineers and technicians within a manufacturing environment.

In light of these challenges, in developing a culture of radiation safety, competent radiation safety professionals need to be within the public and private spaces to educate all professional stakeholders and the general public on the responsible and safe use of radiation and radioactive materials. This remedy came into fruition when the University of the West Indies (UWI) Mona Campus launched its Medical Physics BSc and MSc programs in 2009 and 2011 respectively. To date, this program has graduated approximately under 200 medical physicist graduates.

Further development came in 2015 and 2019 the Government of Jamaica, created the Nuclear Safety and Radiation Protection Act (NSRPA) and the Hazardous Substance Regulatory Authorities (HSRA) respectively, to formalize the use of all forms of radiation generators and radioactive materials. These two pivotal moments made Jamaica the first Caricom Community (CARICOM) nation with radiation laws and an independent regulatory body.

By 2021 to boost the representation and profile of medical physics locally and regionally, the Jamaica Association for Physics in Medicine (JAPM) was incorporated in October of that year. This not-for-profit organization is dedicated to representing and advancing medical physics science and its affiliated professionals.

By 2022, the government, with the support of the IAEA, established its first public nuclear medicine centre. These historical moments had inadvertently led to the development and improvement of the medical sector capacity for diagnosing and treating of cancer and other non-communicable diseases (NCDs).

In the last quarter of 2023, in putting the spotlight on medical physics in Jamaica publicly and across the Caribbean, JAPM hosted its inaugural scientific conference on November 13 -17,2023 in Kingston. This historical conference titled "*Quality Assurance in Radiation Medicine for Sustainable Healthcare*" was a collaborative effort of the JAPM and Ministry of Health & Wellness (MOHW) with heavy support from international organizations such as IAEA, Pan American Health Organization (PAHO), and the International Organization of Medical Physicist (IOMP).

III. CHALLENGES

These events have propelled Jamaica's radiation medicine sector and also stimulated the public discussion about nuclear power generation. These interventions have been appreciated by a burgeoning medical physics community, whose presence predates the laws and regulations. The radiation user landscape for an island is quite sizeable, compared to its Caricom counterparts, with over 1000 personnel, across the professions of dentistry, veterinary, surgery, diagnostic, and interventional radiology. Meanwhile, the medical physics fraternity has under 25 physicists in qualified posts. Furthermore, the treatment and diagnostic capacity has increased significantly. Within each specialism, there have been progressive strides in the development of medical physics resources both publicly and privately. In the Radiotherapy landscape, there are four (4) linear accelerators, one (1) cobalt teletherapy unit, and one (1) LDR Brachytherapy unit (Cs^{137}). In the Diagnostic and Interventional Radiology, there is a minimum of 100 units ranging from X-ray, CT scanner, Fluoroscopy, MRI, and Ultrasound. In nuclear medicine, there is one PET CT, one SPECT unit and few gamma cameras.

However, in light of this, nine (9) years after the law and regulations passed, there is still low radiation compliance by some private radiation user professionals. This occurrence has sparked an identifiable gap in the need for further education and training for all professionals. Firstly, in medical physics, there is a need for a holistic residency program, and a professional refresher course locally is required. The former is underway, and the latter eventually will make headway as resources and professional capacity increase.

Within the dental community, through public lecture engagements, identifiable knowledge gaps found were a preconceived notion that low doses are considered negligible doses due to using digital X-ray systems, lack of the need for personnel radiation monitoring, poor shielding materials, and facility layout configuration. A similar conclusion could be inferred from the observation of general and specialist surgeons who utilize fluoroscopy to conduct diagnostic/ interventional radiology studies/ procedures on patients. Gaps related to lax or non-existent enforcement of the wearing of personal dosimetry badges, full body PPE (especially for the head and eyes) wearing and frequent integrity testing, the consistent use of fixed or mobile architectural shielding, quality control testing of fluoroscopy units, diagnostic reference levels and annual general radiation protection education for the surgical team around the unit. There are currently unknowns about the position of radiation protection practices within veterinary radiology. Further investigation is needed to understand the current status of this sector. This is especially apparent with the introduction of mobile veterinary radiology service vehicles to the public.

Importantly, the general public is a key stakeholder that requires education about radiation usage and protection. This is especially the case where many of the general public are within all these sectors working in close contact with the medical staff. With only 15% of the workforce in Jamaica with a tertiary degree, a high level of ignorance would greatly increase the risk of radiation-related incidents among non-radiation workers. As such, this vulnerable group cannot be overlooked.

In conclusion, continual education in the public domain is deeply required to dispel ignorance related to radiation phobia and apathy toward safety in the presence of an ionizing source. Clinical and dental fraternities need current

and advanced knowledge about every changing landscape of radiation equipment functionalities and radiation protection principles in their practices. However, to assess the depth of the knowledge gap and then rectify issues, surveys need to be implemented on a local to national scale to establish the current education baseline. In the interim, in addressing the gap, activities are underway to engage with these radiation professional communities to assess the current status and then implement remediation actions to boost to a satisfactory level.

IV. ACKNOWLEDGEMENTS

I would like to acknowledge the continued support of the Dr. Anna Barnes and Institute of Physics and Engineering in Medicine (IPEM). Also, I would like to personally to Prof. S Tabakov, for his support in the review of the paper and prospective projects.

REFERENCES

1. Voutchkov, M. (2019). TEN YEARS OF MEDICAL PHYSICS EDUCATION AND CONTINUING PROFESSIONAL TRAINING IN JAMAICA. *MEDICAL PHYSICS INTERNATIONAL Journal*, *7*(1).
2. Brevitt, B., Gordon, A., Voutchkov, M., & Burnett, L. (2018). Enhancing Quality Management through Effective Quality Assurance in Jamaican Radiology Centres. *Journal of Medical Diagnostic Methods*, *07*(02). https://doi.org/10.4172/2168-9784.1000272
3. International Atomic Energy Agency (IAEA). (2018, January 4). *Building Regulatory Capacity in Jamaica: IAEA Welcomes Delegation from New Jamaican Authority | IAEA*. https://www.iaea.org/newscenter/news/building-regulatory-capacity-in-jamaica-iaea-welcomes-delegation-from-new-jamaican-authority"
4. International Atomic Energy Agency (IAEA). (2019, March 28). *Bridging Regulatory Gaps: IAEA Supports Jamaica in Achieving Stronger Radiation Safety | IAEA*. https://www.iaea.org/newscenter/news/bridging-regulatory-gaps-iaea-supports-jamaica-in-achieving-stronger-radiation-safety
5. Power Technology. (2017, November 22). *Inside the Caribbean's only nuclear reactor - Power Technology*. https://www.power-technology.com/features/inside-caribbeans-nuclear-reactor/
6. Alleyne-Mike, K., Sylvester, P., Henderson-Suite, V., & Mohoyodeen, T. (2020). Radiotherapy in the Caribbean: a spotlight on the human resource and equipment challenges among CARICOM nations. *Human Resources for Health*, *18*, 1–13. https://doi.org/10.1186/s12960-020-00489-5
7. Kennedy-Dixon, T.-G., McDonnough, K., Reid, M., & Gossell-Williams, M. (2021). Trends in the utilization of nuclear medicine technology in Jamaica: Audit of a private facility. *World Journal of Nuclear Medicine*, *20*(2), 129. https://doi.org/10.4103/WJNM.WJNM_92_20
8. Yorke, A. A., Williams, V. M., Elmore, S., Alleyne-Mike, K., Addison, E., Kyeremeh, P. O., Tagoe, S. N. A., Trauernicht, C. J., Lazarus, G. L., & Ford, E. C. (2024). Radiation Therapy Physics Quality Assurance and Management Practices in Low- and Middle-Income Countries: An Initial Pilot Survey in Six Countries and Validation Through a Site Visit. *Advances in Radiation Oncology*, *9*(2), 101335. https://doi.org/10.1016/J.ADRO.2023.101335
9. Orellana, P., Mut, F., Estrada, E., Lette, M. M., Pellet, O., Morozova, O., El-Haj, N., Bucheli, J. C., Pynda, Y., Okolielova, T., Cherit, A., Giammarile, F., & Paez, D. (2021). Status of Nuclear Medicine in Latin America and the Caribbean: IAEA Analysis of Development in the Past 6 Years. *J Nucl Med*, *62*(06), 23–29.
10. Walker, D., Paul, T., & Taylor, T. (2021). The growth potential for diagnostic imaging training in the English-speaking Caribbean. *Radiography*, *27*(3), 956–961. https://doi.org/10.1016/J.RADI.2021.01.006
11. Elbanna, M., Pynda, Y., Kalinchuk, O., Rosa, A., & Abdel-Wahab, M. (2023). Radiotherapy resources in Latin America and the Caribbean: a review of current and projected needs based on International Atomic Energy Agency data. *The Lancet Oncology*, *24*(9), e376–e384. https://doi.org/10.1016/S1470-2045(23)00299-1
12. Renha, S. K., Torres Aroche, L. A., Velez, G., Knoll, P., & Tsapaki, V. (2022). *IAEA RLA 6091: ENHANCING CAPACITY BUILDING OF MEDICAL PHYSICISTS IN LATIN AMERICA AND CARIBBEAN*. *10*(2). https://www.iaea.org/projects/tc/rla6091

Contacts of the corresponding author:

Author: Rahje Shields
Institute: PRAD Radiation Partners Limited
City: Kingston, Jamaica
Email: Rshields@pradradiation.com / Rahje.shields@gmail.com

EDUCATIONAL TOPICS

SOME RADIOGRAPHIC QUALITY CONTROL TESTS WITH SPECIFIC IMPORTANCE FOR DEVELOPING COUNTRIES

S. Tabakov[1,2]

[1] President IOMP 2015-2018; [2] King's College London, UK

Abstract— **The paper describes some QC tests which have specific additional importance for assessment the performance of X-ray radiographic systems in developing (aka LMI) countries. The Beam Quantity (Specific output dose – mGy/mAs) and the linearity of the (mGy/mAs) = F (kV^2) graph are QC parameters indicating also the approaching end of life of an X-ray tube. Dose output and kV dependence on Anode current (mA) QC tests are also indicators for the stability of the hospital electrical power supply system. These QC parameters can be used as providers of useful information for improving the performance of X-ray equipment in developing countries (especially in rural hospitals). The paper could be used as a reference material for lecturing and training Quality Control of X-ray Radiographic equipment.**

Keywords **X-ray Tube and Generator, Diagnostic Radiology Quality Control, QC in Low- and Middle-Income countries, QC in developing countries**

I. INTRODUCTION

Quality Control (QC) of X-ray tube and Generator of Radiographic equipment is an important activity for medical physicists in Diagnostic Radiology. QC tests follow specific protocols and are described by a number of reputable institutions [1, 2, 3]. However, the assessment of results of some QC tests can bring additional information about the functioning of the radiographic equipment, which can be very useful for colleagues in developing countries for planning replacement of the X-ray tube, correcting the electrical supply of the equipment or other (often servicing) procedures. The paper will briefly discuss such QC tests.

II. BEAM QUANTITY AND (mGy/mAs) = F (KV^2) GRAPH

It is well known that X-ray tube output (dose) is linearly related to the mA, time or mAs (hence Dose/mAs should be constant at set kV), and quadratically related to the kV.

The Beam quantity (mGy/mAs) for certain kV (e.g. 80 kV) and measured at certain distance and fixed filtration is a stable parameter, specific for the X-ray equipment (namely for its X-ray tube). This parameter is measured both for Broad Focus (BF) and Fine Focus (FF) of the X-ray tube.

The graph/function plotting mGy/mAs against kV^2 for a relatively new X-ray tube (for different set kV but at fixed mA and time) will produce a relatively straight line [5].

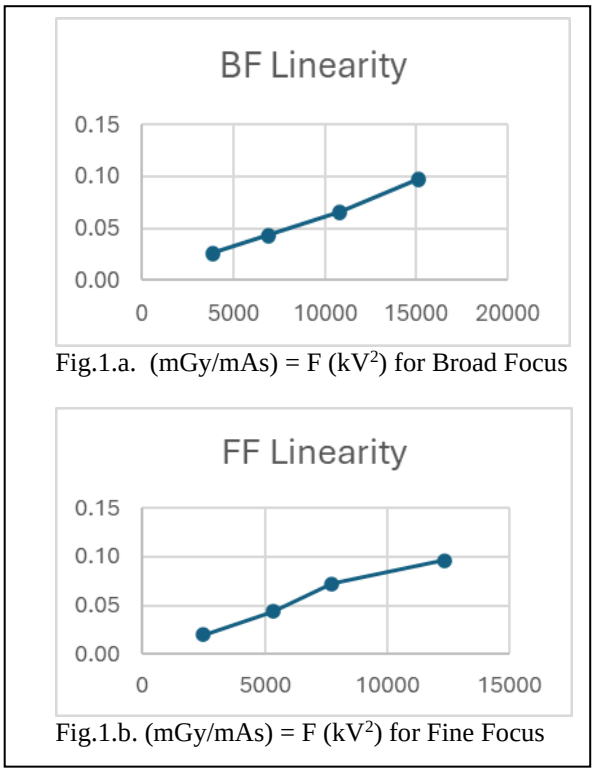

Fig.1.a. (mGy/mAs) = F (kV^2) for Broad Focus

Fig.1.b. (mGy/mAs) = F (kV^2) for Fine Focus

However, if the X-ray tube is exhausted (e.g. one of its focal spots is exhausted), the line will not be straight and most often will bend down at high kV. Fig.1.a and Fig.1.b show such a case for an relatively old X-ray tube (based on the real QC measurements, shown on Table 1).

From the two graphs one can see that while the function (mGy/mAs) = F (kV^2) for Broad Focus on Fig.1.a is relatively linear, the same function for Fine Focus on Fig.1.b shows drop at the end of high kV. This drop is an indicator that in this case the Fine Focus has been used very often and it has decreased its specific output (dose/mAs). The reason for this is related mainly to the cracks over the anode surface. The X-ray exposures heat quickly the anode (to temperatures of the order of 2000-3000 ^{0}C), followed by cooling the anode in between exposures. This causes thermal stress of the anode material, and its Tungsten-coated surface starts to crack with time. This way as a result of many exposure (many cycles of heating and cooling) the number of Anode surface cracks and their sizes increases (Fig.2). This leads to the known effect of enlarging the Actual focal spot (hence the measured Effective focal spot)

[4]. This reduces the radiographic spatial resolution, but also decreases tube output (dose), as significant part of the accelerated thermal electrons from the Cathode fall inside the cracks and produce there X-ray photons, which are absorbed by the cracks sides/walls (hence increase the temperature of the anode, but with decreased production of X-rays towards the patient). The effect is more prominent with the Fine Focus, as there the heat from the thermal electrons distributes over a smaller area, hence the temperature during the exposure is higher and the FF thermal stress becomes prominent earlier, compared with the BF (at an equal number of X-ray exposures). This way the linearity of (mGy/mAs) = F (kV^2) of an X-ray tube can be seen as an indicator for planning the tube replacement. This is also useful for assessing the status of the tube, when its QC assessment starts at unknown time of its clinical use.

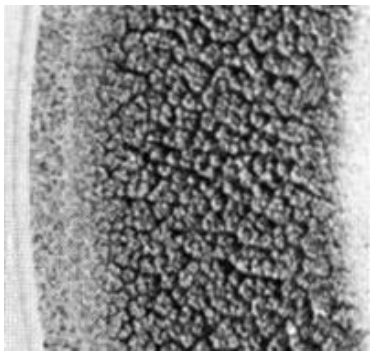

Fig.2 Section of the anode surface of an X-ray tube (rotating anode) showing cracked Anode surface due to thermal stress [4].

If the X-ray tube is QC tested by the Medical Physics Department from its installation – i.e. the Beam Quantity figures (the specific dose output mGy/mAs) are known from the beginning, one can monitor the gradual decrease of this figure (with the years) at specific kV, mAs and distance (focal spot to the dosemeter). From the author's practice, when this parameter drops below 60% from its initial value, replacement of the X-ray tube should be planned.

Depending on the frequency of clinical use of the X-ray equipment, this could be after 5, 10 or more years. This planning is very important for developing countries, where the X-ray tubes are used almost to the end of their life (in many developed countries the X-ray tubes are replaced well before they reach such an exhaustion).

Fig.3 shows the Relative X-ray beam intensity distribution of a new X-ray tube (curve 1) and exhausted X-ray tube (curve 2) [4]. Here can be observed that, additionally to the decreased intensity of curve 2, its pick shifts from the central beam (to the patient) towards the cathode, thus the intensity of the beam towards the Anode drops significantly, what leads to more prominent Heel effect. This effect is difficult to observe in practice [6].

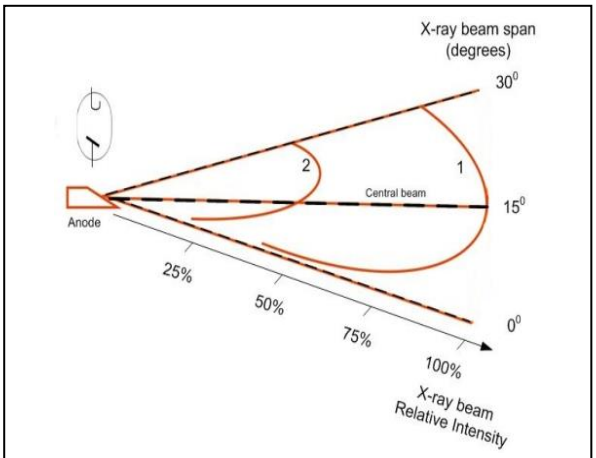

Fig.3 Relative X-ray beam intensity distribution of a new X-ray tube (curve 1) and exhausted X-ray tube (curve 2). Note the significant decrease of intensity towards the anode side (more prominent with exhausted X-ray tube), leading to the well-known Heel effect [4, 6].

Failing to replace an exhausted X-ray tube can lead to X-ray tube arcing, what may lead to fault exposures (hence

Table 1. Real parameters from QC test of an X-ray tube for assessment of (mGy/mAs) = F (kV^2) graph linearity

Focus	set kV	set mA	set msec	set mAs	meas kV	meas mGy	mGy/mAs	(meas kV)2
BF	60	200	100	20	62	0.51	0.03	3844
BF	80	200	100	20	83	0.86	0.04	6889
BF	100	200	100	20	104	1.31	0.07	10816
BF	120	200	100	20	123	1.95	0.10	15129
FF	50	100	200	20	50	0.40	0.02	2500
FF	70	100	200	20	73	0.88	0.04	5329
FF	90	100	200	20	88	1.45	0.07	7744
FF	110	100	200	20	111	1.92	0.10	12321

repetition of exposures and increased patient dose) and further to X-ray equipment failure, what will be associated with significant cost [6, 7].

III. DOSE OUTPUT AND KV DEPENDENCE ON ANODE CURRENT

The dependence of the X-ray tube output (dose) and kV on the Anode current (mA) of the exposure is a parameter related with QC testing of the X-ray Generator. However, this parameter is closely related to the main electrical power circuit of the hospital (it is very prominent in smaller, often rural, hospitals in developing countries [8]).

This effect is really prominent at high mA. We shall demonstrate the effect with a small indicative example (calculation with round figures), which gives an estimate of this dependence, in order to support its understanding.

Each X-ray equipment is connected to the main electrical power circuit of the hospital. Hence between the X-ray equipment and the main transformer of the hospital there are long cables and electrical connections, which have their specific electrical resistance (ohmage). Let us take the following indicative example:

-The X-ray Generator of an X-ray equipment has a High Voltage step-up transformer with transformer ratio 1:500;

-The electrical mains supply the X-ray equipment with 200 Volts (thus the X-ray equipment could produce max 100 kV: 200x500 = 100,000V)

-If this equipment produces a heavy exposure (e.g. in the area of the pelvis) with parameters: 100kV and 100mA (0.1 Amperes Anode current), the required electrical power for this exposure will be of the order of 100,000x0.1 = 10,000 Watts (in this indicative example we do not take into consideration the length of the exposure and the effective voltage);

-This way during the exposure of 100kV and 100mA, the X-ray equipment will consume 10kW from the electrical power circuit of the hospital;

-These 10kW (at 200 V) will require 50 Amperes electrical current entering the X-ray Generator (200x50=10,000);

-These 50A will be delivered by the main power supply of the hospital (its main transformer) and will pass through long hospital cables before coming to the X-ray equipment;

-If we assume that the electrical resistance of these cables is of the order of 0.2 Ohms (what is almost ideal parameter in a small hospital), then this 50A will produce a voltage drop over the cables of the order of 10 Volts (50x0.2=10V). In a rural hospital with high electrical ohmage of the power cables (and their connections) the voltage drop in this example could be twice as much. Similarly, significant voltage drop can be associated with mobile X-ray equipment, where the resistance of the plug connection should also be considered;

-This means that while at the very first moment of the exposure (the first milliseconds) the X-ray Generator will receive 200V, then during the next moment it will receive 200-10=190V;

-After the High Voltage transformer these 190V will supply the X-ray tube with 95kV (190x500=95,000), instead of the required 100kV;

-This way the exposure in this indicative example will just begin with the set parameters of 100kV and 100mA, but will continue with 95kV and 100mA;

-Thus, due to the drop of voltage over the cables of the hospital, the resulting X-ray exposure will be with reduced kV (affecting the image contrast) and reduced dose. The higher is the Anode current (mA) required during the exposure, the more prominent will be this voltage drop in the electrical power supply (in small hospitals one can even observe short dimming of the room lamps light during a heavy X-ray exposure).

Older X-ray equipment (often used in developing countries) have specific Compensatory System, which estimates the expected voltage drop and compensates this voltage drop. This System is between the electrical power supply and the High Voltage transformer (usually using autotransformer). It has variable transformer ratio and usually increases the voltage from the mains to compensate the voltage drop during the exposure. Thus, it provides the High Voltage transformer of the X-ray Generator with specific higher voltage, which compensates the expected voltage drop. Contemporary medium-frequency X-ray Generators use varying frequency of the current through the High Voltage transformer to keep the set kV correct. In any case the voltage drop effect always exists and the correct functioning of the Compensatory System has to be tested

During QC this effect should be tested with high Anode current (as per the maximal clinical requirements) – usually of the order of several hundred mA. Observing the kV waveform could show the effect (and its correction).

The Compensatory system is adjusted regularly by the X-ray service engineers, and if over-adjusted, one could even measure higher kV than the set ones during the exposure. Anyhow, if the dependence of the kV and Dose output from the mA is found during QC tests to be significant, the service engineers should be informed, and they shall decide to either correct the Compensatory System or repair the respective part of the electrical power supply of the hospital (for this X-ray equipment).

Table 2 shows a real QC measurements for assessment Dose output dependence (DOD) and kV dependence (kVD) on the Anode current (mA) of an old X-ray equipment (BF). From Table 2 data one could calculate the % of DOD as:

DOD=100*(stdev of mGy/mAs)/(average of mGy/mAs)

The result is 12% DOD, what is too high (up to 10% can be accepted).

In a similar way one can calculate the % of kVD as:

kVD = 100*average (error/real value) for all 4 meas.

(e.g. from the measured 83, 83, 85, 90 kV the error from the set 80kV is 3, 3, 5, 10 kV, hence in the last measurement at 500mA we have 10/80 = 12.5% error).

The overall kVD in this case is 6.5% what is also unacceptable (up to 5% can be accepted). Both DOD and kVD show that this old X-ray equipment does not function well, it has been overcompensated, perhaps electrical cables ohmage is too high, and all this should be corrected.

In newer X-ray equipment the often-used modern Automatic Exposure Control (AEC) system will correct the drop of dose (usually by some prolongation of the time of the exposure). Considering the image contrast - the Window technique of the digital radiography systems could correct it relatively well (visually). Despite this, the effect of Anode current dependence will always influence the exposure, especially in small hospitals. Its assessment can be an useful indicator for the need of improvement of the electrical power supply circuit of the hospital, or need of adjusting the Compensatory System, what is important for the correct functioning of the X-ray equipment.

IV. CONCLUSION

In the past the above QC tests were performed regularly in developed countries. However, with the time the importance of these decreased. This was due to various factors such as:

-Hospital-Manufacturer Contracts, which require replacement the X-ray equipment (or X-ray tube) well before its expected end of life;

-Improving quality of the Hospital electrical power supply;

-Automatization of the new digital Radiographic X-ray systems, etc.

However, the effects, explained above, continue to exist and they affect the performance of X-ray equipment (especially in developing countries and surely in rural hospitals). Due to this reason the additional information from these QC tests will have to be taken into account in such places.

The assessment of the QC parameters described above formed part of the 1998-published e-learning EMERALD training materials (where the tests are explained in detail) [5].

The explanation of the above effects are also included in the EMITEL e-Encyclopedia of Medical Physics [4] and the author has lectured these at numerous venues and occasions. The paper here, with its examples, can form part of the explanations of the rationale for some QC tests, especially in developing countries - aka Low-and-Middle Income (LMI) countries.

V. FURTHER READING

1. IAEA Human Health Series No.47, Handbook of Basic Quality Control Tests for Diagnostic Radiology, 2023

2. AAPM Report No.74, Quality Control of Diagnostic Radiology, 2002

3. IPEM Report No.32 Part I, Measurement of the Performance Characteristics of Diagnostic X-ray systems used in Medicine (X-ray Tubes and Generators), 1995 (used for many years and replaced by IPEM Report No.77 and later Report 91)

4. EMITEL e-Encyclopedia of Medical Physics, Available free from www.emitel2.eu

5. EMERALD Training materials: Diagnostic Radiology, Available free from: http://www.emerald2.eu/cd/Emerald2/

6. Tabakov S. (2018), X-ray Tube Arcing: Manifestation and Detection During Quality Control, Journal Medical Physics International, v.6, p 157-162

7. MedWrench: X-ray Tube Dying, Accessed 7 May 2018 from : https://www.medwrench.com/thread/99878/x-ray-tube-dying

8. Borras C (Ed), Defining the Medical Imaging Requirements for a Rural Health Center, ISBN 978-9811016110, Springer, 2017

Author: Slavik Tabakov, PhD, Dr hc, FIPEM, FHEA, FIOMP, FIUPESM President IOMP 2015-2018, Institute: King's College London, UK, slavik.tabakov@emerald2.co.uk

Table 2. Real parameters from QC test of an X-ray tube for assessment of Dose output and kV dependence on mA

Focus	set kV	set mA	set msec	mAs	meas kV	meas mGy	mGy/mAs
BF	80	25	100	2.5	83	0.16	0.0640
BF	80	200	100	20	83	0.96	0.0480
BF	80	300	100	30	85	1.72	0.0574
BF	80	500	100	50	90	2.65	0.0530

PROFESSIONAL ISSUES

NEW MEDICAL PHYSICS SPECIALTIES: A STUDY OF THE GENERAL MEDICAL PHYSICIST SPECIALTY IN THE NETHERLANDS: AN INITIAL REPORT

A. Pace[1], C.J. Caruana[1], S. Agius[2], E. Pace[1]

[1] Medical Physics, Faculty of Health Sciences, University of Malta, Msida, Malta
[2] Nuclear Medicine Department, Mater Dei Hospital, Msida, Malta

Abstract — Globally, the Medical Physics profession is mostly delimited to diagnostic and interventional radiology, radiation oncology and nuclear medicine. This is true also in Malta. However, in the Netherlands there are other specialties, among which 'General Medical Physics'. The objectives of this study were to: (i) investigate the role of the General Medical Physicist in the Netherlands (ii) identify aspects of the role which Medical Physicists in Malta do not exercise, (iii) consider the possible introduction of this specialty in Malta. The methodology used in the study can be utilised by Medical Physicists to introduce other specialties to their countries.

Keywords— **Role expansion, general medical physicist, medical physics in the Netherlands.**

I. INTRODUCTION

The scope of the role of Medical Physics (MP) both globally and in Malta is at present largely delimited to solely three specialty areas: diagnostic and interventional radiology (D&IR), nuclear medicine (NM) and radiation oncology (RO). Before the present study the profession has not explored other specialty areas practiced in Europe with a view of expanding the role nationally.

MP in the Netherlands has been successfully advancing for over 50 years and includes other specialties of MP such as Audiology and General Medical Physics (GMP). This study researches the role of the GMP in the Netherlands, a country with a highly developed healthcare system. Outside of the Netherlands, there is little understanding of the role of the GMP as of yet.

By investigating the role of the GMP and analysing the relevance of its role, it would be possible to assess whether introduction of this specialty within the healthcare systems of other countries including the Maltese healthcare system is feasible. The objectives of the study therefore were: (a) To study the role of the GMP within a selected number of hospitals in the Netherlands, (b) To identify aspects of the role which are not yet exercised by Medical Physicists in Malta, and (c) To consider whether and how this specialty of MP could be introduced in Malta.

II. METHODOLOGY

The data collection techniques included semi-structured interviews with Dutch GMPs, document analysis and direct observation. The semi-structured interviews provided a focused approach using pre-planned open-ended questions that allowed flexibility, further discussion and follow-up questions based on the participants' responses. The open-ended nature of the questions also allowed for the emergence of new themes or ideas not initially considered by the researcher.

The purpose of the interviews was to acquire individual perspectives of the GMP role by personally asking the GMPs about their daily duties and responsibilities as well as their perspectives on the specialty. Three different GMPs working in different hospitals with different systems and in different cities were interviewed to ensure a variety of perspectives from different work environments. Analysis of documentation and research articles provided by the participants gave additional information. Moreover, direct observation provided an additional source of primary data during the onsite visits. This variation of data collection methods ensures a well-advised view on the wide spectrum of the work of the GMP.

The sampling method used for this study was judgmental (expert) sampling. The three centers were chosen by an advisor from the Netherlands to ensure sufficient coverage of the role. The participants were in fact recommended by a member of the board of directors of the Dutch Medical Physicist Training Foundation (OKF) and were contacted by the secretary of OKF, which acted as an intermediary for this research. Each interview lasted approximately one hour. Prior to the study, the Dutch curriculum for the competences of the GMP was studied. This curriculum helped in formulating the interview schedule and further enhanced the structure for this research.

The questions were divided into 6 general themes:

Theme 1: General understanding of the role of the GMP in the Netherlands

Theme 2: What distinguishes the GMP from other MPs?

Theme 3: How GMPs interact/work with other healthcare professionals

Theme 4: What special education/training is required to become a GMP?

Theme 5: What specific medical devices and associated physical agents are GMPs involved with?

Theme 6: What was the origin of the GMP in the Netherlands?

The first objective of this study is addressed in themes 1-4, Themes 4 and 5 tackle objective 2, and Themes 4, 5 and 6 set the foundation for objective 3.

III. RESULTS AND DISCUSSION

Theme 1 - *General understanding of the role of the GMP in the Netherlands*

GMPs are a member of the medical staff of general hospitals – they are responsible for overseeing all medical devices (and associated physical agents) utilised within the hospital. While the specialist departmental MP manage the devices in D&IR, RO, and NM, GMPs can also be involved with tasks in these areas as needed, calling for specialists when necessary. GMPs have a broad overview of the medical technology in the hospital, so they can recognise the needs for new medical devices and treatment approaches. They offer guidance on their introduction into the clinic and try to guarantee optimised use. Additionally, they identify potential risks associated with each device and communicate these risks to ensure an overall safe environment in the hospital. The board of directors and medical staff rely on GMPs as their primary contact in events of device malfunction or other technical issues. Moreover, the participants stated that this specialty enhances overall safety, innovation, and financial management of hospitals.

Theme 2 - *What distinguishes the GMP from other Medical Physics Professionals?*

This theme aims to identify aspects of the GMP role, not performed by specialized MPs in D&IR, RO, and NM. Firstly, GMPs adopt a hospital-wide perspective, looking beyond any single department to identify what is best for the entire hospital. They apply successful strategies for all medical departments, leveraging their knowledge of medical devices, medical innovations, and the needs of medical professionals. By doing so, GMPs play a consultative and strategic role in the hospital, rather than solely providing department-specific expertise like other specialist MPs. GMPs also engage in hospital policy discussions and have considerable influence in the decision-making process concerning medical device technology.

GMPs need to have sound knowledge on particular medical devices; if they think additional expertise is required, they can consult other MPs in the hospital or in the country. They leverage their professional relationships and connections with other colleagues in the Netherlands to obtain advice and guidance when initiating new projects or implementing unfamiliar devices.

Theme 3 - *How GMPs interact/work with other healthcare professionals.*

GMPs undertake complex projects for the entire hospital, serving as intermediaries between doctors, the board of directors, and vendors. They try to ensure a balance between purchase of medical device technology and budget constraints. They also serve as intermediaries between doctors and other hospital personnel regarding the use of medical equipment. In addition, GMPs cooperate with IT, estates, purchasing, and medical departments. They have a role in connecting medical device technology to patient databases, provide advice on the layout of examination rooms and help ensuring smooth introduction of medical devices. The participants expressed the importance of a close collaboration with the IT department. This is becoming more important, now that digital health applications are legally considered as medical devices. Any gaps in the connectivity between the medical software and devices can have significant implications in patient diagnosis and treatment. In the hospitals in the Netherlands, all medical departments have a medical manager. As the GMP department is part of the medical staff, the GMP provides a medical manager who has equivalent decision-making power to doctors in hospital-wide decisions. One of the more challenging aspects of the GMP role is getting other healthcare professionals involved in the process of implementation and maintenance of the medical device technology in the hospital. Participants expressed the concern that the risks and hazards associated with outdated medical devices are not always fully realised, even when there is need for urgent replacement.

Theme 4 - *What special education/training is required to become a GMP?*

The diagram illustrated in Figure 1 below, outlines the educational path to become a MP (including GMP), in the Netherlands. The training period involves two years of general training followed by two years of training in the chosen specialty of the trainee (one specialty being GMP).

Figure 1 – Educational path for becoming a Medical Physics Expert (MPE) in the Netherlands.

According to participants, knowledge of hospital business management and organization structure is advantageous for a GMP and it is therefore included in their training. Other essential skills for GMPs include expertise in radiation protection, risk analysis, communication skills, ethical and professional behavior, as well as research skills. In addition, essential skills for GMPs include expertise in radiation protection and risk analysis, robust communication skills, ethical and professional conduct, as well as research skills and IT skills.

Theme 5 - *What specific medical devices are GMPs involved with?*

The GMP addresses medical devices not addressed by MPs specialised in D&IR, RO, and NM. This theme looks into identification of these devices. This can shed light on particular medical devices that are managed by GMPs but have not yet been given attention by MPs in Malta, hence indicating the advantages of the inclusion of GMPs in the Maltese healthcare system. GMPs are generally involved with all medical devices in hospitals. GMPs are involved with all of the stages in the medical device lifecycle depicted in Figure 2 below, with an aim to optimise all medical devices; not only in terms of effective use and safety but also in cost-effectiveness.

Figure 2 – Medical device lifecycle (Van Asten et al., 2023)

The participants work on devices such as infusion pumps and ventilators in intensive care units (ICU), pacemakers and ECG-carts in cardiology, lasers and all imaging devices in ophthalmology and surgery and patient monitoring devices in the operating room, amongst countless others. GMPs ensure appropriate selection and utilization of medical devices in the hospital, with careful consideration of patient-specific factors. For instance, when selecting respiratory equipment for premature infants, they pay great attention to device specifications, including the device's ability to handle the tiny respiratory volumes of newborns. Regarding lasers, GMPs are generally appointed as laser safety experts and ensure compliance with the safety regulations. The participants emphasized that there are various other risks and hazards associated with medical devices used in hospitals, not only regarding ionizing radiation. Improper implementation or usage of these devices, such as infusion pumps, lasers, and electrosurgery equipment, can pose a significant and direct threat to patient safety. All participants stressed the need to pay close attention to these devices. Implementation of medical alarm system in hospitals (e.g., medical device alarms to smartphones) are complex projects, and hospitals involve their GMPs for this.

Theme 6 - *How was the GMP set up in the Netherlands?*

In 1973, the Dutch MPs formed a national society. The group of physicists working in hospitals not only were working with radiation. Physicists working in academic and general hospitals in cardiology, urology or intensive care departments contributed to the society. Therefore, GMP from the beginning was defined as one of the subspecialties of the MPs in The Netherlands. Very importantly, GMPs played a proactive role for the equal treatment of physicists and doctors in Dutch law. The so-called BIG registration (defining professions in Dutch healthcare) provides clarity about their competence. It also defined the MP as a legally protected professional title with which MPs can perform reserved actions independently and requiring a specialist training as doctors (BIG Register. 2022).

IV. CONCLUSIONS AND RECOMMENDATIONS

This section provides a summary of the conclusions derived from the study, and suggestions for professional practice and future research.

The main conclusions of the study were:

(i) **Theme 1:** *General understanding of the role of the GMP in the Netherlands*

The main role of GMPs is to collaborate in healthcare facilities to ensure safe, effective and efficient use of medical device technology in all medical departments.

(ii) **Theme 2:** *What distinguishes the GMP from other MPs?*

GMPs adopt a hospital-wide perspective and are involved in all medical devices and physical agents in the hospital rather than for a specific medical department. They have a consultative and strategic role in the hospital broader than ionizing radiation only.

(iii) **Theme 3:** *How GMPs interact/work with other* healthcare professionals

GMPs act as intermediaries between medics, the hospital management, and vendors of medical equipment in balancing the cost of medical device technology and budget constraints. GMPs also cooperate with various departments, including IT, estates, purchasing, and medical device technology departments, in establishing the safety of patient data, advise on the layout of examination rooms, and help to ensure smooth commissioning of medical devices into clinical practice.

(iv) **Theme 4:** *What special education/training is required to become a GMP*

Master's degree in physics or equivalent, followed by two years of general hospital training and two years of specialised hospital training in GMP.

(v) **Theme 5:** *What specific medical devices are they involved with?*

GMPs are involved with *all* medical devices and all physical agents in the hospital.

(vi) **Theme 6:** *How was the GMP set up in the Netherlands?*

From the early start of the MP society in the Netherlands, the GMPs were present, showing their competency.

The recommendations for professional practice from the study are to (i) expand the scope of MP practice in Malta to introduce and include the role of the GMP and (ii) introduce the specialty in the local MP education and training framework for clinical Medical Physicists. An advantageous arrangement for Malta's healthcare system would entail the employment of GMPs at the main public hospitals (Mater Dei and Gozo General Hospital) whilst also offering consultancy to the small healthcare centres in different locations within Malta and perhaps even to the private sector. This model is similar to the approach used in the Netherlands where some GMPs manage several smaller hospitals for a few days every month in addition to their full-time work at their main larger hospital.

The recommendations for future research are to conduct a comprehensive study to identify the exigencies of the Maltese healthcare system concerning the medical devices that would fall under the purview of the GMP specialty.

ACKNOWLEDGEMENTS

The authors would like to thank the following persons for their generous help during the project: Christiaan van Swol *Advisor of the study*, Hugo Spruijt *GMP*, Jeroen Bosman *GMP*, Vera Lagerburg *GMP*, Priscilla Verbon *Intermediary of the study*.

REFERENCES

1. BIG Register. (2022). CIBG Ministry of Health, Welfare and Sport. Retrieved 13 May 2023, from https://english.bigregister.nl
2. Caruana, C. J., Christofides, S., & Hartmann, G. H. (2014). European Federation of Organisations for Medical Physics (EFOMP) Policy Statement 12.1: Recommendations on Medical Physics Education and Training in Europe 2014. Physica Medica, 30(6), 598-603. 10.1016/j.ejmp.2014.06.001
3. Cheung, A., van Velden, F. H. P., Lagerburg, V., & Minderman, N. (2015). The organizational and clinical impact of integrating bedside equipment to an information system: A systematic literature review of patient data management systems (PDMS). International Journal of Medical Informatics (Shannon, Ireland), 84(3), 155-165. 10.1016/j.ijmedinf.2014.12.002
4. COUNCIL DIRECTIVE 2013/59/EURATOM. (2013). Official Journal of the European Union,
5. Guidelines for the Certification of Clinically Qualified Medical Physicists (2021). IAEA.
6. Hooijschuur, C. A. M., Dijk, W. A., van der Velde, W., Sanon, B., Ammeraal, C., Dassen, W. R. M., & Spruijt, H. J. (2002). Uniform pacemaker and ICD information system in the Netherlands. Paper presented at the 377-380. 10.1109/CIC.2002.1166788 https://ieeexplore.ieee.org/document/1166788
7. IOMP Policy Statement No. 1 The Medical Physicist: Role and Responsibilities (2010). IOMP.
8. Martins Jarnalo, C. O., Linsen, P. V. M., Blazís, S. P., van der Valk, P. H. M., & Dieckens, D. B. M. (2021). Clinical evaluation of a deep-learning-based computer-aided detection system for the detection of pulmonary nodules in a large teaching hospital. Clinical Radiology, 76(11), 838-845. 10.1016/j.crad.2021.07.012
9. OKF. (2021). Integral Curriculum for the Medical Physics Expert. Netherlands: College Consilium of the Stichting Opleiding Klinisch Fysicus https://www.google.com/url?sa=t&rct=j&q=&esrc=s&source=web&cd=&ved=2ahUKEwiWl-vTy-_-AhV_gf0HHbgpAlsQFnoECAwQAQ&url=https%3A%2F%2Fsvmens.nl%2Ff%2Ffiles%2Fdownload%2Fwebsite%2Fonderwijs%2Fintegral-curriculum-medical-physics-expert-01-01-2021-version-1.0.pdf&usg=AOvVaw1G20TvzcQigAxsbnTC6PDq
10. Samei, E., Pawlicki, T., Bourland, D., Chin, E., Das, S., Fox, M., Freedman, D. J., Hangiandreou, N., Jordan, D., Martin, M., Miller, R., Pavlicek, W., Pavord, D., Schober, L., Thomadsen, B., & Whelan, B. (2018). Redefining and reinvigorating the role of physics in clinical medicine: A Report from the AAPM Medical Physics 3.0 Ad Hoc Committee. Medical Physics (Lancaster), 45(9), e783-e789. 10.1002/mp.13087
11. Slegers, A. S., Gültuna, I., Aukes, J. A., van Gorp, E. J. J. A. A., Blommers, F. M. N., Niehof, S. P., & Bosman, J. (2015). Coaching Reduced the Radiation Dose of Pain Physicians by Half during Interventional Procedures. Pain Practice, 15(5), 400-406. 10.1111/papr.12251
12. Van Asten, W., Markidou, E. S., Gromoll, C., Gourzoulidis, G. A., Maguire, S., Guidi, G., Pace, E., Spruijt, H., Martinez-Ortega, J., & Klöck, S. (2023). EFOMP policy statement 17: The role and competences of medical physicists and medical physics experts in the different stages of a medical device life cycle. Physica Medica, 108, 102557. 10.1016/j.ejmp.2023.102557
13. Van der Heide, J. A., Mannaerts, H. F., Spruijt, H. J., van Campen, L. M., de Cock, C., Visser, C. A., & Kamp, O. (2004). Noninvasive mapping of left ventricular electromechanical asynchrony by three-dimensional echocardiography and semi-automatic contour detection. The American Journal of Cardiology, 94(11), 1449-1453. 10.1016/j.amjcard.2004.07.152
14. Van Der Putten, N., Koster, J., Vletter, W., Dijk, W. A., Dassen, W. R. M., Spruijt, H. J., Baljon, M. H., & Gerritsen, M. (2002). Data standards in echocardiography: a Dutch experience. IEEE. 10.1109/cic.2002.1166794
15. Van der Velde, E. T., Atsma, D. E., Hoekema, R., Luijten, J. E., Buddelmeijer, C. I., Spruijt, H. J., & van der Putten, N. H. J. J. (2004). A multicentre PDA project to support the clinical decision process. Paper presented at the 177-179. 10.1109/CIC.2004.1442900 https://ieeexplore.ieee.org/document/1442900

Contacts of the corresponding author:

Author: Amber Pace
Institute: Medical Physics, Faculty of Health Sciences, University of Malta
City: Msida
Country: Malta
Email: amber.pace.19@um.edu.mt

ASSESSMENT OF RADIOLOGY STAFF'S KNOWLEDGE ON RADIATION HAZARDS AND PROTECTION MEASURES IN THE PORT HARCOURT DEPARTMENT OF RADIOLOGY, NIGERIA

W. Igoniye, B.A. Manuel, O.D. Ray-offor

Department of Radiology, University of Port Harcourt Teaching Hospital, Rivers State, Nigeria

Abstract— **While radiology staff work in an environment with ionizing radiation, comprehensive safety protocols and effective protective equipment are crucial in mitigating these risks. These measures include administrative controls, engineering controls, personal protective equipment, continuous education and training, and regular monitoring to ensure radiation exposure is kept as low as reasonably achievable (ALARA). To evaluate the level of knowledge and practice of radiation hazards and radiation protection among radiology staff in Port Harcourt, Nigeria, with the goal of identifying areas for improvement in safety practices. A cross-sectional survey was conducted among 179 radiology staff, including 65 medical doctors (radiologists), 12 nurses, 47 radiographers, and 55 other personnel. All 179 participants returned the survey, providing a 100% response rate. Participants completed a questionnaire consisting of 22 questions covering demographic information, awareness of radiation risks, radiation protection practices, regulatory knowledge, understanding of fluoroscopy units, training and education, radiation protection principles, quality assurance practices, radiation sensitivity awareness, knowledge of radiation effects, familiarity with radiation safety equipment, purpose of radiation dose administration, and understanding of optimizing radiation dose. The survey revealed that 82.1% of the staff understand the risks associated with radiation exposure in diagnostic radiology. All 179 participants (100%) attended a basic lecture on radiation exposure. However, significant gaps were found in regulatory knowledge, as only 88.3% of the staff were aware that Nigeria Nuclear Regulatory Authority (NNRA) approval is required for a machine to dispense radiation. This study emphasizes the need for continuous education and training programs tailored to the specific needs of radiology staff. Addressing these knowledge gaps and improving safety practices can enhance the overall safety and well-being of radiology staff in Port Harcourt, ultimately contributing to better patient care and outcomes.**

Keywords— **Radiation hazards, Radiation protection, Radiology staff, Knowledge assessment, Port Harcourt.**

I. INTRODUCTION

X-ray imaging is a cornerstone of medical diagnosis, but it involves exposure to ionizing radiation, which can damage tissues and potentially lead to cancer. Proper knowledge of radiation hazards and protection measures is crucial for radiology staff like radiologists, radiographers, medical Physicists and nurses [1]. Despite regulations by the Nigeria Nuclear Regulatory Agency (NNRA), studies suggest gaps in radiology staff's knowledge about radiation risks. This research aims to assess the knowledge of staff at the Port Harcourt Department of Radiology regarding radiation hazards and protection measures [2]. By identifying areas for improvement, this study seeks to enhance radiation safety practices in the department. This can lead to better patient care by minimizing radiation exposure for both patients and healthcare workers. The use of X-rays comes with inherent risks, particularly due to their ionizing nature, which can cause damage to living tissues [3, 4]. The ionizing radiation has the potential to cause cellular damage, including DNA mutations that can lead to cancer [5, 6]. The linear no-threshold (LNT) model, which is widely accepted in radiation protection, suggests that any dose of radiation, no matter how small, carries a corresponding risk of cancer [8, 9]. This model forms the basis for radiation protection standards, guiding efforts to minimize radiation exposure.

Optimizing radiation dose is essential in radiology to minimize the risks associated with radiation exposure while ensuring that diagnostically acceptable images are obtained [8]. This principle, known as ALARA (As Low As Reasonably Achievable), guides radiology professionals in balancing the need for diagnostic information with the potential risks of radiation exposure [9, 10]. Abuzaid emphasizes the ALARA principle for radiation protection which aligns with the methodology of ensuring patient safety and complements focus on proper practices. Justification of radiological procedures is equally important, ensuring that the benefits of the procedure outweigh the risks for the individual patient [11]. The International Atomic Energy Agency (IAEA) emphasizes the need for strong radiation safety regulations.

Despite the efforts of regulatory bodies such as the Nigeria Nuclear Regulatory Agency (NNRA), studies have indicated gaps in the knowledge of radiology staff regarding radiation hazards and protection [12] &13). Existing surveys might not be tailored to the specific protocols, equipment, and regulations used in the Port Harcourt Department of Radiology. A new survey can be designed to target these specific aspects, ensuring a more accurate assessment of the staff's knowledge about radiation hazards and protection measures relevant to their daily practice [14, 15]. This study aims to contribute to the ongoing efforts to enhance radiation safety in radiology by assessing the

knowledge of radiology staff and identifying areas for improvement.

Through education, training, and continued research, the field of radiology can continue to advance while ensuring the safety of patients and healthcare workers.

II. METHODOLOGY

Questionnaire Design and Administration

The survey instrument (included as supplementary material) comprised 22 questions, the four demographic questions are Multiple Choice Questions (MCQ) and more than four answer options. The first four questions collected demographic data such as age, gender, and professional experience of the participants. The following 15 multiple-choice questions (MCQs) with four answer options focused on evaluating participants' understanding and application of radiation protection principles. One subjective that probe into understanding of ALARA Principle. One MCQ with six answer options to tick as appropriate concerning the biological effects of ionizing radiation and one MCQ with three answer options on knowledge of the fluoroscopic system. These MCQs covered various aspects of radiation safety, including Biological effects of ionizing radiation, Radiation protection principles (e.g., justification, optimization, dose limitation), Safe operating procedures for X-ray equipment, Use of personal protective equipment (PPE).

The survey was reviewed by radiation safety experts and radiology professionals to ensure its content accurately reflects current practices and targets relevant knowledge areas. A pilot test with a small sample group helped refine the survey for clarity and comprehensiveness. The survey was distributed to a diverse group of participants within the Department of Radiology, including Radiologists, Medical physicists, Radiographers, Radiology technologists, Residents and Students.

Google Forms was chosen for its user-friendly interface and efficient data collection capabilities. The survey link was electronically distributed to the target population. An informed consent statement explained the study's purpose and assured participants of anonymity and confidentiality. Participation was voluntary, and responses did not affect professional standing.

Ethical Considerations

The study adhered to the ethical guidelines of the University of Port Harcourt Teaching Hospital. Measures were implemented to ensure responses were anonymous and confidential.

Data Collection Details

Data collection spanned from 1st November 2023 to 29th February 2024, providing a thorough assessment period. The department comprises a multidisciplinary team including radiologists, nurses, radiographers, medical physicists, radiologic technologists, and residents. Participants received the survey link through departmental platforms, emails, and WhatsApp messages. Additionally, the principal investigator conducted a hardcopy questionnaire survey, overseeing participants as they completed it. Each correct answer was awarded a score of "1," with no negative marking for incorrect responses.

Data Analysis Software

The data was entered into Python software, using Visual Studio Code, for analysis. A descriptive analysis was conducted, along with relevant statistical tests to ascertain the level of knowledge regarding radiation protection among the participants. The knowledge levels were categorized based on the percentage of correct responses: inadequate (<60%), adequate (60–80%), and excellent (80–100%). To compute the p- value and determine the statistical significance using Python, scipy.stats module was used to perform a Chi-square test'. For statistically significant findings from the Kruskal-Wallis H-test, a pairwise post-hoc test with Bonferroni correction was applied. A p-value ≤ 0.05 was considered statistically significant.

III. RESULTS

There's near-equal representation with 53.1% female and 46.9% male staff. A significant portion (53.1%) falls within the 30-39 age group, indicating a core of staff in their prime working years. The presence of staff in the 20-29 (23.5%) and 40-49 (23.5%) age brackets suggests a healthy mix of experience and new talent. Notably, there are currently no staff aged 50-59 or 60-69. Nearly half (46.9%) of the staff have 1-5 years of experience, highlighting a substantial number of early-career professionals. The remaining workforce is spread across experience levels with 29.1% (6-10 years), 17.9% (11-15 years), and a smaller group with 16-20 years of experience.

On knowledge of radiation exposure risks in diagnostic radiology**, t**he results showed in table 2, that 41.3% of respondents of the question “The ways to reduce the risk of radiation exposure for patients in the radiology department” recognized the importance of reducing the time spent performing x-ray procedures. This understanding aligns with the "as low as reasonably achievable" (ALARA) principle, emphasizing the importance of minimizing radiation exposure time to reduce risks. Furthermore, 53.1% of participants acknowledged the main goal of optimizing radiation dose in radiology and as well as listing the three principles of radiation protection in the correct order. Assess knowledge of departmental practices for dose optimization, such as: “What is the main goal of optimizing radiation dose in radiology” this question highlights potential knowledge gaps in implementing dose optimization within the Port Harcourt Radiology departmental workflow. The finding that 53.1% of respondents correctly identified the order of radiation protection principles (Time- Distance-Shielding) is

a positive indicator. This demonstrates a foundational understanding of minimizing radiation exposure. However, the remaining 46.9% who provided incorrect responses (25% Distance-Shielding-Time, 11.8% Distance-Time-Shielding, and 11.8% Shielding-Time- Distance) reveal a crucial knowledge gap. This will foster a culture of safety that prioritizes staff well-being while maintaining optimal image quality for patient care.

Table1: Demographic Characteristics

Serial Number	Demographic Characteristics	Frequency	Percentage (%)
	Gender		
1	Male	84	46.9
2	Female	95	53.1
	Age Groups (In years)		
3	20 – 29	42	23.5
4	30 – 39	95	53.1
5	40 – 49	42	23.5
	Work Experience (In years)		
6	1 – 5	84	46.9
7	6 – 10	52	29.1
8	11 – 15	32	17.9
9	16 – 20	11	6.1
	Job Title		
10	Radiologists	65	36.3
11	Radiographers	47	26.3
12	Nurses	12	6.7
13	Medical Physicists	4	2.2
14	Technologists	15	8.4
15	Health Assistants	36	20.1

Additionally, 53.1% of respondents recognized the thickness of the mobile Protective Barrier (MPB) used in the x-ray room. emphasizes the importance of integrating knowledge into daily practices. Standardized departmental protocols and clear visual signage in the X- ray room serve as constant reminders and reinforce the crucial role of the MPB in radiation safety. This ongoing reinforcement strengthens staff's understanding and promotes consistent application of best practices. The finding that 64.8% of respondents correctly identified pregnant women as the most radiation-sensitive patients demonstrates a good understanding of a critical principle. However, the remaining 35.2% who selected other options (presumably children) highlight a potential knowledge gap that requires a more clinically innovative approach. While recognizing pregnant women's vulnerability is crucial, true innovation lies in risk stratification for different patient populations. This will ultimately lead to a more individualized and risk-stratified approach to patient care.

The finding that 88.3% of respondents correctly identified DNA damage as an effect of radiation exposure in the question "What are some of the effects of ionizing radiation that you are aware of?" demonstrates a good understanding of long-term carcinogenic risks. However, the lower percentages for other effects, particularly regarding acute effects, reveal a potential knowledge gap.

The finding that 53.1% of respondents indicated situational awareness regarding lead apron usage is a positive sign. However, a significant portion (29.4% sometimes, 11.8% never) demonstrates a need for clearer guidelines and training on appropriate lead apron use in various scenarios.

The finding that a significant majority (70.4%) of respondents reported never wearing both thyroid collars and

lead eye glasses reveals a critical gap in radiation protection practices This has significant clinical implications for both staff and patient safety. Thyroid and eye tissues are particularly susceptible to radiation exposure. Consistent non-use of these protective measures significantly increases staff's risk of developing thyroid and eye cancers over time. Abuzaid's findings on areas where adherence might be lower (e.g., thyroid collar usage) due to factors like increased workload or PPE shortages [18].

The high percentage (93.9%) of staff reporting consistent TLD use indicates a strong understanding of their basic function – monitoring radiation exposure. This adherence is crucial for ensuring staff safety and adheres to established radiation protection protocols. However, the additional information that 6.1% reported sometimes wearing TLDs suggests a potential gap in understanding. This might indicate:

Lack of knowledge on proper TLD wear during specific procedures and misconceptions about the importance of consistent data collection for accurate exposure assessment. This gap is addressed by exploring staff understanding of TLD data interpretation.

Results showed that the majority of respondents (88.3%) were aware that NNRA approval is required for a machine to dispense radiation. This indicates a high level of awareness among radiology staff regarding the regulatory process for radiation- emitting machines. However, 11.7% of respondents incorrectly believed that only machines that produce radiation require approval from the NNRA. This misconception highlights the need for further education and clarification regarding the regulatory requirements for all machines that dispense radiation, including those used in diagnostic and therapeutic radiology.

Understanding the type of fluoroscopy unit in use is crucial for optimizing its operation and ensuring safety. In this study, participants were asked about the type of fluoroscopy unit in their institution, specifically whether it is an under-couch or over-couch C-arm system.

This research sheds light on a potential knowledge gap regarding staff familiarity with the specific type of fluoroscopy unit used in their department. While the majority (74.9%) reported using an over-couch C-arm system, a significant portion (18.8%) used an under-couch system, and a concerning 6.2% were unsure of the type altogether.

These findings reveal an opportunity to enhance staff knowledge and optimize radiation safety practices: The research can advocate for clear and consistent labeling of fluoroscopy units within the department. This can be achieved through signage or visual identification markers to ensure staff are always aware of the specific system type they are using. Develop training protocols that are tailored to the specific type of C-arm system used in the department. This ensures staff receive proper instruction on safe positioning techniques and radiation protection considerations relevant to the unit's design (over-couch vs. under-couch exposure).Create a platform (online forum, knowledge base) where staff can share experiences and best practices for specific C-arm systems. This fosters a culture of continuous learning and knowledge exchange, addressing any lingering uncertainties about the equipment used in daily practice

While the finding that 100% of respondents attended a basic radiation exposure lecture demonstrates a commitment to staff education, it doesn't necessarily address a knowledge gap. The 100% attendance rate for the basic radiation exposure lecture indicates a positive trend in staff training. However, it doesn't guarantee complete knowledge retention or preparedness for all radiation safety scenarios encountered in daily practice. Implementing follow-up assessments or knowledge retention tests to gauge staff comprehension of the fundamental radiation safety principles covered in the lecture will yield optimum result. This can help staff apply their theoretical knowledge to practical situations.

The results showed that 88.3% of respondents identified the main justification for administering a radiation dose in radiology as visualizing the anatomy and pathology of the body. This aligns with the primary goal of diagnostic radiology, which is to obtain detailed images for accurate diagnosis and treatment planning. In contrast, 11.8% of respondents incorrectly believed that the main justification was to destroy cancer cells, highlighting a potential misunderstanding of the role of diagnostic radiology in cancer treatment.

Regarding the optimization of radiation dose, 52.9% of respondents identified the main goal as improving image quality. This is crucial for obtaining clear and detailed images for accurate diagnosis while minimizing radiation exposure. Additionally, 47.1% identified the main goal as reducing the risk of radiation-induced cancer, demonstrating an understanding of the importance of minimizing radiation exposure to patients and healthcare workers.

When asked about the main purpose of wearing a Thermoluminescent Dosimeter (TLD), 94.1% of respondents correctly identified it as measuring the amount of radiation exposure. This is essential for monitoring and controlling radiation exposure levels among radiology staff.

Furthermore, 93.9% of respondents correctly identified the purpose of periodic quality assurance tests of x-ray equipment as being useful for maintaining the quality of equipment and ensuring safe operation. These findings highlight the importance of continuous education and training to ensure that radiology staff understand and adhere to best practices for radiation dose administration and optimization.

Finally, when asked about the primary purpose of a Geiger counter in the radiology department, 64.8% correctly identified it as measuring radiation dose. This is essential for monitoring radiation levels in the environment and ensuring safe practices in radiology departments.

IV. DISCUSSION

The staff's demographic distribution underscores the need for continuous education and training to ensure that all staff are well-prepared to handle the challenges of radiological practices (16). Awareness of radiation risks among radiology staff is crucial for safe practices (17). A significant finding is that 82.1% of staff understand the risk of cancer associated with radiation exposure in diagnostic radiology, which is adequate and in agreement with Assiri et al.2020(18). This high level of awareness is promising but further underscores the need for ongoing education and training to maintain and enhance safety practices in the field. These findings indicate a satisfactory level of awareness among radiology staff regarding strategies to reduce radiation exposure for patients. However, continuous education and reinforcement of these principles are essential to ensure consistent adherence to best practices in radiation protection. Effective radiation protection practices are essential for ensuring the safety of both patients and healthcare workers in radiology departments (19). This study aimed to assess the adherence of radiology staff to key radiation protection practices, including the consistent use of lead aprons, thyroid collars, lead eyeglasses, and radiation dosimeters (TLDs). The findings are inadequate and in agreement with. Khamtuikrua, and Suksompong, (2020) study, highlighting the need for increased awareness and education regarding the importance of wearing lead aprons consistently to minimize radiation exposure (20). The Nigerian Nuclear Regulatory Authority (NNRA) mandates approval for machines dispensing radiation to ensure safety. Compliance with NNRA regulations is crucial for radiology departments.

The NNRA requires approval for all radiation-dispensing machines, not just those producing radiation. Proper use of personal protective equipment (PPE), including lead aprons, thyroid collars, and lead eyeglasses, is essential. Compliance with these regulations is necessary to minimize radiation exposure risks and ensure the safety of both patients and healthcare workers. Ongoing education and training are excellent and vital and in an agreement with Mngxekeza, (2019) study, to ensure that radiology staff are aware of and adhere to NNRA regulations, promoting a culture of safety and regulatory compliance within radiology departments (21).

As stated in the International Commission on Radiological Protection (ICRP) publication, The primary purpose of radiological protection is to provide a high level of protection for man and the environment against the harmful effects of ionizing radiation. Fluoroscopy units are essential in diagnostic radiology for real-time imaging procedures. The findings shows knowledge score of adequate indicating staffs awareness towards radiation safety which is also in agreement with the study of Hayashi et al(2021)

V. LIMITATIONS OF THE STUDY

The limitations of this study include the potential for response bias as participants may have provided answers, they deemed socially desirable (23). This study is susceptible to response bias, similar to Abuzaid et al. (2022). Participants might report practices that are considered ideal rather than their actual behavior.

The single-institution design limits generalizability of findings to other radiology departments in Port Harcourt or Nigeria as a whole. The use of self-reported data could introduce recall bias, as participants may not accurately remember past training or experiences (22). This study assesses knowledge but doesn't directly measure actual adherence to safety protocols during radiology procedures. Despite these limitations, this study provides valuable insights into the knowledge of radiation hazards and protection among radiology staff, highlighting areas for improvement in radiation safety practices. Future studies could benefit from longitudinal designs and multi- center collaborations to enhance the generalizability and validity of the findings.

VI. CONCLUSION

In conclusion, this study identified varying levels of knowledge on radiation hazards and protection measures among radiology staff at the institution. While overall awareness seems adequate, specific areas like proper use of lead aprons and thyroid collars require improvement. These findings highlight the critical need for continuous education.

Regularly conducting training programs can enhance radiation safety practices among radiology professionals. These programs should address identified knowledge gaps, such as the importance and proper use of personal protective equipment (PPE) like lead aprons and thyroid collars. Implementing regular audits and quality assurance measures can ensure consistent adherence to established safety protocols within the department. Building on this study, future research could evaluate the effectiveness of training interventions. This would involve implementing targeted training programs and measuring their impact on staff knowledge and adherence to safety protocols.

Supplementing self-reported data with direct observation of practices during radiology procedures could provide a more holistic picture of adherence to safety measures.

Then future studies could involve multiple institutions in Port Harcourt or across Nigeria to enhance the generalizability of findings.

VII. ETHICAL STATEMENT

Hereby, I, Igoniye Williams consciously assure that for the manuscript /insert title/ the following is fulfilled:

1) This material is the authors' ownoriginal work,

which has not been previously published elsewhere.

2) The paper is not currently beingconsidered for publication elsewhere.

3) The paper reflects the authors' own research and analysis in a truthful and complete manner.

4) The paper properly credits the meaningful contributions of coauthors and co- researchers.

5) The results are appropriately placed in the context of prior and existing research.

6) All sources used are properly disclosed (correct citation). Literally copying of text must be indicated as such by using quotation marks and giving proper reference.

7) All authors have been personally and actively involved in substantial work leading to the paper and will take public responsibility for its content.

ACKNOWLEDGEMENT

Authors would like to thank all the radiology staff and students who actively participated in this survey.

REFERENCES

1. Maharjan, S. (2017). Radiation knowledge among radiographers and radiography students. Radiography Open, 3(1), 17-17.
2. Idowu, B. M., and Okedere, T. A. (2020). Diagnostic radiology in Nigeria: a country report. Journal of Global Radiology, 6(1).
3. Leotlela, M. (2021). Establishing an Effective Nuclear Regulatory Regime: A Case Study of South Africa. Policy, 5(1), 1-18.
4. Anurag, L., Gaurav, M., Sanjay, D., and Chandrashekar, M. (2022). The spectrum of the atomic energy regulatory board under the department of atomic energy with respect to a medical radiation facility. Journal of Datta Meghe Institute of Medical Sciences University, 17(3), 766-771.
5. Okawele, K. N., Nathaniel, E. U., and Ekanem, A. M. (2024). Occupational Radiation Dose Absorbed by Radiographers in Port Harcourt, Rivers State. Researchers Journal of Science and Technology, 4(1),21-31.
6. Goula, A., Chatzis, A., Stamouli, M. A., Kelesi, M., Kaba, E., and Brilakis, E. (2021). Assessment of Health Professionals' Attitudes on Radiation Protection Measures. International journal of environmental research and public health, 18(24), 13380.
7. Assiri, H., Dawasaz, A. A., Thobaiti, R. A., Alshehri, Y., Alsahman, L., and Buraidi, A. (2020). Awareness among dental practitioners towards radiation hazards and protection in Abha city, Saudi Arabia. Journal of Dentistry and Oral Sciences, 2(3), 1-14.
8. Abuzaid, M. M., Elshami, W., and Tekin, H. O. (2022). Infection control and radiation safety practices in the radiology department during the COVID-19 outbreak. PLoS One, 17(12), e0279607.
9. Khamtuikrua, C., and Suksompong, S. (2020). Awareness about radiation hazards and knowledge about radiation protection among healthcare personnel: a quaternary care academic center–based study. SAGE Open Medicine, 8, 2050312120901733.
10. Mngxekeza, S. (2019). Realising the right to the highest attainable standard of health in the nuclear industry.
11. Hayashi, S., Takenaka, M., Kogure, H., Yakushijin, T., Maruyama, H., Hori, Y. and Nishida, T. (2021). A questionnaire survey on radiation protection among 282 medical staff from 26 endoscopy-fluoroscopy departments in Japan. DEN open, 1(1), e5.
12. Schell, C., Godinho, A., and Cunningham, J. A. (2021). Examining change in self- reported gambling measures over time as related to socially desirable responding bias. Journal of gambling studies, 37, 1043-1054.
13. Hill, N. L., Mogle, J., Whitaker, E. B., Gilmore-Bykovskyi, A., Bhargava, S., Bhang, I. Y. and Van Haitsma, K. (2019). Sources of response bias in cognitive self- report items: "Which memory are you talking about?". The Gerontologist, 59(5), 912- 924.

Contacts of the corresponding author:

Author: Williams Igoniye
Institute: Department of Radiology, University of Port Harcourt Teaching Hospital
City: Rivers State
Country: Nigeria
Email: williamsigoniye@gmail.com

INVITED PAPERS

DOSIMETRIC COMPARISON IN A HYBRID STUDY OF PATIENTS AND PHANTOM: IMRT VS. FIELD-IN-FIELD (3DCRT)

A.M. Baidoo[1], S.N.A. Tagoe[1,3], E.K. Sosu[2], S.B. Boateng[1], R.B. Awotwe[1], A. Mamoud[1], J.F. Nanevi[4], P.Odonkor[5], A.M. Fatormah[6]

[1] Sweden Ghana Medical Centre/Department of Radiation Oncology, Medical Physicist, Accra, Ghana
[2] University of Ghana/Department of Medical Physics, Head of Department, Accra, Ghana
[3] University of Ghana/Department of Radiography, Exam Officer, Accra, Ghana
[4] Catholic Hospital Battor /Department of Medical Imaging, Radiation Protection Officer, Battor, Ghana
[5] Korle Bu Teaching Hospital/National Centre for Radiotherapy and Nuclear Medicine, Medical Physicist, Accra, Ghana
[6] University of Ghana/Department of Biomedical Engineering, PhD Candidate, Accra, Ghana

***Abstract*—Due to its location, breast radiotherapy necessitates a high degree of accuracy in order to protect adjacent organs at risk while maximizing doses to the tumor. Numerous studies have been conducted to determine the most effective treatment planning technique that results in an optimal breast treatment. In all these research works, data sets and the medium for treatment planning were either a collection of patients or a phantom. Thus far, no study has been conducted to compare the dosimetry of these techniques using both phantom and real patients. The goal of this study is to investigate the dosimetric superiority between 3DCRT Field-in-Field and IMRT techniques for whole breast radiotherapy in a hybrid study of anthropomorphic phantom and real patients. A female Rando Alderson anthropomorphic phantom and image sets of thirty breast cancer patients that have completed whole breast radiotherapy were planned using tangential IMRT and 3DCRT Field-in-Field techniques using a prescribed dose of 50Gy in 25 fractions. The dosimetric superiority between the two treatment planning techniques were investigated by examining the quality of plans generated by each technique, using as criteria, target coverage, OAR sparing, conformity index (CI) and homogeneity index (HI). With an assessment score of 18/18 for real patients, the IMRT technique demonstrates superior dosimetry in terms of the dose parameters designated for this study. Both treatment planning techniques achieved an evaluation score of 15/18 for the phantom, with the IMRT scoring higher in OAR sparing and the FiF outperforming the IMRT in target coverage. The findings of this research indicates that tangential IMRT possesses superior dosimetry for breast cancer radiotherapy since it has the potential to dramatically lower radiation doses to OARs while maximizing target doses compared to 3DCRT FiF.**

Keywords— **Dosimetric parameters, Contralateral breast, Tangential Beam, Phantom.**

I. INTRODUCTION

Approximately 50% of cancer cases globally are treated with radiation therapy[1]. In order to achieve a greater cure rate with acceptable morbidity, the most fundamental principle is to deliver maximum dose to the tumor with minimum dose to the surrounding normal structures. The treatment planning technique and algorithm are among the most essential elements that determine the quality of radiation therapy. With 25.8% of all newly detected cases in 2020 being diagnosed with breast cancer, it is the most common cancer among women globally[2]. Meanwhile, because of its location, radiotherapy of the breast necessitates extraordinary caution in order to protect critical organs at risk (OARs) while delivering maximum doses to the breast treatment volume. Studies have noted that the rate of ischemic heart disease that follows radiation therapy for breast cancer is higher when the heart is exposed to ionizing radiation[3]. Other studies have similarly reported lung toxicities following breast irradiation involving exposure to large volumes of lung[4]. Ensuring the best technique accessible for treatment planning of breast cancer radiation therapy is essential to eliminating the aforementioned complications.

The goal of this study is to investigate the dosimetric superiority between 3DCRT Field-in-Field (FiF) and IMRT techniques for whole breast radiotherapy in a hybrid study of anthropomorphic phantom and real patients. Numerous studies have been carried out to compare the dosimetric superiority of 3DCRT-FiF and IMRT for breast cancer radiotherapy, and the findings of these investigations are being used as a basis for clinical decisions regarding the most effective technique for the best radiation dosimetry of breast cancer treatment. In all these, data sets and the medium for treatment planning were either a collection of patients or a phantom. No research has been done up to this point that compared the dosimetry of the two techniques using both phantom and real patients. The female anthropomorphic phantom is a good representation when taking into account the total PTV of the whole breast that are reported by the majority of these investigations[3]. The total PTV of the phantom in this study was 565.52 cc. However, the whole breast of the female anthropomorphic phantom is significantly smaller than the average breast size of the patients whose data were used as a representation of a typical West African woman, despite the phantom's tissue-equivalent properties. Thus, in order to present both the idealized and the clinically realistic data that might accurately represent the dosimetry of the two techniques

globally, this study was conducted using both patients and the anthropomorphic phantom.

II. MATERIALS AND METHODS

Study design

A female Rando Alderson anthropomorphic phantom was used together with data from images of thirty (30) randomly selected patients, comprising of fifteen (15) each of left and right sided breast cancer patients that have completed intact breast radiation treatment for this study.

Radiotherapy Imaging and Contouring

In this study, an in-house Computed Tomography (CT) simulator, Siemens CT (Somatom Emotion 16 slice scanner) was used to scan a female Rando Alderson anthropomorphic phantom. The patient (same for phantom) was immobilized on an inclined breast board on a flat couch as shown in Figure 1. A wire was placed on the midline at the sternum of the phantom to define boundaries of both breasts. Axial CT scans using slice thickness of 3mm were acquired for the thoracic wall. The image data were exported to a treatment planning system, and 3D reconstruction was digitally obtained.

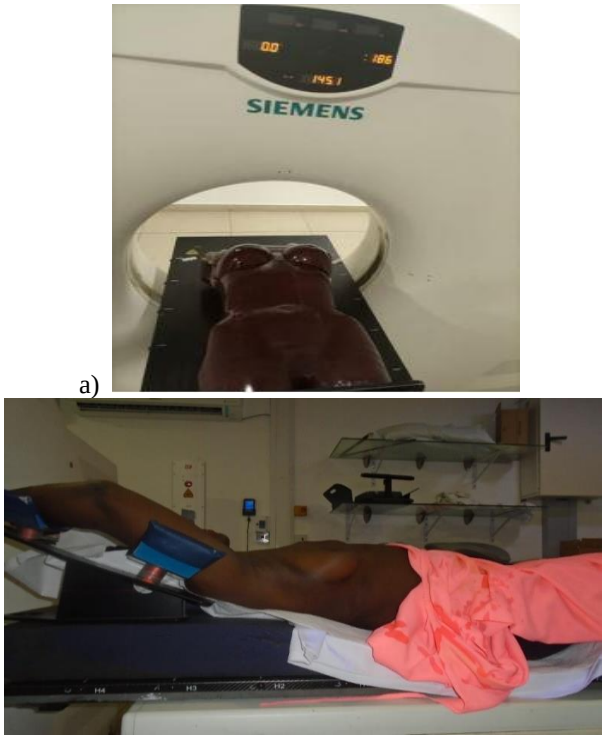

a)

b)

Figure 1: CT Setup: a) Female anthropomorphic phantom; b) Patient Setup

Delineation of the Clinical Target Volume (CTV), Planning Target Volume (PTV) and all OARs including heart, lungs and contralateral breast were done using the Monaco® workstation. For patients unlike the phantom, the CTV could as well include all axillary and parasternal lymph nodes based on tumor histological features, staging and individual characteristics. These were done according to the Radiation Therapy Planning Consensus Definitions of Breast Cancer Atlas of the Radiation Therapy Oncology Group (RTOG)[5] and the Evidence-Based Guideline for Radiation Therapy for the Whole Breast by the American Society for Radiation Oncology (ASTRO)[6]. All contours were made by the same radiation oncologist. The total PTV for the phantom was 565.52 cc. The maximum PTV for the patients was 2197.10 cc, the smallest was 653.22 cc and the average of all thirty (30) patients was 1352.37±845.53 cc. The study involved whole breast radiotherapy without supraclavicular nodes. The prescribed dose was 50.0 Gy in 25 fractions, prescribed according to the ICRU Report 50 recommendations[5], and the dose limits for all OARs were defined according to our clinical protocol.

Ethical considerations

Without any clinical application, the various treatment techniques were applied to the dataset of patients. The regulations of our institution do not require an ethical clearance for this activity.

Treatment Planning

All plans were completed in Elekta Treatment Planning System (Monaco® version 5.11.03) commissioned with beam parameters from an Elekta Synergy® linear accelerator. 3DCRT Field-in-Field (FiF) and Intensity Modulated Radiotherapy (IMRT) treatment planning techniques were used to generate treatment plans for each patient and the phantom. The primary optimization parameters for both planning techniques were the same, and these parameters were adjusted based on individual challenges pertaining to the realization of the dosimetric results with respect to treatment objectives. The planning objectives of both treatment planning techniques were generated following RTOG recommendations and are shown in Table 1. Treatment planning in both techniques for the phantom were completed independently by three Medical Physicists, unlike the patients where all plans were completed by the same Physicist.

Table 1: Optimization Objective for Treatment Planning

Structure	**Planning Aim**
PTV	$V_{50Gy} \geq 90\%$, $V_{47.5Gy} \geq 95\%$, $D_{50\%} \geq 50Gy$, $V_{51Gy} \leq 25\%$, $V_{53Gy} \leq 10\%$
Contralateral breast	$D_{max} \leq 3$ Gy, $V_{5Gy} \leq 15$ %
Ipsilateral lung	$V_{20Gy} \leq 45\%$, $V_{30Gy} \leq 35\%$
Lung (Total volume)	$V_{20Gy} \leq 30$ %, $V_{30Gy} \leq 20\%$
Heart	$D_{max} \leq 40$ Gy, $D_{average} \leq 26$ Gy, $V_{5Gy} \leq 45$ %, $V_{20Gy} \leq 20$ %

3DCRT Field-in-Field Technique

The FiF plans were generated using eight and ten beams for right and left breasts respectively with a single isocenter at the center of mass of the PTV. It involved the use of two open tangential fields and multiple field-in-fields to achieve an optimal dose distribution and desired homogeneity through complex manual fluence map optimization as shown in Figure 3.

The gantry angles of the open tangential fields were selected using the beam's-eye-view (BEV) projections to ensure complete coverage of the PTV, yet minimum beam coverage for lung and heart (for left breast) volumes. The angles were also selected to ensure that the contralateral breast is completely out of the beam with the help of the wire placed on the midline at the sternum during simulation as shown in Figure 2. With the fields carefully selected to encompass less than 2 cm of the affected lung volume from its outermost side in each axial view, the line of intersection of the two tangential fields had no overlap with the contralateral breast. There was an addition of 2 cm jaw margin to the surface of the skin. The open fields used 6MV photons for all calculations. The technique also involved calculation and plan optimization to achieve desired dose distribution with the two open fields. The open fields were given equal weighting, contributing to the entire dose distribution before introduction of the subfields. Plan dose optimization involved identification of the appropriate calculation point within the target to achieve desired dose distribution using global normalization.

When isodose lines were displayed on the 3D viewer interphase, the regions of overdose within the target became clear. A subfield was introduced for each of the two open fields with which the part of the lung that was within the beam was fully blocked with MLCs. In the case of the left breast, another subfield per angle was employed to shield the heart in a similar process to that of lung blocking.

Regarding the treatment planning of the phantom, three (3) subfields each were added, resulting in five (5) subfields per angle. These subfields were created with 15 MV photons to manually cover hot areas in a reduction sequence such as 112%, 109%, 106% using MLCs. The beam weight per subfield was 5% of its corresponding open field, and the equivalent monitor unit (MU) was 12.50. Monitor units for the subfields were calculated and the resulting isodose distribution was observed.

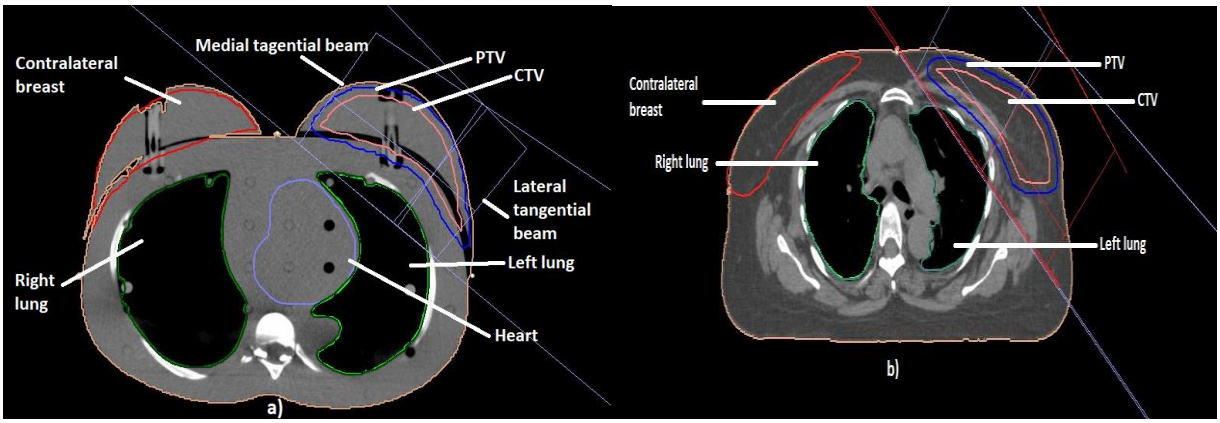

Figure 2: Axial view of 3DCRT beam arrangements: a) Phantom; b) Actual patient

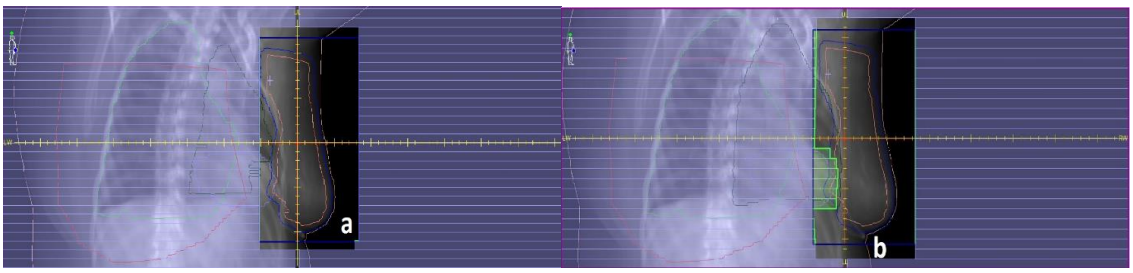

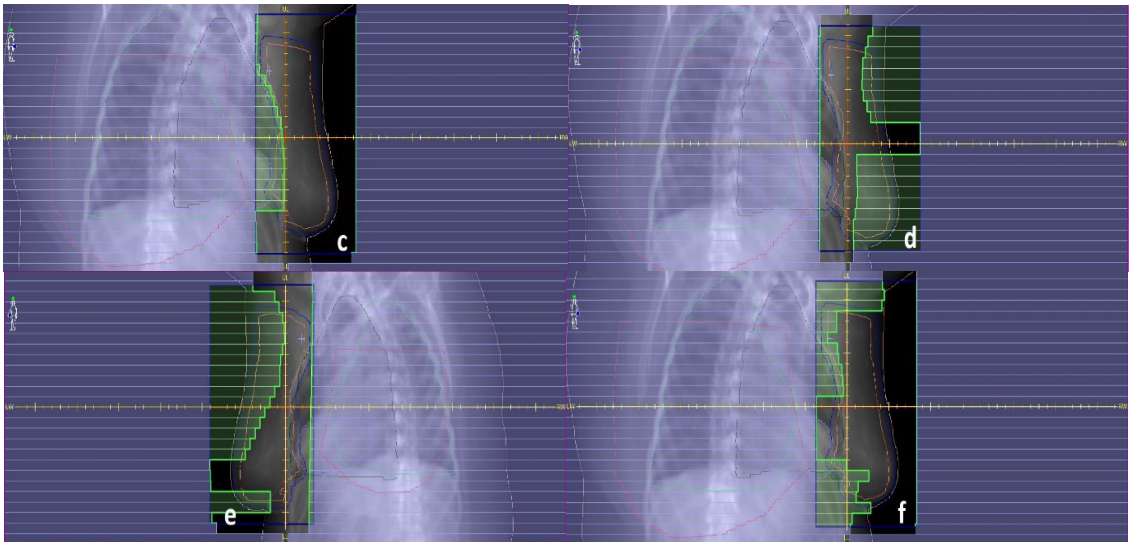

Figure 3: Manual fluence map optimization steps: a) Open field; b) Heart block; c) Lung block; d) 115% isodose block; e) 112% isodose block; f) 109% isodose block

The procedure, involving treatment fields and number of subfields used for the treatment planning of the patients were the same as that used for the phantom, except that there was no heart blocking field for right sided breast cancer patients. The subfield MUs per patient varied depending on their individual response to beam weighting. Nonetheless, the subfields were carefully weighted to reduce the respective open field MU by a percentage that was useful in maintaining good coverage and reducing hot spots. Each subfield was used in the most optimal way to acquire the best PTV coverage, homogeneity and OAR sparing.

Intensity Modulated Radiotherapy (IMRT) Technique

The IMRT gantry angles and the field parameters were similar to that of the FiF, with analogous planning goals leading to comparable initial optimization parameters to achieve the best realistic plan. As a result, the IMRT technique employed tangential IMRT (T-IMRT) planning approach, and the optimization objective is shown in Table 1.

For the phantom, the tangential IMRT (T-IMRT) plans were generated in the Monaco TPS using two tangential beams (306^0 and 129^0) with a single isocenter at the center of mass of the PTV as shown in Figure 4. This was achieved by introducing the best achievable optimization parameters to augment the medial and lateral tangential fields. The gantry angles were selected to avoid direct exposure to the contralateral breast.

For each patient, the T-IMRT plan was generated in imitation of the treatment planning of the phantom. The difference, however, is that the tangential beams had no fixed angles for all patients, as they were individually selected to suit the varying breast sizes, shapes and contours to achieve the planning objectives whilst avoiding the contralateral breast. All IMRT plans were generated in constrained optimization mode, and the appropriate optimization parameters were to make treatment planning faster and less tedious.

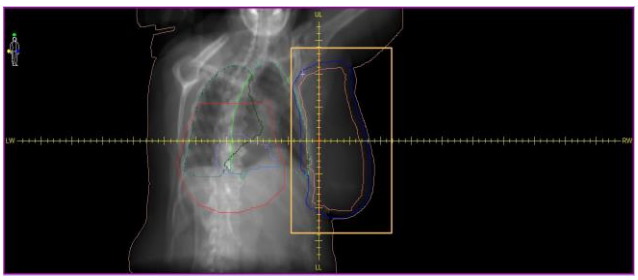

Figure 4: Lateral tangential IMRT beam

Dosimetric Criteria and Analytical Method

Global maximum dose (GD_{max}), prescription dose coverage (V_{50Gy}), conformity index (CI) and homogeneity index (HI) were then compared between FiF and IMRT as well as the percentage of target volumes receiving at least 95% of the prescribed dose ($V_{47.5Gy}$). Values for these parameters were obtained from the display of DVH statistics of the individual plans. DVH statistics were displayed, and the degree of OAR sparing between the two techniques were compared.

The conformity index (CI) was defined as the ratio of the reference isodose (95% isodose) volume to the target (PTV) volume[7], using the ICRU recommendations[5] and the ideal value was 1. Following the RTOG criteria for a defined range of CI values, and juxtaposing it with our clinical protocols, a CI range of 0.9 to 1.1 was considered tolerable. The CI was estimated as:

Conformity Index, $CI = \frac{V_{RI}}{TV}$ (equation 1),

where V_{RI} is the reference isodose volume and TV is the target volume.

The homogeneity index (HI) was defined as the ratio of the global maximum dose to the prescription dose, and the ideal value was 1[7]. In this case, it was ensured that the global maximum dose was within the target volume. A range of 0.95 to 1.07 was considered acceptable in this study. The HI was estimated as:

Homogeneity Index, $HI = \frac{GD_{max}}{D_p}$ (equation 2),

where GD_{max} is the maximum point dose and D_p is the prescription dose[8].

All data were recorded on Microsoft Excel 2016, which was used for the statistical analysis of the dosimetric parameters. The t-test comparative analysis was used to compare the dosimetric parameters and evaluate the differences between the two techniques, and a p value of 0.05 was considered statistically significant. Mean values of dose parameters were considered for 30 patients except the heart which was considered for 15 left sided breast cancers. The dose parameters presented for the phantom were mean values of the independent treatment plans generated by three Medical Physicists. With the phantom, only the left sided breast was considered.

III. RESULTS

Table 2 presents the FiF and IMRT dose parameters for target coverage. It shows the dose parameters recorded for treatment planning of the anthropomorphic phantom, and that of the 30 patients. The dosimetric values recorded for all OARs in the study are expressed under their respective techniques in Table 3. All values in Table 2 and 3 are expressed in mean ± standard deviations. Assessment of all dosimetric parameters in consideration for this study have been presented in Table 4, with 0 and 1 representing failed and passed objectives respectively.

Figure 5 provides a visual display of the performance of the two techniques on patients through their Dose Volume Histograms (DVH).

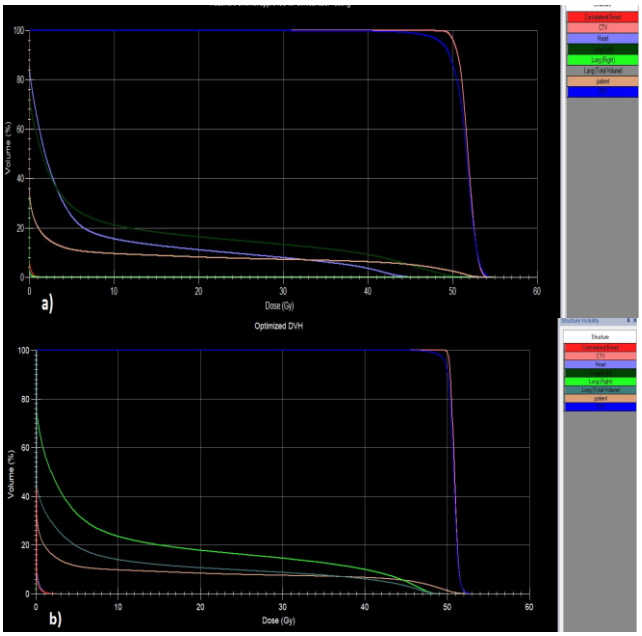

Figure 5: Dose Volume Histograms (DVH): a) 3DCRT FiF Patient DVH; b) IMRT Patient DVH

Table 2: PTV Dosimetric Parameters for FiF and IMRT $(\bar{x}\pm SD)$

Ptv Optimization Objective	**Phantom**		**Patient**	
	FiF	IMRT	FiF	IMRT
GD_{max} (Gy)	53.55 ± 0.28	52.19 ± 0.16	53.09 ± 0.78	51.92 ± 0.92
V_{53Gy} (%)	3.04 ± 0.90	0.03 ± 0.05	7.90 ± 1.43	0.91 ± 1.52
V_{51Gy} (%)	44.71 ± 12.58	0.78 ± 0.66	31.30 ± 9.80	23.96 ± 7.56
V_{50GY} (%)	91.69 ± 5.24	86.29 ± 5.32	83.22 ± 8.68	94.05 ± 2.64
$V_{47.5GY}$ (%)	95.94 ± 1.53	96.04 ± 2.23	96.94 ± 1.47	98.77 ± 0.81
$D_{50\%}$ (GY)	50.96 ± 0.32	49.98 ± 0.49	50.74 ± 0.50	50.64 ± 0.38
CI	0.96 ± 0.02	0.96 ± 0.02	0.97 ± 0.01	0.99 ± 0.01
HI	1.07 ± 0.01	1.04 ± 0.00	1.06 ± 0.02	1.04 ± 0.02

Table 3: OAR Dosimetric Parameters for FiF and IMRT $(\bar{x}\pm SD)$

Structure	OAR Constraints	Phantom		Patient	
		FiF	IMRT	FiF	IMRT
Contralateral breast	D_{max} (Gy)	4.77 ± 0.23	1.20 ± 0.23	2.73 ± 1.16	1.75 ± 0.90
	V_{5Gy} (%)	0.00 ± 0.00	0.00 ± 0.00	0.00 ± 0.00	0.00 ± 0.00
Ipsilateral lung	V_{20Gy} (%)	9.75 ± 2.20	4.16 ± 0.16	17.45 ± 2.23	13.57 ± 2.07
	V_{30Gy} (%)	6.31 ± 0.32	3.95 ± 0.13	13.52 ± 1.63	11.29 ± 1.27
Lung (Total volume)	V_{20Gy} (%)	4.02 ± 0.24	1.90 ± 0.31	9.24 ± 0.99	7.69 ± 0.74
	V_{30Gy} (%)	2.22 ± 0.31	1.00 ± 0.09	7.20 ± 1.29	4.56 ± 0.73
Heart	D_{max} (Gy)	9.55 ± 0.69	7.68 ± 1.04	42.06 ± 2.64	39.50 ± 2.63
	$D_{average}$ (Gy)	1.49 ± 0.34	0.92 ± 0.17	6.79 ± 1.07	4.59 ± 0.69
	V_{5Gy} (%)	0.58 ± 0.37	0.09 ± 0.04	25.12 ± 3.18	20.07 ± 3.15
	V_{20Gy} (%)	0.00 ± 0.00	0.00 ± 0.00	10.09 ± 1.35	7.80 ± 0.29

Table 4: Assessment Table Based on Optimization Objectives for Both Techniques on Phantom and Patients

Structure	Optimization Objective	Phantom		Patients	
		FiF	IMRT	FiF	IMRT
PTV	GD_{max} (Gy)	0	1	0	1
	V_{53Gy} (%)	1	1	1	1
	V_{51Gy} (%)	0	1	0	1
	V_{50Gy} (%)	1	0	0	1
	$V_{47.5Gy}$ (%)	1	0	1	1
	$D_{50\%}$ (Gy)	1	0	1	1
	CI	1	1	1	1
	HI	1	1	1	1
Contralateral breast	D_{max} (Gy)	0	1	1	1
	V_{5Gy} (%)	1	1	1	1
Ipsilateral lung	V_{20Gy} (%)	1	1	1	1
	V_{30Gy} (%)	1	1	1	1
Lung (Total volume)	V_{20Gy} (%)	1	1	1	1
	V_{30Gy} (%)	1	1	1	1
Heart	D_{max} (Gy)	1	1	0	1
	$D_{average}$ (Gy)	1	1	1	1
	V_{5Gy} (%)	1	1	1	1
	V_{20Gy} (%)	1	1	1	1

IV. DISCUSSIONS

This study compared the dose parameters between the two treatment planning techniques taking into consideration the volume of the PTV covered by the prescribed dose (V_{50Gy}) and at least 95% of the prescription ($V_{47.5Gy}$), the conformity index (CI) and homogeneity index (HI), as well as OAR sparing. The OAR sparing criteria involved D_{max} (Gy) and V_{5Gy} (%) of the contralateral breast, V_{20Gy} (%) and V_{30Gy} (%) of the ipsilateral lung, V_{20Gy} (%) and V_{30Gy} (%) of the whole lung, D_{max} (Gy), $D_{average}$ (Gy), V_{5Gy} (%) and V_{20Gy} (%) doses to the heart.

The global maximum dose (GD_{max}) that resulted in the best possible treatment plans were higher in FiF. The IMRT produced relatively lower GD_{max} for a desired coverage, as shown in Table 2, with a p-value of 0.00. The FiF plans of the phantom had a GD_{max} slightly above 53.5Gy (107% of prescription dose). Considering the planning objectives of the study, based on our departmental protocols, using as a guide the ICRU report 50 recommendations[5], this is above

the required range for acceptable plans. However, the result was different when the technique was applied on real patients. Although the GD_{max} for the FiF plans remained relatively higher compared to the IMRT in real patients, the patients FiF plans produced a GD_{max} (Gy) of 53.09 ± 0.78, which is clinically acceptable. Although, it has been shown that using FiF can greatly improve dose uniformity and reduce hot spots in comparison to other techniques such as tangential wedge fields (TW)[9], this study suggests that it is easier to achieve a global maximum dose that falls within the ICRU recommendations (95% to 107%) of the prescribed dose in IMRT than in FiF. Getting a good GD_{max} in FiF is possible with the use of the sub-fields to manually block hot areas within the target, but this process is sometimes difficult to achieve depending on patient characteristics. Sometimes, in treatment planning, it becomes impossible to achieve the desired GD_{max} without compromising on complete coverage of the PTV. This limitation is mostly observed in FiF technique than in IMRT, which makes the latter preferable in realizing the best global maximum dose without compromising on coverage. Additionally, in cases where the hot spot gets so close to the point of normalization, where blocking with MLC will lead to covering the norm point in FiF, achieving a desired global maximum dose become extremely difficult. In order to achieve quality radiotherapy treatment by minimizing normal tissue toxicities, it is recommended that the global maximum dose falls within a range of 95% to 107% according to the report 50 of the ICRU[5]. Although, the ICRU report 62 recommends a smaller range of values for IMRT planning[5], it was necessary to use a common criteria for the comparison of the two techniques in the study. Conversely, recent studies have suggested that local radiotherapy for cancer can cause spontaneous regression of non-directly treated malignancies, implying the involvement of systemic antitumor immune responses. So even though, some investigations have suggested that the FiF approach reduces hot spots in PTV, as reported by a dosimetric study conducted for whole breast irradiation[10], the results from this study has proven the supremacy of IMRT over FiF in terms of lower global maximum doses.

Table 2 also shows the percentage of the PTV receiving the full prescribed dose (V_{50Gy} (%)) for both techniques with a p-value of 0.00. The FiF recorded higher coverage of the prescribed dose in the phantom with 91.69 ± 5.24 than the IMRT with 86.29 ± 5.32, which implied that the IMRT could not meet the V_{50Gy} objective of the study. The higher FiF V_{50Gy} (%) value recorded in the phantom could possibly be influenced by the corresponding high global maximum dose, as clinical experience prior to this study suggests that in FiF planning, higher GD_{max} have the tendency to retain prescribed doses to a larger target volume. Despite this observation being clinically common, it could not be applied to patients, though the patients' GD_{max} was equally higher in FiF than IMRT. Rather, the IMRT produced better prescribed dose coverage in real patients with 94.05 ± 2.64 than the FiF which recorded 83.22 ± 8.68. This current study shows that target coverage in IMRT is not influenced by higher GD_{max}. This is in accordance with other findings that highlight the potential for IMRT techniques to enhance PTV uniformity and coverage[8]. This is also reinforced by a recent study which revealed that, the tangential IMRT plans, which have fewer monitor units and a shorter delivery period, is an appropriate plan for treating left sided breast cancer because they achieve good coverage of the PTV and spare OARs other than the heart and coronary arteries[11]. Consequently, IMRT has presented a dosimetric advantage of complete coverage with desirable global maximum doses in human tissues, resulting in very steep PTV curves in DVH as displayed in Figure 5. Results from the treatment planning of the phantom and that of the patient have presented conflicting results for prescription dose coverage of the PTV, this may require further investigation.

The results show that the percentage of target volumes receiving at least 95% of the prescribed dose ($V_{47.5Gy}$ (%)) was higher in IMRT than in FiF in both media. This is evident in Table 2, as the FiF produced 95.94 ± 1.53 and 96.94 ± 1.47 for phantom and patients, with the IMRT producing 96.04 ± 2.23 and 98.77 ± 0.81 for phantom and patients respectively, and 0.00 p-value. Regarding the phantom, the two treatment techniques produce contrasting results for V_{50Gy} and $V_{47.5Gy}$. Just as it was explained earlier that higher GD_{max} has the tendency to retain prescribed doses to a larger target volume, it was as well expected that the FiF would result in a higher PTV $V_{47.5Gy}$ (%) in the phantom. Yet the IMRT technique resulted in a higher $V_{47.5Gy}$ in both treatment planning media. The comparative results of $V_{47.5Gy}$ between the two techniques is consistent with the preceding results of V_{50Gy} in patients. It is also consistent with the $V_{47.5Gy}$ coverage that have been reported in literature for a range of planning studies to be from 90% to 97% of the PTV[12].

The conformity index (CI) values were observed to be better in IMRT, recording 0.99 ± 0.01 for patients, extremely close to the ideal value of 1. Since improved conformity could aid in providing the lowest exposure to OARs and the maximum dose to the target volume[13], it generates a preceding hypothesis that IMRT might be a superior technique in terms of organ sparing. Even though the CI for the FiF resulted in a competitive value of 0.97 ± 0.01 for the patients, it was slightly lower than that of the IMRT, with 0.00 p-value. The CI in this case was useful in estimating, on one hand the extent to which adjacent healthy tissues around the breast are exposed to radiation, and on the other hand the extent of coverage of the breast target volume depending on whether the CI value was greater or less than 1 respectively. It is apparent that both techniques produce seemingly equitable CI values, and this is evidenced by the equivalent CI values recorded by the two techniques in the phantom. Using the understanding that conformity indices help to assess how well treatment plans correspond to the parameters of contemporary radiation treatment, which stipulate that a 95% isodose should cover the PTV, the mathematical expression of CI in this study

makes it directly proportional to the percentage of target volumes receiving at least 95% of the prescribed dose ($V_{47.5Gy}$). It is as well a common observation that the percentage of target volumes receiving at least 95% of the prescribed dose increases with better dose conformity. Consequently, the IMRT technique yields superior CI values since it demonstrates higher values for $V_{47.5Gy}$, especially regarding calculations for the actual patients. Recent research works have also shown that IMRT significantly improves CI when compared to 3DCRT. But there was no significant change in HI[14]. So while the homogeneity between the two techniques stays comparable in that study, IMRT significantly increased the plan's conformity[14].

The homogeneity index (HI) values recorded by the IMRT plans were closer to the ideal value of 1 with approximately a constant value of 1.04 ± 0.00 for calculations in both phantom and patients. Since the HI was used to analyze the uniformity of dose distribution within the target[8], the IMRT proved to provide a more uniform dose. The HI values for the FiF technique were equally close to the ideal value with 1.07 ± 0.01 and 1.06 ± 0.02 for calculations in phantom and patients respectively, and a p-value of 0.00. This is inconsistent with the report of a study that suggested that IMRT did not significantly improve either HI or CI[15]. This dosimetric tool was necessary to confirm that the entire treatment volume was being irradiated with approximately the same amount of tolerable radiation dose. The formula used for HI in this study makes it solely reliable on the global maximum dose. This suggests that the HI value is determined by how close the GD_{max} is to the prescription. The closer the GD_{max}, the better the homogeneity, and the closer the HI will be to the ideal value, and the vice versa. Accordingly, the worst HI value observed from Table 2 is that of the FiF plan of the phantom which correspondingly recorded the highest GD_{max} of 53.55 ± 0.28, approximately 107.1%. Similarly, the best HI value recorded is that of the IMRT plan of the patients, recording 51.92 ± 0.92, approximately 103.84%. This mathematical expression of HI makes it a coherent dosimetric parameter in treatment planning in the patients. Work done by Beckham et al. found that IMRT considerably improved both CI and HI[16]. Additional studies comparing the dosimetric characteristics of IMRT to 3D-CRT for the chest wall have shown that the conformity and homogeneity indices have improved[10].

Both treatment planning techniques present competitive advantages in terms of target coverage, conformity and homogeneity for whole breast radiotherapy planning. Nevertheless, the IMRT technique demonstrates superior dosimetry regarding the dose parameters for the real patients in this study. Also, just as it has been reported by similar studies, since the treatment planning system can do automatic fluence optimization to obtain the ideal dose distribution, inverse planning techniques are typically simpler than forward planning[9]. The FiF outperformed the IMRT when the phantom was used as the treatment planning medium. This is consistent with other previous works but differs in some parameters with others[3]. It has equally been reported that when treating breast cancer following a mastectomy and immediately after breast reconstruction, the IMRT technique is appropriate[17]. Also, following breast conserving surgery, patients who received IMRT showed improved clinical outcomes and acceptable acute toxicity[17]. In contrast to the conventional technique, T-IMRT plans significantly improved the PTV, HI, heart, and whole lung sparing in another research comparing 2D plans for adjuvant radiotherapy of the whole breast in cases with early breast cancer[10].

The contralateral breast in this study has far more been spared by IMRT than FiF as shown by the D_{max} of the contralateral breast recorded for both techniques in phantom and patients in Table 3. The FiF recorded D_{max} of 4.77 ± 0.23 in the phantom and 2.73 ± 1.16 in patients. The IMRT recorded D_{max} of 1.20 ± 0.23 and 1.75 ± 0.90 for phantom and patients respectively. This implies that the D_{max} constraint for the contralateral breast was met by all IMRT plans. Other findings imply that compared to other techniques, T-IMRT and FFF-IMRT techniques may be able to lower the exposure dose and volume to contralateral breast[17]. Considering the phantom, the FiF recorded a higher D_{max} for the contralateral breast with a value above the limits of the planning objectives in Table 1. The FiF however recorded an acceptable D_{max} value in patients although the value is relatively higher compared to the IMRT value recorded in patients. Both treatment techniques also met the contralateral breast's V_{5Gy} constraint, as they both recorded 0.00 ± 0.00 in phantom and patients. This value is consistent with their corresponding D_{max} values, since all contralateral breast D_{max} values were less than 5Gy. The IMRT outperforms the FiF in this objective, making it reliable for prevention of secondary cancer probability since a number of studies have reported that the risk of developing a secondary cancer rises as the radiation exposure to the contralateral breast increases[18]. According to some research works, when IMRT was used instead of traditional 3DCRT, the contralateral breast dose was decreased. Another study confirmed this, with tangential IMRT demonstrating lower contralateral breast doses than 3DCRT. With 5-field IMRT, on the other hand, this is not the case because more fields were used, which led to a low dose spill to a larger contralateral breast volume. Given that patients under 40 are more likely to develop secondary contralateral breast cancer, this can be quite important[19]. Other studies, however, discovered that the scatter dose to the contralateral breast is highly influenced by the size of the ipsilateral breast[3].

The IMRT resulted in lesser ipsilateral and whole lung doses than the FiF in both media. Observing from Table 3, the FiF plans recorded V_{20Gy} (%) of 9.75 ± 2.20 for phantom and 17.45 ± 2.23 for patients, whilst the IMRT recorded 4.16 ± 0.16 and 13.57 ± 2.07 for phantom and patients respectively for the ipsilateral lung. With the ipsilateral lung V_{30Gy} (%), the FiF resulted in 6.31 ± 0.32 for phantom and

13.52 ± 1.63 for patients, whilst the IMRT recorded relatively lesser values of 3.95 ± 0.13 and 11.29 ± 1.27 for phantom and patients respectively. Concerning the whole lung doses as shown in Table 3, the V_{20Gy} (%) of the FiF resulted in 4.02 ± 0.24 and 9.24 ± 0.99 for phantom and patients respectively, with the IMRT producing significantly smaller values of 1.90 ± 0.31 for phantom and 7.69 ± 0.74 for patients. Similarly, the FiF technique recorded relatively higher V_{30Gy} (%) values of 2.22 ± 0.31 and 7.20 ± 1.29 for phantom and patient respectively, whilst the IMRT recorded 1.00 ± 0.09 for phantom and 4.56 ± 0.73 for patients. Considering how small the recorded V_{20Gy} and V_{30Gy} lung doses are for both treatment techniques, it is easier for one to overlook the comparative differences between the two, however, it is significant to make a decision about the dosimetric superiority between them using as part of the factors, the constraint in question. It is also obvious that both planning techniques have lung sparing advantages based on the results of Table 3, though, the IMRT is incredibly a good choice based on this study.

The IMRT technique proved to possess heart sparing advantages than the FiF in all the aspects of heart constraints specified for the study. Generally, the heart doses recorded for the phantom were significantly low for both techniques with the V_{20Gy} (%) constraint in the phantom recording 0.00 ± 0.00 for both techniques. In the patients, the heart D_{max} (Gy) values were very high for both planning techniques, with the FiF failing to meet the planning objective with a heart D_{max} of 42.06 ± 2.64. In spite of the fact that the IMRT doses were lesser and fairly within the specified limit, the recorded D_{max} of 39.50 ± 2.63 is still high and very close to the limit. The other heart constraints such as the $D_{average}$ (Gy), V_{5Gy} (%) and V_{20Gy} (%) were all lesser in IMRT than FiF. This upholds the report of previous studies suggesting that the use of IMRT offers the possibility of better local-regional treatment without increasing cardiac toxicity[19]. In line with the report of Liu et al., who discovered that double-arcs VMAT and 5-field IMRT both had larger cardiac doses than 3DCRT, a recent study demonstrated that tangential beam approaches can result in lower heart doses, underscoring the benefit of enhanced organ sparing in comparison to the usage of multi-fields or arcs employing methodologies[20]. Consequently, Rudat et al. reports that, tangential beam IMRT significantly decreased the mean heart dose by 20% and the V55 by an average of 43%[21]. This is similar to the findings of Beckham et al. who suggested that, IMRT substantially reduced the volume of the heart that receive more than 30 Gy[16].

The lung and heart doses were observed to be quite minimum in phantom than in patient for both treatment techniques. This observation could be as a result of a number of things. Visible among these factors is how close the target is to the heart and lungs. This hypothesis resulted in a further analysis to investigate the cause of the above-stated observation by physically examining the distances between the breast target and the OARs in question. The breast PTV of the phantom encompassed the whole breast, but the breast PTV of the patients encompassed the whole breast and sometimes covered axillary and parasternal lymph nodes depending on the clinical need. Thus, the patients' PTV were averagely huge and closer to the heart and lungs than that of the phantom. Considering that the volume of the phantom PTV was 565.52 cc, whilst the average PTV of all 30 patients was 1352.37±845.53 cc, it advances to suggest that treatment of smaller breast sizes has lower the risk of exposure to the lung and heart. Although this investigation proved to uphold this notion based on visual comparison of PTV-to-OAR distance and breast treatment volumes of the 30 patients involved in the study, the fear of digressing from the objectives of this study kept the work from such further investigation. But generally, the IMRT technique ensures higher target volume coverage while minimizing the exposure to contralateral breast, with tolerable doses to the ipsilateral lung and heart, according to recent study findings[17]. Finally, compared to 3DCRT, IMRT offers the possibility of a large reduction in the mean dose and high-dose volumes of the ipsilateral lung and heart, even when used for chest wall irradiation in patients with left-sided breast cancer who have undergone a mastectomy[14].

Each treatment planning technique has been evaluated based on its overall score on various dose parameters that are part of the comparative criteria in Table 4, with 0 and 1 signifying failed and passed objectives, respectively. With an assessment score of 18/18 for real patients, the IMRT stands out as the best technique in human tissues. Both techniques receive an evaluation score of 15/18 for the phantom, with the IMRT scoring higher in OAR sparing and the FiF outperforming it in target coverage. While 3DCRT is often recommended for radiation treatment of breast cancer, research indicates that IMRT use can dramatically lower radiation doses to OARs while providing superior target coverage over 3DCRT[17]. In terms of target coverage, mean dose, and OAR sparing in early breast cancer, a comparison study between 3DCRT and IMRT treatment plans found that the IMRT technique significantly reduced the dose to OARs and normal tissue, with a better target coverage than 3DCRT[14]. In a single therapy delivery phase, IMRT provides an opportunity to increase doses to specific regions within the target volume. For normal tissues or critical structures around the target volume, the treatment technique offers improved dose sparing[22]. According to other studies, over 90% of patients continue to live disease-free for years following IMRT, indicating that the patient's quality of life either stays stable or improves with time[23]. In radiotherapy, IMRT is known for its steep in-field dose gradient, which promotes improved OAR sparing and dose conformity to the PTV. Based on many dosimetry investigations on linac-based IMRT treatments of various anatomical sites, it provides substantial dosimetric advantages over conventional techniques. Numerous studies have documented the potential benefits of IMRT over 3DCRT, including the decrease in the probability of an in-

field recurrence, the reduction of treatment-related morbidity, and the enhancement of local control[22]. Baidoo reported that while IMRT might potentially improve target dose conformity, reduce exposure to normal tissues, and allow for dose escalation, it has superior dosimetric advantages over 2D and 3DCRT techniques, and that includes FiF planning[22]. Several studies have also addressed the decision-making process about radiation therapy for breast cancer and have been suggested that T-IMRT is the optimum method for treatment[3].

Limitations

It is imperative to acknowledge the following as part of the key limitations in this study. First of all, the procedure followed to conduct the investigation is a standard one, yet it is subject to our perfection to avoid human errors. As a result, additional research may be necessary to confirm the study's methodology while taking the resources into account. Secondly, although the results regarding the phantom may be able to offer a standardized and universal representation, the entire work may not be able to provide such a global representation of breast dosimetry because all the patients involved in this study, with the exception of one, were natives of the West African region.

V. CONCLUSIONS

This study shows that T-IMRT planning results in low global maximum doses for the desired target coverage in both anthropomorphic phantom and actual human tissues. Regarding the percentage of target volume covered by the prescribed dose (100% isodose), the two planning techniques show contradictory results in the two media, with the IMRT providing the best coverage in human tissues and the FiF outperforming it in the phantom, an observation that may require further investigation in the field. But generally, the IMRT demonstrates superior dosimetry in terms of PTV coverage, CI and HI in real patients.

Inasmuch as both treatment planning techniques demonstrate organ sparing competences, the T-IMRT results in lesser ipsilateral and whole lung doses than FiF in phantom and patients. The findings of the study suggest that the T-IMRT has a better heart sparing significance in both media, and a higher potential to spare the contralateral breast. Consequently, IMRT demonstrates superior advantage of OAR sparing to FiF.

ACKNOWLEDGMENT

Our sincere gratitude to Mr. Joseph Kwadjo Lano for his support in terms of imaging setup on the CT machine.

REFERENCES

1. Baskar R, Lee KA, Yeo R, Yeoh KW. Cancer and Radiation Therapy: Current Advances and Future Directions. *Int J Med Sci*. 2012;9(3):193-199. doi:10.7150/ijms.3635
2. Mohthash MT, Shah SK, Thirupathi A. KRAS Gene Polymorphism (rs61764370) and Its Impact on Breast Cancer Risk among Women in Kerala Population, South India. *Biology and Medicine*. 2020;11(2).
3. Jin GH, Chen LX, Deng XW, Liu XW, Huang Y, Huang XB. A comparative dosimetric study for treating left-sided breast cancer for small breast size using five different radiotherapy techniques: conventional tangential field, filed-in-filed, Tangential-IMRT, Multi-beam IMRT and VMAT. *Radiat Oncol*. 2013;8(1):89. doi:10.1186/1748-717X-8-89
4. Cho B. Intensity-modulated radiation therapy: a review with a physics perspective. *Radiat Oncol J*. 2018;36(1):1-10. doi:10.3857/roj.2018.00122
5. Jones D. ICRU Report 50—Prescribing, Recording and Reporting Photon Beam Therapy. *Medical Physics*. 1994;21(6):833-834. doi:10.1118/1.597396.
6. Tumanova K, Nidal S, Tumanova K, Popodko A, Stolbovoy A. Most Appropriate Radiation Therapy Techniques for The Breast Cancer Treatment: Dosimetric Analysis of Three Different Radiation Therapy Methods. *RCO*. Published online June 19, 2023:1-8. doi:10.31487/j.RCO.2023.01.01.
7. Petrova D, Smickovska S, Lazarevska E. Conformity Index and Homogeneity Index of the Postoperative Whole Breast Radiotherapy. *Open Access Maced J Med Sci*. 2017;5(6):736-739. doi:10.3889/oamjms.2017.161.
8. Kataria T, Sharma K, Subramani V, Karrthick K, Bisht S. Homogeneity Index: An objective tool for assessment of conformal radiation treatments. *J Med Phys*. 2012;37(4):207. doi:10.4103/0971-6203.103606
9. Acquah GF, Kyeremeh PO, Doudoo CO, Ahiagbenyo P, Edusa C, Beecham K. Breast Dosimetry : A Phantom study between Tangential Wedge Fields and Multiple Open field-in-field 3D Conformal Forward Planning. *IJSRST. 2017:*173629 [(3)6 : 196-200]
10. Jha B, Lamichhane HP, Prasiko G, Srivastava RP. Clinical Experience and Dosimetry Outcome in Treating Breast Cancer with Field-in-Field Technique. *ABCR.* 2021;10(03):35-43. doi:10.4236/abcr.2021.103003
11. Zhao H, He M, Cheng G, et al. A comparative dosimetric study of left sided breast cancer after breast-conserving surgery treated with VMAT and IMRT. *Radiat Oncol*. 2015;10(1):231. doi:10.1186/s13014-015-0531-4
12. Barnett GC, Wilkinson J, Moody AM, et al. A randomised controlled trial of forward-planned radiotherapy (IMRT) for early breast cancer: Baseline characteristics and dosimetry results. *Radiotherapy and Oncology*. 2009;92(1):34-41. doi:10.1016/j.radonc.2009.03.003
13. Al-Rawi SAI, Abouelenein H, Khalil MM, et al. Evaluation of Conformity and Homogeneity Indices Consistency Throughout the Course of Head and Neck Cancer Treatment With and Without Using Adaptive Volumetric Modulated Arc Radiation Therapy. *Advances in Radiation Oncology*. 2022; 7(5): 100905. doi:10.1016/j.adro.2022.100905
14. Tali TA, Amin F, Ahmad J, Ahmad Khan A. Dosimetric Comparison of IMRT Versus 3DCRT for Post-mastectomy Chest Wall Irradiation: An Analytical Observational Study. *Asian Pac J Cancer Care*. 2022;7(4):669-673. doi:10.31557/apjcc.2022.7.4.669-673
15. Li W, Wang J, Cheng H, Yu X, Ma J. IMRT versus 3D-CRT for post-mastectomy irradiation of chest wall and regional nodes: a population-based cmparison of normal lung dose and radiation pneumonitis.
16. Beckham WA, Popescu CC, Patenaude VV, Wai ES, Olivotto IA. Is Multibeam IMRT Better Than Standard Treatment for Patients With Left-Sided Breast Cancer? *International Journal of Radiation Oncology*Biology*Physics*. 2007;69(3):918-924. doi:10.1016/j.ijrobp.2007.06.060
17. Zheng H, Lai YQ, Zhou Y, et al. A comparative dosimetric study of seven radiation techniques for breast cancer after mastectomy and

immediate breast reconstruction. *Transl Cancer Res.* 2017;6(4):788-797. doi:10.21037/tcr.2017.06.38
18. Horn PL, Thompson WD. Risk of contralateral breast cancer associations with histologic, clinical, and therapeutic factors. *Cancer*. 1988;62(2):412-424. doi:10.1002/1097-0142(19880715)62:2<412::AID-CNCR2820620228>3.0.CO;2-3
19. Stovall M, Smith SA, Langholz BM, et al. Dose to the Contralateral Breast From Radiotherapy and Risk of Second Primary Breast Cancer in the WECARE Study. *International Journal of Radiation Oncology*Biology*Physics*. 2008;72(4):1021-1030. doi:10.1016/j.ijrobp.2008.02.040
20. Liu H, Chen X, He Z, Li J. Evaluation of 3D-CRT, IMRT and VMAT radiotherapy plans for left breast cancer based on clinical dosimetric study. *Computerized Medical Imaging and Graphics*. 2016;54:1-5. doi:10.1016/j.compmedimag.2016.10.001
21. Rudat V, Aziz Alaradi A, Mohamed A, AI-Yahya K, Altuwaijri S. Tangential beam IMRT versus tangential beam 3D-CRT of the chest wall in postmastectomy breast cancer patients: A dosimetric comparison. *Radiat Oncol*. 2011;6(1):26. doi:10.1186/1748-717X-6-26
22. Baidoo AM, Tagoe SNA, Addison EK, Sasu E. Piloted Pretreatment Patient-Specific Quality Assurance in Preparedness for Clinical Implementation of Intensity Modulated Radiotherapy. *JJ Oncol Clin Res* 4: 1-14. 2023;4: 104
23. Pasquier D, Bataille B, Le Tinier F, et al. Correlation between toxicity and dosimetric parameters for adjuvant intensity modulated radiation therapy of breast cancer: a prospective study. *Sci Rep*. 2021;11(1):3626. doi:10.1038/s41598-021-83159-3

Contacts of the corresponding author:

Author:	Alhassan Mohammed Baidoo
Institute:	Sweden Ghana Medical Centre
Street:	East Legon Hills
City:	Accra
Country:	Ghana
Email:	ambaidoo1@gmail.com

PHITS MONTE CARLO STUDY OF DEPTH-DOSE PROFILES OF PROTON (^{1}H), ALPHA (^{4}HE), CARBON (^{12}C) AND OXYGEN (^{16}O) IONS IN CORTICAL BONE

C.G. Dalumpines [1,2], G.F. Peñonal [1,2], H. Aringa [1,2], V. Convicto [1,2]

[1] Computational Medical and Radiation Physics Group, Department of Physics, Mindanao State University, 9700 Marawi City, Lanao del Sur, Philippines
[2] Department of Physics, Mindanao State University, 9700 Marawi City, Lanao del Sur, Philippines

Abstract— **Particle therapy has garnered significant interest in the medical field due to its enhanced energy deposition, which peaks sharply at the end of the particle range, minimizing the dose to surrounding healthy tissue. This study uses the Particle and Heavy Ion Transport code System (PHITS) to simulate and analyze the dose distribution of light and heavy ions, such as proton, alpha, carbon, and oxygen ions, in a cortical bone phantom. Additionally, it visualizes the fluence of secondary particles like electrons, positrons, and neutrons. A 30 × 30 × 30 cm³ box-shaped cortical bone phantom with a Source-to-Surface-Distance (SSD) of 100 cm is irradiated with 200 million primary particles. The initial energies used are 54.19 MeV/u for proton, 56.44 MeV/u for alpha particle, 100.07 MeV/u for carbon ion and 117.20 MeV/u for oxygen ion. The energy source is a mono-energetic axial source, and the radial source has a size of 0.10 cm. The results show that the alpha particle peak is at 1.68 cm, while the proton, carbon, and oxygen ion peaks are all at 1.56 cm. The visualization of secondary particle fluence highlights their concentration a few centimeters from the cortical bone surface, supporting the Bragg peak phenomenon. Additionally, dose of secondary particle imparts less than 1% to the total absorbed dose.**

Keywords— **PHITS, SSD, light and heavy ion, particle therapy**

I. INTRODUCTION

Robert Wilson first suggested using protons and heavier ions to cure cancer in 1946. Particle treatment has attracted a lot of attention in the medical community over the years because of its increased energy deposition with penetration depth up to a sharp maximum at the end of their range, where nearly no dosage is deposited in normal tissue [1]. As charged particles travel through matter, they decelerate and lose energy due to atomic or nuclear interactions [2]. The density of the material determines the extent to which protons and heavy ions interact with numerous electrons per centimeter traversed. This interaction process is nonlinear, with the energy loss rate as a function of the material traversed (expressed as *dE/dX*) described by the Bethe-Bloch formula as follows [3]:

$$-\frac{dE}{dx} = R\rho\frac{Z}{A}\frac{z^2}{\beta^2}\left[\ln\left(\frac{2m_e\gamma^2v^2T_{max}}{I^2}\right) - 2\beta^2 - \delta - 2\frac{C}{Z}\right] \quad (1)$$

where, $R = 2\pi N_a r_e^2 m_e c^2 = 0.1535\ \frac{MeV cm^2}{g}$, ρ is the density of target material, Z is an atomic number of the target material, A is an atomic weight of the target material, z is the charge of the incident particle, $\beta = \frac{v}{c}$ is the relativistic velocity of the incident particle with respect to the speed of light. m_e is an electron mass, $\gamma = \frac{1}{\sqrt{1-\beta^2}}$ is the relativistic correction factor, T_{max} is the maximum energy transfer in a single collision expressed as $T_{max} \cong 2m_e c^2\eta^2$ $(\eta = \beta\gamma)$. Furthermore, I is the mean excitation potential refers to the average energy required to remove an electron from an atom or a molecule. It is a key parameter in determining the rate at which this energy loss occurs. Density correction δ accounts for variations in the target material's density and C is the shell correction which considers the electronic structure of the target material. The rate at which charged particles lose energy during penetration is correlated with the particle's mass and can be quantified as linear energy transfer (LET) [4] [5].

In medical radiation physics, the Monte Carlo (MC) technique is recognized as the most accurate analytical approach for creating treatment plans for tumors. Numerous fields have found use for it, and thorough evaluations have been released. Numerous studies have shown that when compared to traditional radiation therapy treatment planning methods, the MC technique performs better in calculating doses, especially in complex geometries. [6] [7] [8] [9] [10] [11]. The PHITS code system is a general-purpose MC Particle and Heavy Ion Transport code system which can estimate the transport of particles through any medium across a broad energy range using various nuclear reaction models and data libraries. Nevertheless, limited research has been done utilizing PHITS to examine the dosage distribution of heavy ions. The purpose of this study is to investigate the percentage depth dose (PDD) profiles of distinct light and heavy ions (oxygen, carbon, proton, and alpha) irradiated in a biological medium such as cortical bone at different energies. Additionally, particle fluence of secondary particles (i.e., electrons, positrons, and neutrons) produced from these interactions is investigated.

II. METHODOLOGY

A. Simulation parameters and platform

In this study, a box-shaped phantom with dimensions of 30 × 30 × 30 cm³ is used. Cortical bone (ρ = 1.85 g/cm^3) is utilized as the phantom material. The Source-to-Surface-

Distance (SSD) is 100 cm. The phantom is irradiated with 2 million primary particles at different radiation sources such as proton (^{1}H), alpha (^{4}He), carbon (^{12}C), and oxygen (^{16}O) ions. The bin size is 0.6 cm. The initial energies are 54.19 MeV/u for proton, 56.44 MeV/u for alpha particle, 100.07 MeV/u for carbon ion and 117.20 MeV/u for oxygen ion. The compositions of the cortical bone are adopted from the National Institute of Standards and Technology (NIST) database [12]. The energy source is a mono-energetic axial source, and the radial source has a size of 0.10 cm. See Figure 1 for the simulation setup.

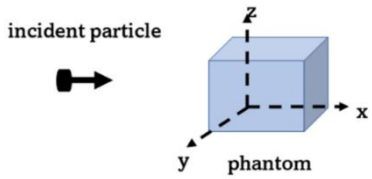

Fig. 1 Simulation set-up

This study utilized the Particle and Heavy Ion Transport code System (PHITS) [13] [14] version 3.30. The usefulness and accuracy of PHITS has been demonstrated in several research areas, including heavy ion radiotherapy, space radiation dosimetry and accelerator-shielding experiments [15] [16].

B. Simulation assessment

Utilizing tally deposit, the PHITS program computes dose data. Subsequently, the data is extracted for analysis. The electron, positron, and neutron flux visualization process begin at the source and extends to the surface of a cortical bone phantom. The PHITS program is utilized for visualizing and calculating the flux of electrons, positrons, and neutrons using tally tracks.

Furthermore, calculation of percentage dose difference between the measured and calculated in terms of range is given by this expression:

$$\%\ Difference = \frac{Range_{measured} - Range_{MC}}{Range_{measured}} \times 100 \qquad (2)$$

Computed or simulated range, that is, the depth at maximum dose deposition in PHITS for proton (1H) and alpha (4He) ions are compared with the available measured data from the National Institute of Standards and Technology (NIST) [12][https://www.nist.gov/].

III. RESULTS

The PDD curve generated by PHITS in cortical bone that is irradiated by light and heavy ions such as proton (^{1}H), alpha (^{4}He), carbon (^{12}C), and oxygen (^{16}O) shown in Fig.2. The initial energies of 54.19 MeV/u for proton, 56.44 MeV/u for alpha particle, 100.07 MeV/u for carbon ion and 117.20 MeV/u for oxygen ion. Table 1 presents the percentage dose difference in terms of range. In addition, Tables 2-4 show the percentage dose of the secondary particles particularly electron, positron and neutron in the total dose absorbed. Fig. 3-5 show the spatial distribution of particle fluence of the secondary particle particularly electron, positron and neutron.

Table 1 Comparison of the simulated values of range of the proton beams in cortical bone to the values of range from NIST proton and helium database [12].

Ion	Energy (MeV)	Range (cm)		% Difference
		CSDA (NIST Data)	Monte Carlo Simulated	
^{1}H	54.19	1.610	1.560	3.11
^{4}He	56.44	1.683	1.680	0.24
^{12}C	100.07	-	1.560	-
^{16}O	117.20	-	1.560	-

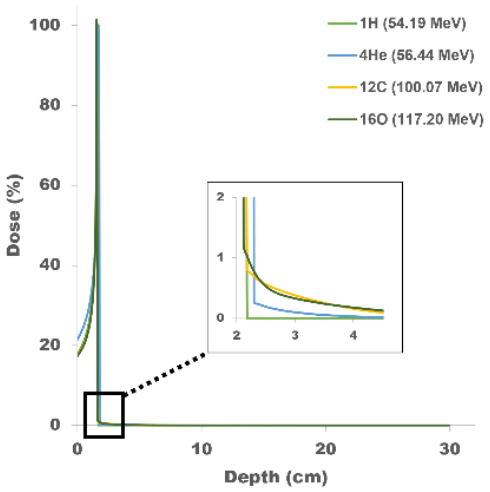

Fig. 2 The depth-dose profile curves in cortical bone phantom from (a.) proton (^{1}H), (b.) alpha (^{4}He), (c.) carbon (^{12}C), and (d.) oxygen (^{16}O) at corresponding initial energies respectively. Inset image shows the variations in the dose tail at different radiation sources.

Table 2 Percentage of electron dose on the total absorbed dose.

Ion	Energy (MeV)	Total Absorbed Dose (Gy)	Electron Absorbed Dose (Gy)	Percentage (%)
^{1}H	54.19	4.33×10^{-1}	2.4×10^{-6}	5.54×10^{-4}
^{4}He	56.44	1.79	4.44×10^{-6}	2.48×10^{-4}
^{12}C	100.07	9.51	1.23×10^{-5}	1.29×10^{-4}
^{16}O	117.20	14.86	1.70×10^{-5}	1.14×10^{-4}

Table 3 Percentage of positron dose on the total absorbed dose.

Ion	Energy (MeV)	Total Absorbed Dose (Gy)	Positron Absorbed Dose (Gy)	Percentage (%)
^{1}H	54.19	4.33×10^{-1}	4.81×10^{-5}	0.01
^{4}He	56.44	1.79	9.54×10^{-5}	5.33×10^{-3}
^{12}C	100.07	9.51	2.28×10^{-4}	2.40×10^{-3}
^{16}O	117.20	14.86	3.03×10^{-4}	2.04×10^{-3}

Table 4 Percentage of neutron on the total dose absorbed dose.

Ion	Energy (MeV)	Total Absorbed Dose (Gy)	Neutron Absorbed Dose (Gy)	Percentage (%)
^{1}H	54.19	4.33×10^{-1}	2.21×10^{-5}	5.10×10^{-3}
^{4}He	56.44	1.79	1.66×10^{-4}	9.27×10^{-3}
^{12}C	100.07	9.51	5.81×10^{-4}	6.11×10^{-3}
^{16}O	117.20	14.86	6.81×10^{-4}	4.58×10^{-3}

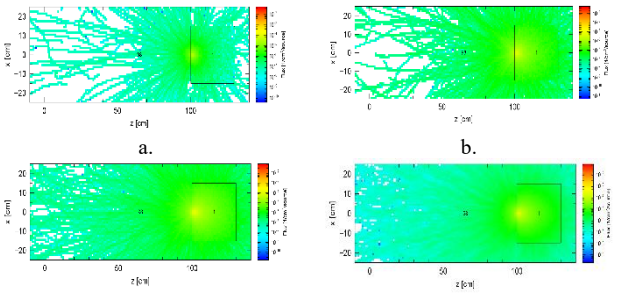

Fig. 3 The spatial distribution of electron fluence in cortical bone phantom from (a.) proton (^{1}H), (b.) alpha (^{4}He), (c.) carbon (^{12}C), and (d.) oxygen (^{16}O) at energy of 54.19 MeV, 56.44 MeV, 100.07 MeV and 117.20 MeV, respectively.

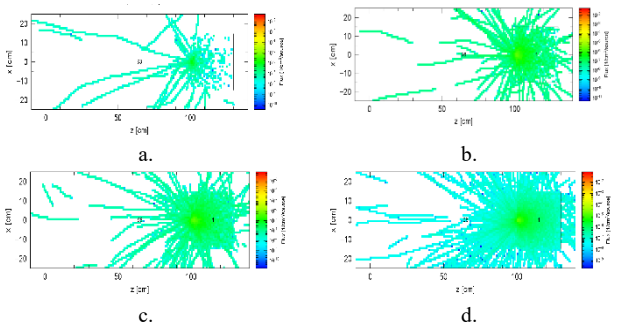

Fig.4 The spatial distribution of positron fluence in cortical bone phantom from (a.) proton (^{1}H), (b.) alpha (^{4}He), (c.) carbon (^{12}C), and (d.) oxygen (^{16}O) at energy of 54.19 MeV, 56.44 MeV, 100.07 MeV and 117.20 MeV, respectively.

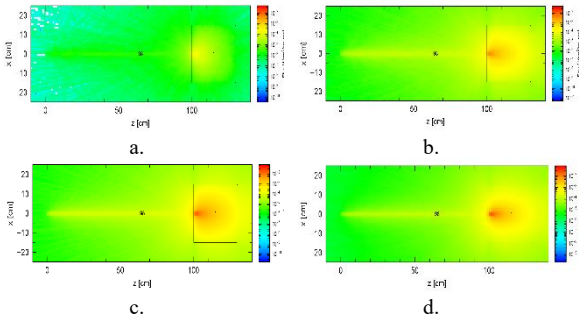

Fig.5 The spatial distribution of neutron fluence in cortical bone phantom from (a.) proton (^{1}H), (b.) alpha (^{4}He), (c.) carbon (^{12}C), and (d.) oxygen (^{16}O) at energy of 54.19 MeV, 56.44 MeV, 100.07 MeV and 117.20 MeV, respectively.

IV. DISCUSSION

The PDD curves of proton (^{1}H), alpha (^{4}He), carbon (^{12}C), and oxygen (^{16}O) irradiated in the cortical bone phantom, the results indicate that the maximum dose occurs at 1.56 cm, except for alpha particles, which peak at 1.68 cm as shown in Table 1. As shown that as the ion becomes heavier the tail becomes broader. The depth dose curve of light and heavy ions is the main advantage as compared to high energy X-rays. It results primarily from the gradual energy loss of the charged particles, as compared to the exponential loss in fluence of X-rays, when penetrating tissue. The mean energy loss of ions per path length is given by the Bethe-Bloch equation presented equation (1). Due to the dependence on $1/\beta^2$ this leads to a remarkable increase of the energy loss per path length with decreasing velocity of the projectile, which results in the Bragg peak in the depth dose curve of ion beams. Beyond the Bragg peak, the ions will stop, and the dose will sharply drop to zero. This is clearly seen for the proton curve. For heavier ions, a tail arises, which is due to a built-up of nuclear fragments with ranges longer than that of the primary ions [17] [18]. In addition, the simulated ranges are compared with the experimental data from the NIST database [12] particularly the continuous-slowing-down approximation (CSDA) ranges. The result gives a good agreement with a percentage difference of not more than 3.11%.

The percentage of the secondary particle dose for electron, positron and neutron imparts less than 1% to its total absorbed dose as tabulated in Table 2-4. Some percentage of the total absorbed dose may influence by incident particle and some other secondary particle or nuclear fragment which is not considered in this study.

For electrons, positron, and neutron flux its corresponding intensity is represented by color gradients, where red denotes the maximum intensity and blue the lowest density. The fluence concentration of secondary particles (electrons, positrons, and neutrons) is observed a few centimeters from the surface of the cortical bone (Fig. 3-5). This supports the Bragg peak for protons, alpha particles,

carbon ions, and oxygen ions, indicating that the peak occurs a few centimeters from the surface. In radiation therapy, a higher particle concentration in a specific area or phantom results in higher energy deposition and thus a higher absorbed dose.

V. CONCLUSION

PHITS successfully simulates the dose profile of proton (^{1}H), alpha (^{4}He), carbon (^{12}C), and oxygen (^{16}O) that irradiates cortical bone. It shows that alpha is at 1.5 cm, while the proton, carbon, and oxygen ions all share the same Bragg peak site at 1 cm. The behavior of secondary particles produced by the interaction of primary ions with the phantom is further explained by the visualization of electron, positron, and neutron fluence. The electron, positron, and neutron concentrations are found to be a few centimeters from the cortical bone phantom's surface, supporting the Bragg peak. This implies that higher particle concentrations lead to increased energy deposition and absorbed dose. In addition, electron, positron and neutron influence less than 1% to its total absorbed dose.

ACKNOWLEDGMENT

We thank Dr. Hiroshi Takemiya of the Japan Atomic Energy Agency for access to the PHITS program, and the DOST Learning Resource Center for providing computer resources for our simulations.

CONFLICT OF INTEREST

The authors have declared that no competing interest exists with publication of the study.

REFERENCES

1. Schulz-Ertner, D., & Tsujii, H. (2007). Particle radiation therapy using proton and heavier ion beams. Journal of clinical oncology, 25(8), 953-964.
2. Schulz-Ertner, D., Jäkel, O., & Schlegel, W. (2006, October). Radiation therapy with charged particles. In Seminars in radiation oncology (Vol. 16, No. 4, pp. 249-259). WB Saunders.
3. Lomax, A. J. (2009). Charged particle therapy: the physics of interaction. The Cancer Journal, 15(4), 285-291.
4. Schulz-Ertner, D., & Tsujii, H. (2007). Particle radiation therapy using proton and heavier ion beams. Journal of clinical oncology, 25(8), 953-964.
5. Jäkel, O. (2007, November). State of the art in hadron therapy. In AIP Conference Proceedings (Vol. 958, No. 1, pp. 70-77). American Institute of Physics.
6. Parodi, K., Mairani, A., Brons, S., et al. (2012). Monte Carlo simulations to support start-up and treatment planning of scanned proton and carbon ion therapy at a synchrotron-based facility. Physics in Medicine & Biology, 57(12), 3759.
7. Padilla-Cabal, F., Pérez-Liva, M., Lara, E., et al. (2015). Monte Carlo calculations of an Elekta Precise SL-25 photon beam model. Journal of Radiotherapy in Practice, 14(3), 311-322.
8. Zaidi, H., Andreo, P. (2022). Monte Carlo techniques in nuclear medicine dosimetry. In Monte Carlo Calculations in Nuclear Medicine (Second Edition) Therapeutic applications (pp. 1-1). Bristol, UK: IOP Publishing.
9. Sheikh-Bagheri, D., Rogers, D. W. O. (2002). Monte Carlo calculation of nine megavoltage photon beam spectra using the BEAM code. Medical physics, 29(3), 391-402.
10. Fix, M. K., Keall, P. J., Dawson, K., et al. (2004). Monte Carlo source model for photon beam radiotherapy: photon source characteristics: Monte Carlo source model. Medical physics, 31(11), 3106-3121.
11. Durán-Nava, O. E., Torres-García, E., Oros-Pantoja, R., et al. (2019, June). Monte Carlo simulation and experimental evaluation of dose distributions produced by a 6 MV medical linear accelerator. In Journal of Physics: Conference Series (Vol. 1221, No. 1, p. 012079). IOP Publishing.
12. Berger, M.J., Coursey, J.S., Zucker, M.A., et al. (2005). *ESTAR, PSTAR, and ASTAR: Computer Programs for Calculating Stopping-Power and Range Tables for Electrons, Protons, and Helium Ions* (version 1.2.3). Available: http://physics.nist.gov/Star
13. Sato, T., Niita, K., Matsuda, N., et al. (2014). Overview of particle and heavy ion transport code system PHITS. In SNA+ MC 2013-Joint International Conference on Supercomputing in Nuclear Applications+ Monte Carlo (p. 06018). EDP Sciences.
14. Sato, T., Iwamoto, Y., Hashimoto, S., et al. (2018). Features of particle and heavy ion transport code system (PHITS) version 3.02. Journal of Nuclear Science and Technology, 55(6), 684-690.
15. Puchalska, M., Sihver, L. (2015). PHITS simulations of absorbed dose out-of-field and neutron energy spectra for ELEKTA SL25 medical linear accelerator. Physics in Medicine & Biology, 60(12), N261.
16. Iwamoto, Y., Hashimoto, S., Sato, T., et al. (2022). Benchmark study of particle and heavy-ion transport code system using shielding integral benchmark archive and database for accelerator-shielding experiments. Journal of Nuclear Science and Technology, 59(5), 665-675.
17. Jäkel, O. (2020). Physical advantages of particles: protons and light ions. The British journal of radiology, 93(1107), 20190428.
18. Convicto, V., Pamisa, D.R., Lintasan, A., & Quiñones, C.T. (2020). Monte Carlo study of nuclear fragmentation in water irradiated with protons and 12C ions for particle therapy applications. Journal of Physics: Conference Series, 1505(1), 012009.

Contacts of the corresponding author:

Author: Clyde Gibb M. Dalumpines
Institute: Mindanao State University
Street:
City: Marawi City
Country: Philippines
Email: clydegibb.dalumpines@msumain.edu.ph

COMPARISON OF SELECTED MATERIALS EFFICIENCY FOR SFRT GRID COLLIMATOR USING TOPAS MONTE CARLO MODELING METHOD

P.K. Muka[1], A.Z. Ibitoye[2], S.O. Adeneye[3], P.A. Sandwall[4], O.M. Oni[1]

[1] Department of Pure and Applied Physics Ladoke Akintola University of Technology, Ogbomoso, Nigeria
[2] Department: Radiation Biology and Radiotherapy, College of Medicine, University of Lagos, Nigeria
[3] Department: Radiation Biology and Radiotherapy, NSIA-LUTH Cancer Centre, College of Medicine, University of Lagos, Nigeria
[4] Department of Radiation Oncology, OhioHealth Mansfield, Ohio, USA

Abstract— **This study evaluated block materials for delivery of spatially fractionated radiation therapy (SFRT). SFRT is a technique for delivering radiotherapy within spaced, grid-like patterns to treat bulky tumors in a single fraction. Particularly relevant to low-and-middle-income countries, where late-stage disease presentation is common. The geometry and design of the grid block as well as the radiation transport and dose scoring were carried out using Monte Carlo Toolkit for Particle Simulation (TOPAS). Phase space files capturing particle attributes such as position, direction, and energy were obtained from the manufacturer for a 6 MV medical linear accelerator (TrueBeam, Varian Medical Systems). A grid collimator was modeled as a solid rectangular structure with dimensions of 22 cm x 22 cm x 7.5 cm, divergent circular holes were arranged in a hexagonal pattern. The dose distribution in a water phantom was evaluated for multiple materials; steel, brass, and Cerrobend (alloy of barium, lead, tin, and cadmium). Peak-to valley dose ratio (PVDR) of stainless-steel, brass, and Cerrobend grid blocks at a depth of 10 cm in water were determined (4.01, 4.13 and 4.78 respectively). PVDR of stainless steel was observed to be near brass, a commonly used material. This study provides support for potential use of steel as an alternate material in grid therapy.**

Keywords— **TOPAS, grid-block, Monte Carlo code.**

I. INTRODUCTION

SFRT (Spatially Fractionated Radiation Therapy) is a radiation treatment approach that delivers a non-uniform dose of radiation to the tumor site, alternating between high and low doses. Research by Mohiuddin et al. (1990) showed surprisingly positive outcomes for patients treated with SFRT compared to traditional radiation therapy. SFRT has advantages when treating large tumors, offering a combination of high-dose "hot spots" and low-dose "cold spots" throughout the tumor. This approach is also known as grid or Lattice SFRT [1,2]

The grid SFRT technique was pioneered by Alban Köhler in 1909 [3]. At the time, orthovoltage beams delivered the highest dose to the skin's surface, limiting the dose that could be given to deeper tumors. SFRT was created to allow for higher doses to be delivered to hard-to-reach tumors while keeping skin dose at a safe level. The grid collimator or block helped reduce skin damage by creating areas of protected skin and tissue that could regenerate. However, with the introduction of medical linear accelerators that produce megavoltage photon beams and modern skin-sparing techniques, the original motivation for SFRT with grid was no longer a concern.

Although grid radiotherapy has shown promise, its use in clinical settings is hindered by a lack of understanding of the underlying radiobiological processes. Historically, these blocks were made of materials like Cerrobend or brass alloys with perforations that created the grid pattern, yet access to these blocks is limited, especially in low-and-middle-income countries. Several studies have explored fabrication techniques. For instance, Zhu et al. examined the possibility of producing Cerrobend grid blocks through 3D printing [4]. Almendral et al. proposed a straightforward method for creating a hybrid grid pattern combining both block and multi-leaf collimator (MLC) technologies [5].

Previous studies have employed grid blocks manufactured from dense materials that can radiation, including: Cerrobend, brass, lead and tungsten. In the current study we investigate and unexplored material, stainless steel, which has promising characteristics including readily availability in limited resource settings. Dosimetric characteristics of brass, Cerrobend, and stainless steel have been compared using computational methods.

II. METHODOLOGY

Geometry of simulation

The grid block is a solid rectangular structure with dimensions of 22 cm × 22 cm × 7.5 cm, made from different materials for its radiation attenuation properties. The upper stream of the block features a hexagonal pattern of holes and arranged in a closely packed lattice which are diverging in size as they progress from the upper stream to the downstream portion of the grid. Each hole is circular and characterized by its diameter. Starting from the upper stream portion, the holes have a diameter of 0.6 cm. These holes are spaced apart with a center-to-center distance of 1.14 cm. As we move downstream, the holes size gradually increase to 0.85 cm while maintaining the same center-to-center distance of 1.14 cm.

The divergent holes size help in achieving the desired spatial distribution of the radiation beam. The smaller holes at the upper stream region focus the radiation, while the larger holes at the downstream region permit the passage of the divergent of the radiation beam. Properties of materials used in this study are shown in Table 1.

Table 1: Physical properties of different materials suitable for fabrication of grid block

Material	Density (g/cm)	Advantages	Disadvantages	References
Cerrobend	9.30	High density, effective radiation attenuation	Expensive, toxic	Zhu et al. [4]
Lead	11.34	High density, effective radiation attenuation	Toxic, requires special handling	Trapp et al. [6]
Tungsten	19.30	High density, effective radiation attenuation	Expensive, difficult to machine	Kijima et al. [7]
Brass	8.50	Good radiation attenuation, cost effective, easy to machine	Lower density	Karimi et al. [8]

Model Validation

Percentage depth dose curves were calculated for depths from 0 cm to 40 cm for field size 10 cm × 10 cm in water phantom. To validate the TOPAS model, twenty phase space files were used to calculate the percentage depth dose for the open beam. The commissioning data obtained with 3D scanning tank; golden beam was used as reference data were used for comparison with the TOPAS simulation. The commissioning data, golden beam and the Monte Carlo simulated results of the percentage depth dose are shown in Figure 2. Both the reference and evaluated data were normalized to the value of maximum dose along the central axis of the beam. The depth at maximum dose for commissioning data, golden beam and the Monte Carlo simulated results are 1.59 cm, 1.5 cm and 1.5 cm. The Monte Carlo simulation results were bench marked against golden beam and commissioning data in term of absolute dose difference.

The geometry and design of the grid as well as the radiation transport and dose scoring in the water phantom was performed with the Monte Carlo based Tools for Particle Simulation (TOPAS). TOPAS is an easy-to-use extended Monte Carlo based GEANT4 simulation Toolkit for Medical Physicists. The description of TOPAS platform for research and applications are detailed in the publication [9].

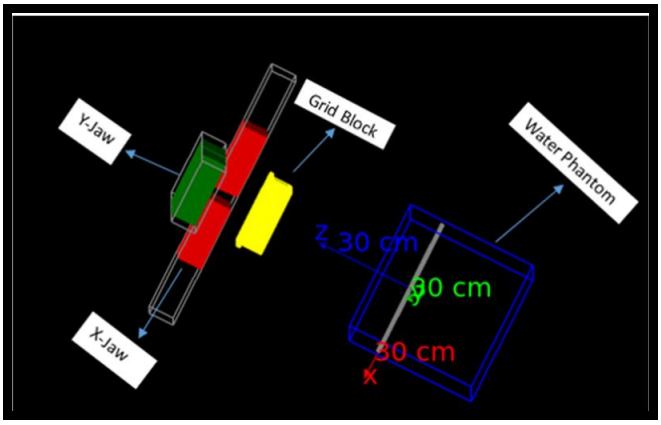

Figure 1: Schematic diagram of the Varian TrueBeam Linac

Monte Carlo Simulations

Using a 6 MV phase space file, the Varian TrueBeam Monte Carlo was modeled in TOPAS (Version 3.8) [10,11]. The Phase space file was placed 26.7 cm downstream from the target position, as described by Varian [11]. For both upper and lower Jaws, TOPAS TsJaws was used in order to simulate the collimators, although not a precise model of the TrueBeam's collimators, the diverging angles provide a close approximation. The upper and lower jaws were placed below the phase space plane, collimated to a 10 cm × 10 cm field at 100 cm source to surface distance (SSD) with the grid block at the distance of 56 cm which is the distance to the block tray. Five billion histories were simulated with an open field using common calibration parameters to validate the TOPAS model [12].

III. RESULTS

Model validation

The validation results from our Monte Carlo model indicate a high level of accuracy when compared to the actual data from commissioning scan and golden beam data. This is evident in the alignment of the model output with the data of the depth dose for 10 cm × 10 cm field size. This suggest that our model is a reliable representation the TrueBeam machine.

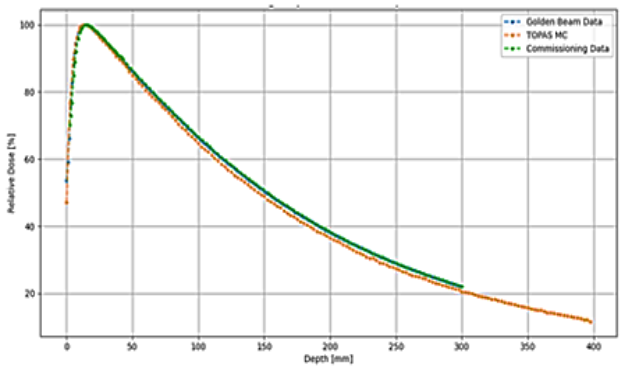

Figure 2: The 6 MV depth dose curve for golden beam, simulation and commissioning data for open field 10 cm × 10 cm

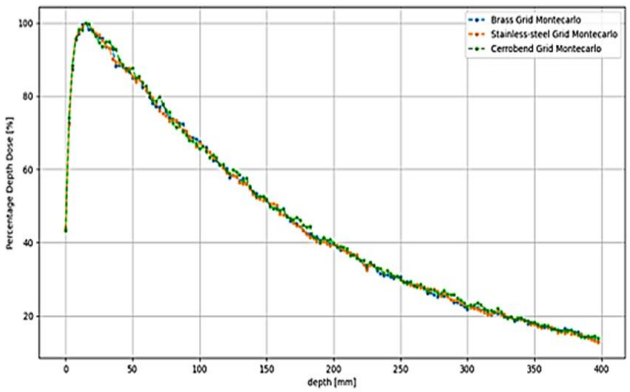

Figure 3: The 6-MV depth dose curves for materials with Brass, Stainless steel and Cerrobend for grid field 10 cm × 10 cm

The three materials exhibit similar depth dose curves, with a rapid increase in dose up to 13 mm depth, follow by a gradual decrease in the tail region. The dose distribution is relatively homogeneous at a shallow depth, with variations of less than 5% among the materials.

Peak to Valley Dose Ratio

The peak to valley dose ratio (PVDR) is defined as the ratio between the high-and low dose points in the cross-plane profile created by grid block. A peak to valley dose ratio of one indicates a perfectly uniform dose distribution, while higher PVDR values indicate a less uniform distribution. In this study, we utilized a Python script to analyze the data collected.

PVDR values of 4.04, 4.13, and 4.78 for stainless steel, brass, and Cerrobend at 10 cm depth for 6-MV and 10 cm × 10 cm calculated along the cross-plane profile. The PVDR of Cerrobend is the highest, demonstrating greatest difference between min and max dose of the three materials. The graphical representation is shown in Figures 4, 5 and 6.

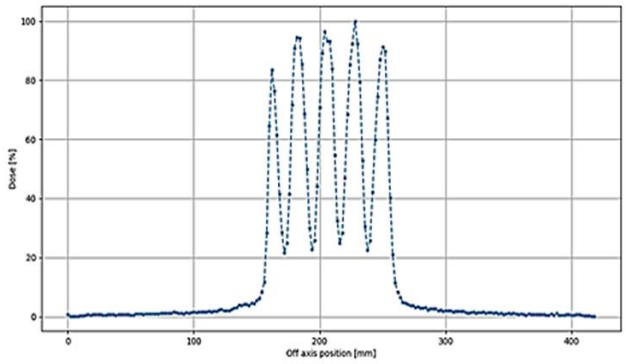

Figure 4: The Monte Carlo simulated beam profile of a 6-MV spatially fractionated photon beam at 10 cm depth in a water phantom for brass

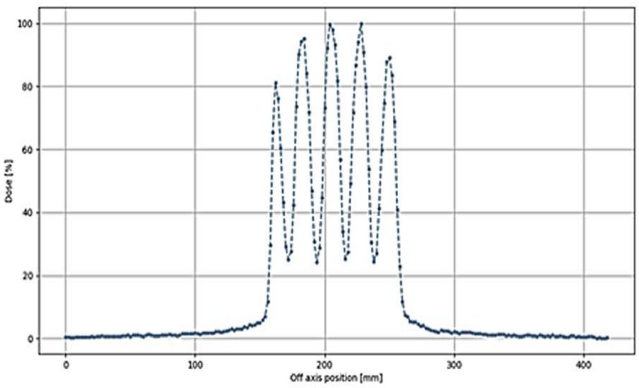

Figure 5: The Monte Carlo simulated beam profile of a 6-MV spatially fractionated photon beam at 10 cm depth in a water phantom for Cerrobend

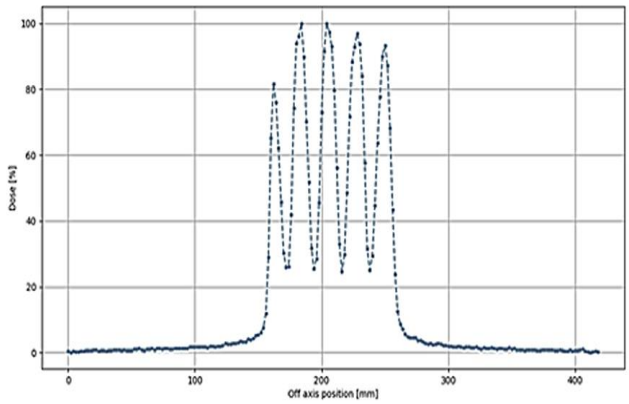

Figure 6: The Monte Carlo simulated beam profile of a 6-MV spatially fractionated photon beam at 10 cm depth in a water phantom for stainless steel

Table 2: Peak to valley dose ratio of 6 MV for different grid blocks

Grid material	Peak Dose	Valley Dose	Peak to Valley Dose ratio
Stainless steel	100	24.75	4.04
Brass	100	24.21	4.13
Cerrobend	100	20.92	4.78

IV. CONCLUSION

This study reveals that stainless steel offers a PVDR similar to brass, often used in the fabrication of grid block collimators for clinical applications. This thus translates that the stainless-steel has a potential use as an alternative material for grid collimators in radiotherapy, most especially to extend access to radiation treatment, improve efficiency, optimize treatment outcomes for bulky tumours, and reduce financial expenses in low-resource settings.

REFERENCES

1. Yan W, Khan MK, Wu X, Simone CB 2nd, Fan J, Gressen E, Zhang X, Limoli CL, Bahig H, Tubin S, Mourad WF. Spatially fractionated radiation therapy: History, present and the future. Clin Transl Radiat Oncol. 2019 Oct 22; 20:30-38. doi: 10.1016/j.ctro.2019.10.004. PMID: 31768424; PMCID: PMC6872856.
2. Tubin S et al. Novel stereotactic body radiation therapy (SBRT)-based partial tumor irradiation targeting hypoxic segment of bulky tumors (SBRT-PATHY): improvement of the radiotherapy outcome by exploiting the bystander and abscopal effects. *Radiat Oncol*. 2019;14(1):21.
3. Laissue, J.A.; Blattmann, H.; Slatkin, D.N. Alban Köhler (1874–1947): Erfinder der Gittertherapie. *Z. Für Med. Phys.* 2012, *22*, 90–99.
4. Zhu X, Driewer J, Li S, Verma V, Lei Y, Zhang M, et al. Technical note: Fabricating Cerrobend grids with 3D printing for spatially modulated radiation therapy: A feasibility study. Med Phys 2015; 42:6269-73.
5. Almendral P, Mancha PJ, Roberto D. Feasibility of a simple method of hybrid collimation for megavoltage grid therapy. Med Phys 2013; 40:051712
6. Trapp, J.V., Warrington, A.P., Partridge, M., Philps, A., Leach, M.O. and Webb, S. 3D measurement of absolute radiation dose in grid therapy. Journal of Physics: Conference Series 3, 2004; 280–283. Institute of Physics Publishing, doi:10.1088/1742-6596/3/1/047.
7. Kijima K, Krisanachinda A, Tamura M, Nishimura Y, Monzen H. Feasibility of a Tungsten Rubber grid Collimator for Electron grid Therapy. Anticancer Res. 2019 Jun;39(6):2799-2804. doi: 10.21873/anticanres.13407. Erratum in: Anticancer Res. 2020 Feb;40(2):1183. PMID: 31177116.
8. Karimi, A.H., Das, I.J., Chegeni, N. et al. Beam quality and the mystery behind the lower percentage depth dose in grid radiation therapy. Sci Rep 14, 4510 (2024). https://doi.org/10.1038/s41598-024-55197-0
9. Perl J, Shin J, Schumann J, Faddegon B, Paganetti H. TOPAS: an innovative proton Monte Carlo platform for research and clinical applications. Med Phys. 2012 Nov;39(11):6818-37. doi: 10.1118/1.4758060. PMID: 23127075; PMCID: PMC3493036.
10. "Monte Carlo," Varian. https*://www.myvarian.com/s/montecarlo* (accessed Oct. 10, 2023).
11. Constantin M, Perl J, LoSasso T, Salop A, Whittum D, Narula A, Svatos M, Keall PJ. Modeling the truebeam linac using a CAD to Geant4 geometry implementation: dose and IAEA-compliant phase space calculations. Med Phys. 2011 Jul;38(7):4018-24. doi: 10.1118/1.3598439. PMID: 21858999.
12. Constantin M. Varian's Monte Carlo Community Newsletter: Phase Space Update. Feb. 2013. [Online]. Available: *https://www.myvarian.com/s/montecarlo*

Contacts of the corresponding author:

Author: Paul Kehinde Muka
Institute: Ladoke Akintola University of Technology, ,
City: Ogbomoso
Country: Nigeria
Email: mukapaul022@gmail.com

DOSIMETRIC COMPARISON BETWEEN GATED AND UNGATED SBRT PLANS USING VMAT WITH FFF BEAMS

T.Y. Nam [1], Q.C. Chen[2], M.C. Ng [1,3]

[1] Oncology Centre, St. Teresa's Hospital, Hong Kong
[2] Department of Diagnostic Radiology, Li Ka Shing Faculty of Medicine, The University of Hong Kong, Pokfulam, Hong Kong
[3] Department of Clinical Oncology, Li Ka Shing Faculty of Medicine, The University of Hong Kong, Pokfulam, Hong Kong

Abstract— **Repeated stop-and-go beams and interplay effect during gated and ungated treatment can have an impact on dose accuracy. We compared the dosimetric impact between gated and ungated SBRT using 6 MV FFF with maximum dose rate (DR_{max}) of 1400 MU/min and 10MV FFF beams with DR_{max} of 2400 MU/min and analyzed factors that would correlate with the dosimetric deviation. Fifteen SBRT lung clinical cases using 6 MV FFF RapidArc with DR_{max} of 1400 MU/min were chosen. 10 MV FFF SBRT plans were then generated by re-optimizing the 6 MV FFF plans with 10 MV FFF beams and 2400 MU/min DR_{max}. CIRS Dynamic Thorax Phantom with a lung equivalent rod and PTW 3D pinpoint detector were used in the verification plans. The target moved sinusoidally with 2 cm amplitude and 4 s period. The verification plan for each case was calculated on average intensity projection computed tomography volume across all phases and across 40% - 60% phases of the breathing cycle for the gated and ungated plans respectively using AcurosXB (AXB) and Anisotropic Analytical Algorithm (AAA). Wilcoxon signed-rank tests were performed on the absolute dose deviation (ADD; measured versus calculated dose in the planning system) between gated and ungated cases. Correlation tests between ADD and the dose coefficient of variation (CV) among the voxels inside the internal target volume of the active volume of the chamber (ITV_{acv}), beam on time/MU and number of cycles of stop-and-go motion were conducted. A significant difference was found on ADD between gated and ungated 10 MV FFF beams with 2400 MU/min DR_{max} (Wilcoxon signed-rank test; $p \leq 0.015$), but not the 6 MV FFF beams with 1400 MU/min DR_{max}. It also revealed that there were significant correlation coefficients r of 0.5947 (AAA) and 0.5470 (AXB) between the ungated 10 MV FFF ADD and the dose CV among the voxels inside ITV_{acv}.**

Keywords— **gating, ungating, VMAT, FFF, SBRT**

I. INTRODUCTION

Some previous studies [1, 2, 3, 4, 5] had investigated dosimetric deviation caused by interplay and stop-and-go effects for gated and ungated radiotherapy. It was noted that the dosimetric impact were dependent on the machine models and delivery methods. Kanai *et al.* [1] studied the mechanism regarding respiratory gated volumetric modulated arc therapy (VMAT) using 6MV beams with Clinac iX (Varian Medical Systems, Palo Alto, CA, USA). They found that the passing rate of gamma analysis for the gated and ungated plans were comparable. In their study, the rotation speed of gated VMAT was decreased by 30% in comparison with that of the ungated VMAT. The reduced dose rate led to decreased multi-leaf collimator (MLC) leaf speed, which then reduced the MLC positioning error and gap size error. However, Yoon *et al.* [2] found that the dosimetric error was greater in gated RapidArc delivery than continuous RapidArc delivery by using Novlis Tx linear accelerator (Varian Medical Systems, Palo Alto, CA, USA). This was due to the stop-and-go motion of the heavy gantry which would offset the gantry restart position due to momentum effects. This also reduced the accuracy of the MLC position and dose rate in RapidArc delivery. Wiersma *et al.* [3] also found that gating was inferior to ungating in dosimetric precision in step-and-shoot intensity-modulated radiation therapy (IMRT) plans, because dosimetric errors would be induced by interruption of the "overshoot phenomena" [4, 5], which was an overshoot of the initial segment dose of each beam on. The average timing deviation for intermediate segments was longer for gating when compared with non-gating.

The study presented in this paper used a TrueBeam linear accelerator (Varian Medical Systems, Palo Alto, CA, USA) with two different beams, 6 MV Flattening Filter Free (FFF) with 1400 MU/min maximum dose rate (DR_{max}) and 10MV FFF with 2400 MU/min DR_{max}. This study aims at comparing the absolute dose deviation (ADD) between gated and ungated beams and investigating any unexplored factors that might correlate with the ADD. Another purpose of this study is to find out if the stop-and-go effect would have a prominent role affecting accuracy of gated radiotherapy by using number of cycles of beam on-and-off ($NC_{stop\text{-}and\text{-}go}$) to quantify the stop-and-go effect suggested by Yoon *et al.* [2]. Preliminary results have been reported in the form of conference publication. [6]

II. METHODOLOGY

Fifteen Stereotactic Body Radiotherapy (SBRT) lung clinical cases using RapidArc were chosen for retrospective analysis. The age of the patients in these fifteen cases ranged from 47 to 82. More than 70% of them were confirmed to have adenocarcinoma of lung. All patient information was anonymized in this study and ethic approval was granted. The fractionated scheme for the

patients varied from 6 to 18 Gy/fraction with 3 to 10 treatment fractions. The radiotherapy plans consisted of either 2 or 3 half arcs (half gantry rotation) or 2 partial arcs with 200 degrees at 6 MV FFF energy and a DR_{max} of 1400 MU/min in the TrueBeam linear accelerator (version 2.7, Varian Medical Systems, Palo Alto, CA, USA) equipped with a 120 leaf Millennium MLC. 10 MV FFF SBRT plans were generated by re-optimizing the fifteen 6 MV FFF plans using 10 MV FFF beams with 2400 MU/min DR_{max} keeping the same objective functions in the plan optimization using Eclipse treatment planning system (version 15.5, Varian Medical System, Palo Alto, CA, USA).

The Dynamic Thorax Phantom (model 008A, CIRS, Norfolk, VA, USA) in Fig. 1 representing an average human thorax in shape, proportion and composition was used for the verification plans. A lung equivalent rod (0.21 g/cc) containing a spherical 20 mm target and a PinPoint 3D ion chamber (PTW, Freiberg, Germany) with sensitive volume of 0.016 cm^3 was inserted for integrated dose measurement. The target in the lung equivalent rod was programmed to move in a sinusoidal fashion of ±2 cm in the inferior/superior direction with a period of 4s while a surrogate (marker block) was moved ±1cm in the anterior/posterior direction with a period of 4s. Acquisition of the four-dimensional computed tomography (4DCT) of the phantom was performed using computed tomography (CT) scanner (SOMATOM Definition Flash, Siemens Healthineers, Erlangen, Germany).

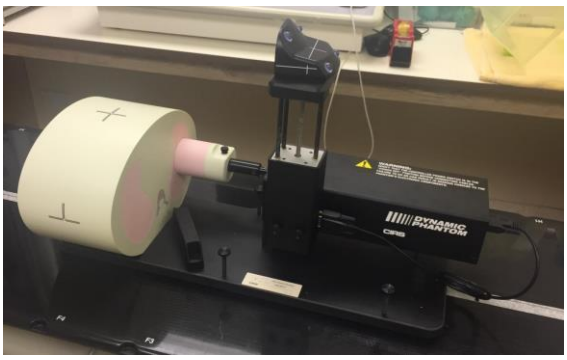

Fig. 1 The Dynamic Thorax Phantom for point dose measurements

The verification plans for each treatment plan were then calculated on the average intensity projection CT volume across all the phases (for ungated cases) and across 40%-60% phases (for gated cases) of the sinusoidal cycle of the phantom using AcurosXB (AXB, version 15.5) and Anisotropic Analytical Algorithm (AAA, version 15.5), where the peak of inhalation is defined as 0% (Fig. 2). All calculations were based on dose to water.

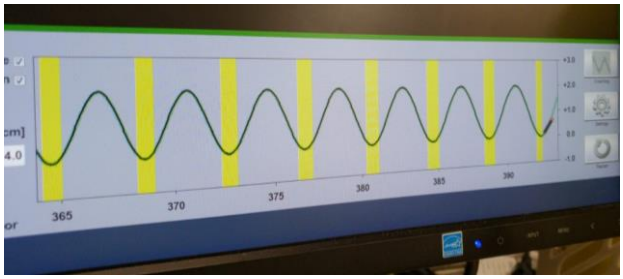

Fig. 2 Sinusoidal cycle of the phantom (green) and the planned phases 40-60% (yellow)

The ITV_{acv} is defined as a single volume encompassing all the active volumes of the chamber across all the phases (Fig. 3) and 40%-60% exhalation breathing phases of the sinusoidal cycle for ungated and gated cases respectively. The voxel-average doses of the ITV_{acv} were compared with the measured values, namely dose deviation. The Hounsfield units (HU) of the ITV_{acv} as well as the stems in both CTs were overridden to 0 HU.

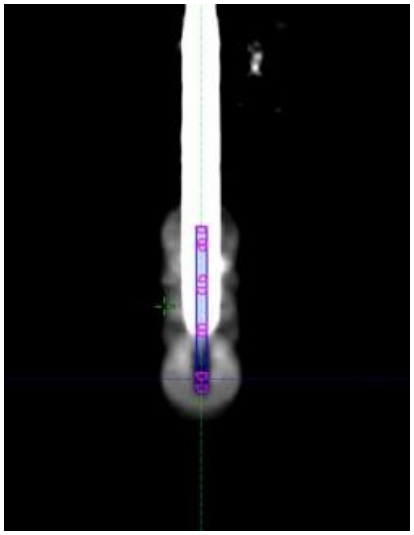

Fig. 3 The chamber is shown in the average CT set. The pink small volumes are the active volumes of the chamber in ten phases of the 4DCT. The blue volume is a single volume encompassing all the pink volumes, namely Internal Target Volume (ITV) of the active chamber volume (ITV_{acv}) for the ungated cases.

The inclusion criteria of the SBRT cases were that: 1) The superior-inferior dimension of the PTV was larger than 4.1 cm to fit the phantom motion. 2) The Internal Target Volume (ITV) encompassing the active volumes of the chamber in different phases did not fall into the penumbra region of the verification plan. (Fig. 4)

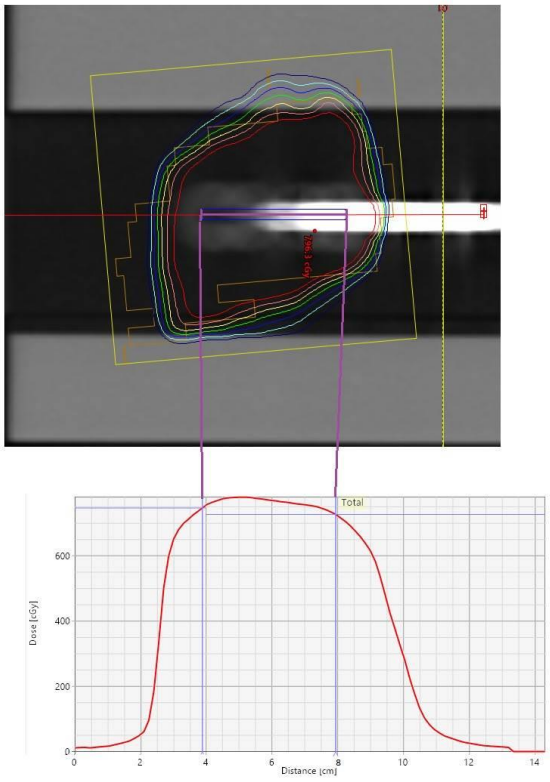

Fig. 4 Example of dose profile of the ungated ITV_{acv} with the penumbra region avoided

Interplay effect is the potential deterioration in dose distribution that results from the simultaneous movement of internal structures and targets and dynamic MLCs motion. It leads to either underdosage or overdosage of the organs-at-risk or target. Therefore, this study only focuses on the magnitude of the dose deviation – absolute dose deviation (ADD). ADD is defined as $|$measured dose – calculated dose$|$ / calculated dose. Friedman test and Wilcoxon signed-rank test were performed for the ADD of both the 6 MV FFF and 10 MV FFF beams to see if there was any significant dosimetric difference on ADD.

Dose Coefficient of Variation (CV) of ITV_{acv}, depicts the ratio of the dose standard deviation among the voxels inside the ITV_{acv} to the mean dose of the ITV_{acv} in the treatment planning system, was studied to see if there was correlation with ADD. Correlation between the ADD and beam on time/MU was also studied.

$NC_{stop\text{-}and\text{-}go}$ is defined as the beam on time divided by the period of a sinusoidal cycle, which was 4 seconds in our study. $NC_{stop\text{-}and\text{-}go}$ of the gated cases with two energies were compared to study the contribution of stop-and-go effect to the ADD, so as to find out if the stop-and-go effect would have a significant role affecting the accuracy of the gated radiotherapy. Paired t-tests and correlation tests were conducted to see how $NC_{stop\text{-}and\text{-}go}$ would correlate with the ADD.

Plan complexity in terms of number of MU / prescribed dose was also investigated to see if there was a statistically significant difference in plan complexity between the 10 MV FFF and 6 MV FFF treatment plans.

Normality tests for all the data were conducted before the analysis. All the tests were performed by SPSS Statistics (version 25, International Business Machines Corporation, Armonk NY, USA).

III. RESULTS

Absolute Dose Deviation (ADD)

All the data were put into eight groups. It consisted of two main groups, 6MV FFF and 10MV FFF. Each energy beams had two subgroups: gated and ungated, which were further broken down into two calculation algorithms. Fig. 5 illustrates the ADD of all the groups. It was noted that the mean ADD in the ungated cases were higher than that of the gated cases in both energies, 3.16% vs 2.50% for 6MV FFF and 4.43% vs 2.59% for 10 MV FFF. The ADD of the AXB cases were found always less than that of the AAA cases. All data groups passed the Shapiro-Wilk Normality Test, i.e. their p-values were larger than 0.05. However, Mauchly's test of sphericity for 10 MV FFF group was violated ($p<0.05$). As such, Friedman tests (non-parametric alternative to one-way ANOVA with repeated measures) and Wilcoxon signed-rank test were conducted for both 10 MV FFF and 6 MV FFF groups.

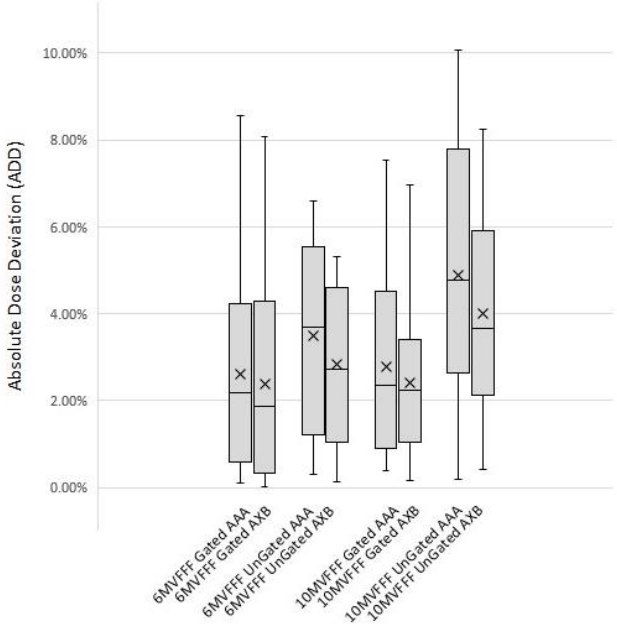

Fig. 5 ADD of the eight groups

Table 1 illustrates the results of Friedman test and Wilcoxon signed-rank test. For the Friedman tests, significant difference was observed in 10 MV FFF group with 2400 MU/min DR_{max}, but not in 6 MV FFF group with 1400 MU/min DR_{max}. For the Wilcoxon signed-rank tests, significant difference in ADD was shown between 10MV FFF gated and ungated cases but not in 6 MV FFF. Significant differences in ADD between AAA and AXB were also observed in ungated cases in both energies.

Table 1 Results of Friedman test and Wilcoxon signed-rank test

		p-value of Wilcoxon signed-ranks test			
	Friedman Test	Gated vs UnGated		AAA vs AXB	
Energy	P-value	AAA	AXB	Gated	Ungated
10MV FFF	0.020*	0.011*	0.015*	0.088	0.023*
6MV FFF	0.184	0.256	0.551	0.363	0.036*

*significantly difference, p<0.05

Dose Coefficient of Variation (CV) of ITV_{acv}

Pearson correlations among ADD and dose CV of ITV_{acv} were performed. All the groups of ADD and dose CV passed the Shapiro-Wilk Normality Test, i.e. larger than 0.05. Table 2 shows the results of the correlation tests between ADD and dose CV of ITV_{acv}. It proved that the dose CV of ITV_{acv} significantly correlated with ADD in ungated 10 MV FFF cases with 2400 MU/min DR_{max} for both AAA and AXB, but not gated cases and in 6 MV FFF cases with 1400 MU/min DR_{max}. Fig. 6 shows the trend of the correlation. The Pearson correlation coefficient for AAA was 0.5947, and for AXB was 0.5470, of which the p values were less than 0.05.

Table 2 Correlation Test between ADD and dose CV of ITV_{acv}

			Pearson Correlation Coefficient **r**	p value
6XFFF	Gated	AAA	0.2983	0.2801
		AXB	0.3398	0.2153
	UnGated	AAA	0.2102	0.4520
		AXB	0.0531	0.8510
10XFFF	Gated	AAA	-0.1605	0.5678
		AXB	-0.0259	0.9269
	UnGated	AAA	0.5947	0.0194*
		AXB	0.5470	0.0348*

*significantly correlated, p<0.05

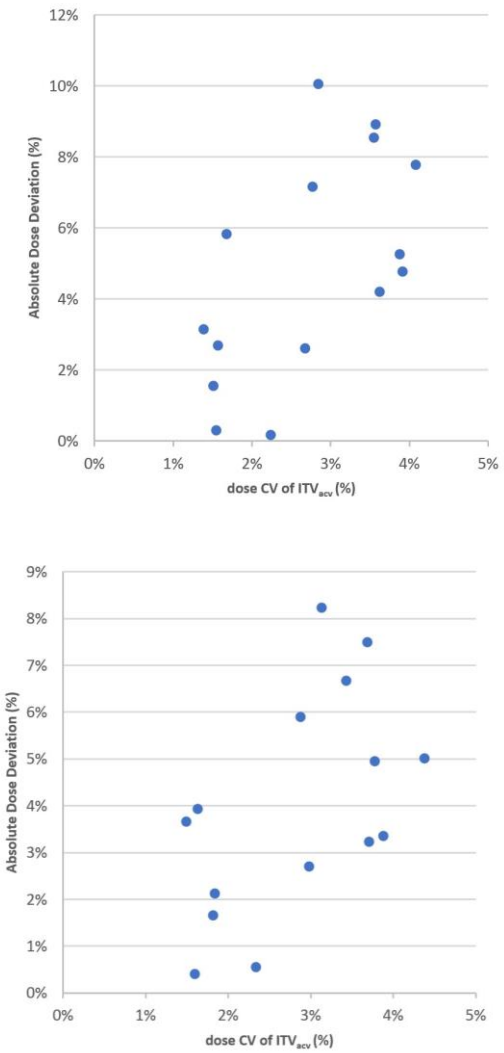

Fig. 6 ADD vs dose CV of ITV_{acv} in 10MV FFF ungated beams using AAA algorithm (upper) and AXB algorithm (lower)

Beam On Time per MU

Fig. 7 shows the beam on time per MU for both gated and ungated cases of both energies. Three groups, namely the 6 MV FFF gated and ungated and the 10 MV FFF ungated, failed the Shapiro-Wilk Normality Test, i.e. less than 0.05, thus a non-parametric equivalent for paired t-test, Wilcoxon signed-rank test, was used. Table 3 illustrates the results of the Wilcoxon signed-rank tests with one-tailed and two-tailed hypothesis. Significant differences were observed among 10 MV FFF and 6 MV FFF for ungated and gated cases with one-tailed hypothesis. Spearman's Rho correlation (non-parametric alternative to Pearson correlation) was also conducted between the ADD and beam on time per MU, however no significant correlation was found.

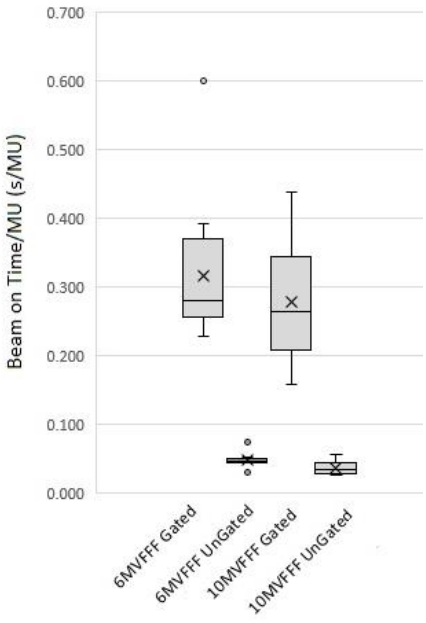

Fig. 7 Beam on time per MU

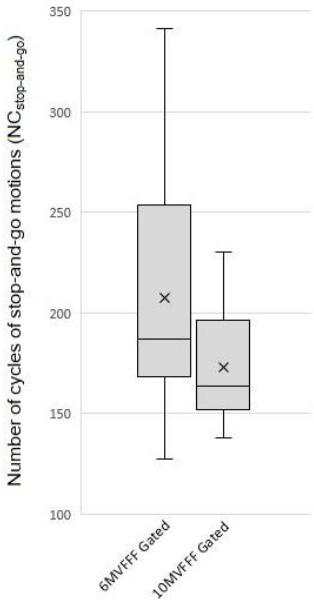

Fig. 8 $NC_{stop\text{-}and\text{-}go}$ for the gated cases of 6MV FFF and 10MV FFF

Table 3 Wilcoxon signed-rank test for Beam On Time/MU

			p-value of Wilcoxon signed-ranks test	
		mean of beam on Time / MU (s/MU)	One-tailed Hypothesis	Two-tailed Hypothesis
6MV FFF	Gated	0.317	0.037*	0.074
10MV FFF		0.278		
6MV FFF	UnGated	0.047	0.001*	0.003*
10MV FFF		0.036		

*significant difference, p<0.05

Table 4 Results of paired t-test of ADD and $NC_{stop\text{-}and\text{-}go}$

ADD Comparison			mean ADD	p-value of paired t-test
6MV FFF	Gated	AXB	2.39%	0.97
10MV FFF			2.40%	
6MV FFF	Gated	AAA	2.61%	0.77
10MV FFF			2.77%	

$NC_{stop\text{-}and\text{-}go}$ Comparison		mean $NC_{stop\text{-}and\text{-}go}$	
6MV FFF	Gated	207.7	0.03*
10MV FFF		173.2	

*significant difference, p<0.05

Number of cycles of stop-and-go motions ($NC_{stop\text{-}and\text{-}go}$)

The ADD and $NC_{stop\text{-}and\text{-}go}$ of the gated cases were studied for the stop-and-go effect. All the groups passed the normality test, i.e. their p-value were larger than 0.05. Thus, paired t-test for ADD and $NC_{stop\text{-}and\text{-}go}$ comparison, and also Pearson correlation were conducted.

Fig. 8 summarizes the $NC_{stop\text{-}and\text{-}go}$ for the gated cases of both energies. Table 4 shows the results of the ADD comparison and $NC_{stop\text{-}and\text{-}go}$ comparison between 6 MV FFF and 10 MV FFF in gated cases. Significant difference in $NC_{stop\text{-}and\text{-}go}$ was observed between the two energies with different DR_{max} but it showed no significant difference in ADD in AAA and AXB. Also, no significant correlation was found in Pearson correlation between ADD and $NC_{stop\text{-}and\text{-}go}$.

Plan complexity

The number of MU per prescribed dose (Gy) was used for evaluating the plan complexity. Both groups, 6 MV FFF and 10 MV FFF, passed the normality test. Paired t- test in plan complexity was conducted for the two energies. It was found that no statistically significant difference was observed in the test (p=0.699).

IV. DISCCUSION

This study evaluated the dosimetric impact of the stop-and-go effect and interplay effect between gated and ungated SBRT using 6MV FFF and 10MV FFF energy beams with targets motion ±2cm inferior/superior motion with period of 4s. According to Court *et al.* [12, 13] and

Ong *et al.* [14, 15], greater target motion would lead to larger dose discrepancies, so a relatively large motion of ±2cm was used for amplifying the motion effect as well as the interplay effect. A relatively short period of 4s was chosen, so as to maximize the stop-and-go effect.

From the Friedman tests shown in table 1, statistically significant difference was shown in 10 MV FFF with 2400 MU/min DR_{max} (p value = 0.020), but not in 6 MV FFF with 1400MU/min DR_{max} (p value = 0.184). The difference of the mean ADD of AAA and AXB between gated and ungated cases for 10 MV FFF was 1.84%, compared with that 0.66% of 6 MV FFF. The difference was due to the higher dose rate used in the cases of 10MV FFF. High dose rate is more susceptible to interplay effects, leading to larger dose deviation [14, 16, 20]. The results of the Wilcoxon signed-ranks tests that the 10 MV FFF ungated ADD was significantly larger than the 10 MV FFF gated ADD means the 10 MV FFF with the ungated beams are more susceptible to interplay effect, compared with the gated beams to both interplay and stop-and-go effect.

It was known that there were several proposed solutions to reduce the dosimetric impact due to interplay effect, for example, using lower dose rate [11, 13, 14, 20], avoiding highly modulated plans [12, 15, 20] or providing sufficient target margin [23]. In this study, less target dose inhomogeneity is also proved to be one of the solutions for reducing ADD in ungated 10 MV FFF with 2400 MU/min DR_{max} cases. It was found that the dose CV of ITV_{acv} statistically correlated with the ADD in ungated 10MV FFF cases. Again, this did not happen in the 10MV FFF gated cases, 6 MV FFF gated and ungated cases. The positive correlation between the ADD and dose CV of ITV_{acv} in ungated 10 MV FFF with 2400 MU/min DR_{max} implied that the ADD could be decreased by using a target dose with reduced dose inhomogeneity.

Due to the complicated technical nature of VMAT on gated radiation therapy, backlash of gantry rotation and MLC position may affect the precision of radiation dose delivery. Yoon *et al.* [5] reported that the more stop-and-go motions will result in more dosimetric errors. Since dose rate of 2400 MU/min was used for 10MV FFF and 1400 MU/min for 6 MV FFF, there was significant difference in $NC_{stop\text{-}and\text{-}go}$ between the two energies. $NC_{stop\text{-}and\text{-}go}$ of 10 MV FFF groups are much smaller than that of 6 MV FFF. Thereby significant difference in stop-and-go effect between 10 MV FFF and 6 MV FFF would be expected and could be reflected in the difference in ADD according to Yoon *et al.* [5]. However, the expected result did not appear in this study. It was observed from table 4 that there was significant difference in $NC_{stop\text{-}and\text{-}go}$ between 6 MV FFF and 10 MV FFF, but no significant difference in ADD between two energies implying that the stop-and-go effect was not significant in gated SBRT.

Jiang *et al.* [11] performed single point measurements on the IMRT plans with a 0.6cc Farmer chamber moving in a one-dimensional sinusoidal fashion. This study used similar setup to that of Jiang's. They had 30% variation for one IMRT field in one fraction and 18% for five IMRT fields over one fraction. When compared with Jiang *et al.* [11], the maximum ADD of this study was approximately 10% over two RapidArc fields. Some improvements were made in this study to reduce the dose deviation. (1) Instead of using a 0.6cc Farmer chamber, a 0.016cc PinPoint 3D ion chamber was used to avoid dose averaging. (2) The measured dose was compared with the planned dose of the ITV_{acv} instead of the corresponding static point dose. (3) The ITV_{acv} used for dose comparison did not fall into the penumbra region of the verification plan to avoid the dose blurring effect [11].

Despite considerable evidence demonstrating the dosimetric effects of interplay averaging out for multiple fractions [11, 12, 14, 21, 22], the effects for individual fractions is still of importance and a topic of interest due to the unknown biological effect applied to this averaging. Moreover, hypofractionation is becoming increasingly popular, in which radiotherapy is delivered in fewer fractions. This will inevitably result in the averaging effect being reduced. Likewise, it is well known that the dosimetric effects of interplay are of little significance to the gross tumor volume (GTV) coverage as long as a sufficient margin is given [23]. However, the effects for ITV dose deviation is still important due to the tighter margins afforded by the increased availability of image-guided radiotherapy (IGRT) and improved machine accuracy and precision.

The pre-set maximum dose rate in 10 MV FFF was higher than that of 6 MV FFF for both gated and ungated cases, thus one-tailed hypothesis of Wilcoxon signed-rank test was used for the beam-on time/MU comparison. For ungated SBRT, the beam-on time/MU of 10 MV FFF was, as expected, significantly shorter than that of 6 MV FFF. Whereas in gated SBRT, a certain amount of time was required for ramping up the dose rate. Combined with the short gating window, the dose rate for the gated cases might not reach its maximum (1400 MU/min for 6 MV FFF and 2400 MU/min for 10 MV FFF) before the gated period was over. However, our results showed that 10 MV FFF had significantly shorter beam on time/MU than 6 MV FFF for the 40%-60% gating window. This implied that the 10 MV FFF still had a higher average dose rate within the gating window than 6 MV FFF beams in gated cases.

Since the dosimetric accuracy affected by the interplay effect would be decreased by increasing the dose rate [14, 16, 20], it was therefore thought that there would also be correlation between the ADD and the beam on time/MU for ungated 10 MV FFF. However, no significant correlation was found. It was then proposed that instead of studying the

beam on time/MU alone, the effect by instantaneous dose rate can be further studied.

With the re-optimization of the 6 MV FFF treatment plans to be 10 MV FFF treatment plans, different MLC patterns were used in the 6 MV FFF and 10 MV FFF plans. Plan complexity of the two energies plans was of concern whether this would have partially accounted for the differences in ADD, beam on time/MU and $NC_{stop\text{-}and\text{-}go}$, as well as correlation tests, since multiple proof of dosimetric effects of interplay generally increased with the plan complexity [10, 15, 20]. The plan complexity in terms of number of MU/Gy among the groups of two energies was compared. No significant difference was found. Therefore, it is interpreted as plan complexity having no significant impact on the results in this study.

A significant difference of ADD was observed between AAA and AXB in ungated cases for 10MV FFF and 6 MV FFF (table 1). Although there was no significant difference for the gated groups, Fig. 1 shows the ADD of AXB cases were always lower than that of AAA cases in all groups. Our findings therefore agreed with the results reported by previous studies on the superiority of AXB over AAA in dose calculation in heterogeneous media [17, 18, 19].

Limitations and improvements

The influence of the interplay effect on dosimetric accuracy and the delivery accuracy of respiratory gating was evaluated only in the superior-inferior direction, where the tumor motion was the most significant. Secondly, the analysis encompassed only the target area. Thirdly, the analysis was conducted by using a phantom with regular simulated motion, which could not accurately represent true motion of a human patient motion. Fourthly, due to the re-optimization in the 10 MV FFF plans, different MLC patterns were used for the 6 MV FFF and 10 MV FFF ADD comparison though there was no significant difference in plan complexity. Moreover, as only single point measurements were made, there was no multi-dimensional measurement results. Shift and change in the shape of the dose distribution caused by interplay effect were not accounted in this study. Finally, the limited sample size led to only the ungated data showing a significant difference between AAA and AXB. Therefore, false negative error would be reduced, if the sample size could be increased.

V. CONCLUSIONS

This study found that the interplay effect had a statistically significant adverse dosimetric impact in 10MV FFF ungated SBRT due to the high DR_{max} 2400MU/min. This adverse impact on ADD could be decreased by using a target dose with reduced dose inhomogeneity due to the significant correlation found between ADD and dose CV of ITV_{acv}. On the other hand, the stop-and-go effect showed no significant effect to the ADD. To conclude, the interplay effect outweighed the stop-and-go effect for the TrueBeam linear accelerator. Lastly, SBRT using 10 MV FFF with DR_{max} 2400 MU/min had significantly shorter beam-on time/MU than that when using 6 MV FFF with DR_{max} 1400 MU/min in both gated and ungated cases.

ACKNOWLEDGMENT

The authors would like to thank Sr. Timothee Chow, managing director of St. Teresa's Hospital and Dr. Gordon Au, department head of Oncology Centre, St. Teresa's Hospital for their full support on this study.

REFERENCES

1. Kanai K, Kotabe K, Kijima K, Ishikawa Y, Nakayama H. (2018) Multileaf Collimator Position Accuracy of Respiratory Gated VMAT. 38(1):2-9. doi:10.11323/jjmp.38.1_2
2. Yoon M, Kim Y, Jeong J et al. (2015) Dosimetric Analysis of Respiratory-Gated RapidArc with Varying Gating Window Times. Progress in Medical Physics. 26(2):87. doi:10.14316/pmp. 2015.26.2.87
3. Wiersma R, Xing L. (2007) Examination of geometric and dosimetric accuracies of gated step-and-shoot intensity modulated radiation therapy. Med Phys. 34(10):3962-3970. doi:10.1118/1.2776671
4. Ezzell G. (2001) The overshoot phenomenon in step-and-shoot IMRT delivery. J Appl Clin Med Phys. 2(3):138. doi:10.1120/1.1386508
5. Ezzell G, Galvin J, Low D et al. (2003) Guidance document on delivery, treatment planning, and clinical implementation of IMRT: Report of the IMRT subcommittee of the AAPM radiation therapy committee. Med Phys. 30(8):2089-2115. doi:10.1118/1.1591194
6. Nam T, Chen Q, Ng M (2023) Dosimetric comparison between gated and ungated SBRT plans using VMAT with FFF beams [Abstract]. In Proceedings of the Annual Conference of the European Society for Radiotherapy & Oncology (ESTRO), Vienna, Austria. PO-1782. Retrieved from https://user-swndwmf.cld.bz/ESTRO-2023-Abstract-Book/1518/
7. Thiyagarajan R, Sinha S, Ravichandran R et al. (2016) Respiratory gated radiotherapy-pretreatment patient specific quality assurance. J Med Phys. 41(1):65. doi:10.4103/0971-6203.177279
8. Rouabhi O, Gross B, Bayouth J, Xia J. (2018) The Dosimetric and Temporal Effects of Respiratory-Gated, High-Dose-Rate Radiation Therapy in Patients With Lung Cancer. Technol Cancer Res Treat. 18:153303381881607. doi:10.1177/1533033818816072
9. Tyler M. (2016) Quantification of interplay and gradient effects for lung stereotactic ablative radiotherapy (SABR) treatments. J Appl Clin Med Phys. 17(1):158-166. doi:10.1120/jacmp.v17i1.5781
10. Court L, Wagar M, Berbeco R et al. (2010) Evaluation of the interplay effect when using RapidArc to treat targets moving in the craniocaudal or right-left direction. Med Phys. 37(1):4-11. doi:10.1118/1.3263614
11. Jiang S, Pope C, Jarrah K, Kung J, Bortfeld T, Chen G. (2003) An experimental investigation on intra-fractional organ motion effects in lung IMRT treatments. Phys Med Biol. 48(12):1773-1784. doi:10.1088/0031-9155/48/12/307
12. Court L, Wagar M, Bogdanov M et al. (2010) Use of reduced dose rate when treating moving tumors using dynamic IMRT. J Appl Clin Med Phys. 12(1):28-34. doi:10.1120/jacmp.v12i1.3276

13. Court L, Wagar M, Ionascu D, Berbeco R, Chin L. (2008) Management of the interplay effect when using dynamic MLC sequences to treat moving targets. Med Phys. 35(5):1926-1931. doi:10.1118/1.2896083
14. Ong C, Dahele M, Slotman B, Verbakel W. (2013) Dosimetric Impact of the Interplay Effect During Stereotactic Lung Radiation Therapy Delivery Using Flattening Filter-Free Beams and Volumetric Modulated Arc Therapy. International Journal of Radiation Oncology*Biology*Physics. 86(4):743-748.
15. Ong C, Verbakel W, Cuijpers J, Slotman B, Senan S. (2011) Dosimetric Impact of Interplay Effect on RapidArc Lung Stereotactic Treatment Delivery. International Journal of Radiation Oncology*Biology*Physics. 79(1):305-311. doi:10.1016/j.ijrobp. 2010.02.059
16. Rao M, Ye J, Spiegel J, Takamiya R, Mehta V, Wu J. (2014) Interplay Effect During Lung SBRT with VMAT Delivered by Flattening Filter–Free Beams. International Journal of Radiation Oncology*Biology*Physics. 90(1):S192 doi:10.1016/j.ijrobp. 2014.05.727
17. Krishna G, Srinivas V, Reddy P. (2016) Clinical implications of Eclipse analytical anisotropic algorithm and Acuros XB algorithm for the treatment of lung cancer. J Med Phys. 41(4):219. doi:10.4103/0971-6203.195185
18. Han T, Mikell J, Salehpour M, Mourtada F. (2011) Dosimetric comparison of Acuros XB deterministic radiation transport method with Monte Carlo and model-based convolution methods in heterogeneous media. Med Phys. 38(5):2651-2664. doi:10.1118/ 1.3582690
19. Krabch M, Chetaine A, Nourreddine A, Erradi F, Baddouh L. (2018) 29 Dosimetric comparaison of the anisotropic analytical algorithm and acuros XB algorithm in dose calculation for lung cancer heterogeneity. Physica Medica. 56:53. doi:10.1016/j.ejmp. 2018.09.111
20. Edvardsson A, Nordström F, Ceberg C, Ceberg S. (2018) Motion induced interplay effects for VMAT radiotherapy. Physics in Medicine & Biology. 63(8):085012. doi:10.1088/1361-6560/aab957
21. Rao M, Wu J, Cao D et al. (2012) Dosimetric Impact of Breathing Motion in Lung Stereotactic Body Radiotherapy Treatment Using Image-Modulated Radiotherapy and Volumetric Modulated Arc Therapy. International Journal of Radiation Oncology*Biology*Physics. 83(2):e251-e256. doi:10.1016/j.ijrobp. 2011.12.001
22. Duan J, Shen S, Fiveash J, Popple R, Brezovich I. (2006) Dosimetric and radiobiological impact of dose fractionation on respiratory motion induced IMRT delivery errors: A volumetric dose measurement study. Med Phys. 33(5):1380-1387. doi:10.1118/1.2192908
23. Li X, Yang Y, Li T, Fallon K, E Heron and D, Huq M. (2013) Dosimetric effect of respiratory motion on volumetric-modulated arc therapy-based lung SBRT treatment delivered by TrueBeam machine with flattening filter-free beam. J Appl Clin Med Phys. 14(6):195-204. doi:10.1120/jacmp.v14i6.4370

Contacts of the corresponding author:

Author:	Dr. Man Cheuk Ng
Institute:	St. Teresa's Hospital
Street:	327 Prince Edward Road
City:	Hong Kong
Country:	Hong Kong
Email:	mcng.thomas@gmail.com

HOW TO

IMPLEMENTING A ROBUST QUALITY ASSURANCE PROGRAM IN AN LMIC CLINIC AFTER TRANSITIONING FROM CO-60 TO LINAC TELETHERAPY UNIT

K. Akosah[1], E.K. Addison[1], L. Furnari[2], G. Dos Santos[2], A.A. Yorke[3]

[1] Komfo-Anokye Teaching Hospital, Kumasi, Ghana
[2] Instituto De Radiologia – Hospital Das Clínicas Da Usp, São Paulo, Brazil
[3] University of Washington Fred Hutch Cancer Center, Seattle, WA, USA

Abstract— **To provide emerging and existing radiotherapy centers in sub-Saharan Africa a blueprint to transition from Cirus Co-60 teletherapy units to Linac quality assurance (QA) tailored to the current availability of devices and equipment and to electronically track the data to trend and adjust when necessary. After 8 weeks of virtual training quality assurance (QA) documentation and the impact quality control (QC) and patient safety we instituted an electronic method of record keeping following AAPM TG 142 and 198 recommendations. Our clinic transitioned from a cirus cobalt-60 unit to a Varian Clinac iX with two photon energies (6 and 16 MV), four electron energies (6, 9, 12, and 16 MeV), an EPID, and a 120 millennium MLC installed. We developed an institutional QA program tailored to our institutional resources. The results demonstrate reproducibility in all quality assurance processes, with average daily radiation output constancy for 6MV and 16MV photons being (2.25%±0.25) and (2.61%±0.13) with a maximum deviation of 4.23% and 4.47% respectively whiles safety checks (door interlock and console, video monitors, beam on light indicator, and audio intercom system) and mechanical/optical checks (collimator size indicators, laser localization, distance indicator (ODI), collimator size indicator, gantry/collimator angle indicators, couch walk, collimator walk and treatment couch position indictors) were functional and within operational limits (1 mm, 2 mm and 1°). The average monthly radiation output constancy for 6 MV and 16 MV were 2.07%±0.45 and 2.185%±0.37 with a maximum of 2.32% and 2.63% respectively. This demonstrated that the beam is adjusted as the values are above the tolerance. The electronic data tracking has made it easier to track and trend our QA output values and as well as safety and mechanical checks for better record keeping. Through this, some new monthly QA tests (couch walk, collimator walk and treatment couch position indictors) have been added to the already existing ones. It was essential that centers similar to ours implement a robust yet simple QA program following recommendations from AAPM TG 142, 198 and MPPG 8a.**

Keywords— **Quality assurance, Co-60, Linac, low- and middle-income country.**

I. INTRODUCTION

Komfo Anokye Teaching Hospital is one of three radiotherapy centers in Ghana Equipped with a Varian Clinac iX which has two photon energies (6 and 16 MV), four electron energies (6, 9, 12, and 16 MeV), an EPID, and a 120 millennium multi leaf collimator. The Center offers 3-Dimensional conformal radiotherapy services and 2D treatments on a Cirus Co-60 unit.

Periodic quality assurance of the external beam radiotherapy device is essential for the device to function at a level needed for creating custom plans unique for each patient's treatment. Efficient and effective QA procedures are needed in radiotherapy centers to ensure the machines integrity is not compromised (i.e., machine characteristics do not deviate significantly from their baseline values acquired at the time of acceptance and commissioning). [3, 4, 5, 6, 7] This study was conducted to provide emerging and existing radiotherapy centers in sub-Saharan Africa a blueprint to transition from Cirus Co-60 teletherapy units to Linac quality assurance (QA) tailored to the current availability of devices and equipment and to electronically track the data to trend and adjust when necessary.

All QA protocols have been adapted from the American Association of Physicists in Medicine Task Group (AAPM TG) report numbers 142, 198 and Medical Physics Practice Guidelines 8a recommendations for periodic checks on the Linac.

A QA program takes into account the procedures necessary for checking the performance of radiotherapy equipment and for measuring the characteristics of the output as well. The program is designed to specify the method of testing equipment, the parameters to be tested and the frequency of testing, the responsibilities of different members of staff, the baseline values and tolerances for these values, action levels and documentation guidelines. A clinical linear accelerator must in all circumstances function within tolerances obtained during acceptance testing [9]. It is therefore expected that a QA program designed specifically for an institution will meet those standards.

It is recommended that a QA committee should constitute professionals such as radiation oncologists, physicists, dosimetrist, therapists, engineers, and administrators, according to the American College of Radiology (ACR) [10]. Dosimetric accuracy, mechanical accuracy, safety, imaging, and unique Procedures, should all be included in the QA report. As a guideline for establishing the baseline for upcoming dosimetric studies of beam performance consistency, Acceptance Testing Procedure (ATP) Standards are established. This demonstrates that the apparatus is mechanically sound and functions within predetermined tolerances of accuracy.

According to their tolerance, three action levels are established and followed: level 1 (inspection), level 2 (planned activities), and level 3 (immediate/ stop treatment/ corrective actions) [7]. In this study we implement a quality assurance and an electronic method of tracking the data for a level 1, 2 or 3.

II. MATERIALS AND METHODS

The Clinac version 9.1 Linac system with 3D conformal treatment modality, Exradin A19 ionization chamber, Max 4000 Plus Electrometer, Designed A4 Sheet for collimator walk, Thermometer, Barometer, Blue Water PMMA Slabs, Front Pointer and Accessories, a Jig, a Leveler, and an electronic generated excel worksheet to keep track and record our QAs were used for the study. The linac has two photon energies (6, and 16 MV) with Flattening Filter Free (FFF) mode and four electron energies (6, 9, 12, and 16 MeV). The linac is equipped with a Varian Millennium MLC system comprising of 120 leaves

We performed x-ray output constancy, laser localization, distance indicator (ODI), collimator size indicator, door interlock, audiovisual monitor, radiation area monitor, and beam on indicator were performed on a daily, monthly basis and tracked the results for a total of 6 months setting action levels and making adjustments when needed.

Daily QA:

Prior to treating patients that day, the daily QA procedures were carried out. Mechanical checks, which included laser localization, distance indicator (ODI), and collimator size indicator were performed. Dosimetric checks, which includes photon and output constancy, and safety, which includes door interlock, audiovisual interlocks, radiation area monitor, and beam on indicator, are the three main categories into which these tests can be divided. In our clinic a certified medical physicist conducts such tests. For the dosimetric outputs we used Exradin A19 calibrated ionization chamber, a deviation of less than 3% is recommended, with errors of less than 2 mm for laser localization, distance indicator, and collimator size indicator being considered acceptable. Safety checks are done to check the functionality of, the door interlocks, audiovisual monitors, radiation area monitor, and beam on indicator. In our clinic, if any of these parameters are out of tolerance treatment is put on hold and issue is investigated and fixed. All daily check results must be within limits for the Linac to be approved for clinical use

Monthly QA:

More comprehensive tests of the mechanical, safety, and radiation dosimetry parameters were performed on a monthly basis. The mechanical system, gantry/collimator angle indicators, treatment couch position indicators, couch accuracy, localizing lasers, light/radiation field coincidence, door interlocks, optical distance indicator accuracy, photon output constancy and typical dose rate constancy, are among the things that are tested as part of the quality assurance approach.

1. ***Laser Localization***

This test was done with the jig aligned with the lasers installed and cross hair of the linac head. The surface of the jig was set to 100 cm SSD using the front pointer and the plate of the jig rotated through the angles of 90° and 270° to check deviations of the lasers from the cross marks on the plate. The deviation is then recorded.

2. ***Optical Distance Indicator or Distance Indicator (ODI)***

The front pointer and the jig were used for this test. With the gantry at 0°, the front pointer was set at 100 cm SSD and the jig moved till the flat surface touches the tip of the front pointer. The 100 cm SSD coincides with the radiation or machine isocenter as it grazes the surface of the illuminated field light. The pointer is removed and the ODI checked for 100 cm SSD. The value and its deviation were recorded.

3. ***Collimator Size Indicator***

This test was done with the jig set up on the treatment couch and set to 100 cm SSD. The field sizes are moved with the cross marks on the surface of the jig to fill the area. Various field sizes ranging from 5×5 cm to 20×20 cm was used, and the deviations recorded.

4. ***Gantry Angle Indicator***

The test was done with mechanical movement of the gantry at 0°, 90°, 180°, and 270°. The angles moved were verified by attaching a digital leveler to the head of the linac. This test is necessary for checking couch and machine isocenter. The measured or readout values were recorded.

5. ***Collimator Angle indicator***

The test was done with mechanical movement of the collimator at 0°, 45°, 90°, 135°, 180°, and 315° with the jig set up and aligned with the laser and the cross hair in the head of the linac. The angles moved were verified from the digital readings on the gantry of the linac. The readout values were recorded and well documented in the developed excel spreadsheet.

6. ***Iso Walk***

a. Couch walk

Couch is kicked to various angles as indicated on the base plate. Couch rotation angle indicated on the base plate is compared with the angle indicated on the in room monitor. The deviations were recorded.

b. Collimator walk

Set the sheet with the field markings on the couch and align cross hairs. Move collimator through various selected angles. (30, 60, 90, 200, 315, etc.). Check at

what point the center of the cross hair move from the center of the markings. The deviations were recorded.

7. Safety Checks

These checks are paramount to the safety of the patient and people authorized to work within the radiation area. Patients are monitored and communicated with through the audiovisual monitor. Staff and authorized people are warned of radiation beam on or off with the functionality of the beam light indicator. The door interlock also helps prevent unnecessary exposure to staff as treatment is in session as one attempts entering the treatment room.

The data taken were well documented and analyzed in the developed electronic excel spreadsheet which will also help track data of all QA tests performed for the future.

8. Photon Beam Output factor

The output factor for the two photon energies of the energy were measured. The blue solid PMMA slabs phantom was arranged on the treatment couch and aligned with the lasers. An SSD of 90 cm using the front pointer, a reference field size of 10×10 cm and a depth of 10 cm were set. The electrometer was switched on and warm up done. The A19 ionization chamber was connected to the electrometer. Series of five readings were taken for the 6 and 16 MV photon energies. Initial and final temperature and pressure readings were recorded as well. The deviation in the output was calculated using the equation:

$$\frac{measured\ reading - reference\ reading\ (nC)}{reference\ reading\ (nC)} \times 100 \quad (1)$$

9. Couch Position Indicators

For couch position indicators, the couch vertical and longitudinal were done. For couch vertical, a 30 cm rule was held to the couch with a cellotaph. The 15 mark was used as the zero mark with the corresponding value on the in-room monitor and ODI recorded. Series of values were taken in steps of ±5 cm and the corresponding digital values on the in-room monitor and ODI noted as well.

For couch longitudinal, a 100 cm rule was held to the couch with a cellotaph. The 50 mark was used as the zero mark with the corresponding value on the in-room monitor recorded. Series of values were taken in steps of ±10 cm and the corresponding digital values on the in-room monitor recorded as well.

III. RESULTS

A. Photon Beam Output factor

The output factor is a field size–dependent correction for the output of the linear accelerator. It is the ratio of absorbed dose of a particular field size relative to the dose at a reference field size. Field size is determined by choice of collimator size and SDD. In the measurements carried out, the reference field size was 10×10 cm with additional field sizes (5×5 cm, 15×15 cm, 20×20 cm) and the depth of measurement was 10 cm. The results for the daily and monthly output are presented in the Table 1.

Table 1: Photon Beam Output for 6 MV and 16 MV with average daily and monthly deviations

	6 MV	Deviation (%)	16 MV	Deviation (%)	Tolerance (%)
Monthly	16.82	2.32	20.00	2.88	3
Daily	16.78	2.07	19.44	2.40	2

B. Laser Localization

The laser alignment for patient setup was done for the angles 90° and 270°. This helps to set up patients per treatment planning parameters to deliver the right dose to patients. The results for the test are presented in Table 2. Tolerance ± 1 mm.

Table 2: Laser Alignment with average deviations

	Horizontal	Vertical
Left	0	0
Right	0	0
Sagittal	0	0

C. Optical Distance Indicator or Distance Indicator (ODI)

The 100 cm SSD test was done using the ODI at a gantry angle of 0 and collimator angle of 0. The average result for the test is summarized in Table 3.

Table 3: Optical Distance Indicator or Distance Indicator (ODI) with deviations

SSD (cm)	ODI (cm)	Deviation (%)
100	100	0

D. Collimator Size Indicator

During patient treatment, the radiation beam which is defined by field size results from the closing and opening of the collimator jaws to an extent. The results of the collimator size indicator for 5×5 cm to 20×20 cm is summarized in Table 4. Tolerance ± 2 mm.

Table 4: Collimator Size Indicator with average deviations

Jaws (mm)		Expected (mm)		Measured (mm)		Difference (mm)	
X=5	Y=5	5.0	5.0	5.0	5.0	0.0	0.0
X=10	Y=10	10.0	10.0	10.1	10.0	0.1	0.0
X=15	Y=15	15.0	15.0	15.0	15.1	0.0	0.1
X=20	Y=20	20.0	20.0	20.0	20.0	0.0	0.0

E. Gantry Angle Indicator

During the treatment of patient gantry moves through various planned angles to deliver the right dose to patients during the process. The results of the test done from selected angles are summarized in Table 5. Tolerance ± 1º.

Table 5: Gantry Rotation with average deviations

Level	Digital	Mechanical	Difference
0	0.0	0.0	0.0
90	90.1	90.0	0.1
180	180.1	180.0	0.1
270	270.0	270.0	0.0

F. Collimator Angle indicator

Collimator rotation is key in treatment planning as better dose coverage and sparing of critical organs is concerned. A summary of the test done on various collimator angles is presented in Table 6. Tolerance ± 1º.

Table 6: Collimator Rotation with average deviations

Level	Digital	Difference
0	0.0	0.0
45	45.1	0.1
90	90.1	0.1
180	180.0	0.0

G. Couch Position Indicators

A quality control test on the movement of couch necessary since patient setup and treatment is dependent on this as well. This is done to maintain the integrity of the couch. A summary of the results from the tests performed is shown in Tables 7 and Table 8. Tolerance ± 0.2 cm.

Table 7: Couch Position Indicators (longitudinal)

Ruler	Digital (cm)	Mechanical (cm)	Difference (cm)	Deviation (cm)
0	0.0	0.0	0.0	0.0
-10	133.0	123.1	9.9	-0.1
+10	113.1	123.1	10.0	0.0

Table 8: Couch Position Indicators (vertical)

Ruler	Digital (cm)	Mechanical (cm)	Difference (cm)	ODI (cm)
0	0	N/A	N/A	100
-5	-5.1	5.0	-0.1	105
5	4.9	5.0	0.1	95
-10	-10.1	10.0	-0.1	110

H. Iso Walk

Couch and collimator isocenter tests are important quality control tests performed on the machine since one has to make sure of reproducing the same baseline isocenter settings attained during acceptance. The results are summarized in Table 9. Tolerance ± 1 mm.

Collimator	0.1	0.18
Couch	0.1	0.16

I. Safety Checks

The safety check is very key to the safe and comfortable treatment delivery to patients undergoing radiotherapy. This also helps warn and prevent staff and authorized people of any unnecessary radiation exposure. The summary of the results obtained is found in Table 10.

Table 10: Safety checks with operational status.

Check	Status
Door interlock and console	Functional
Video monitors	Functional
Beam-on light indicator	Functional
Audio intercom system	Functional

Eighty percent (80%) of the measured dosimetric data was below ±2% tolerance,10% above ±2% and with 10% above the tolerance value of ±3% from the commissioning value from fig.1. Daily measurements over the period shows an average percentage difference of 1.39% and 0.83% for 6 and 16 MV photon energies as compared to the values obtained during commissioning.

The monthly photon output had four of values within the ±3% of the reference values and the one above the tolerance value fig.2. Output measurements over the period show an average percentage difference of 2.16% and 2.18% for 6 and 16 MV photon energies as compared to the values obtained during commissioning.

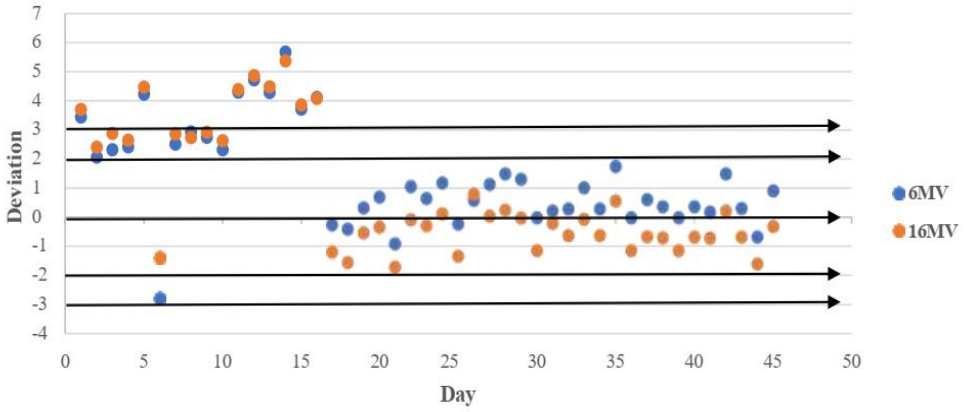

Fig.1 A graph of daily photon output deviation

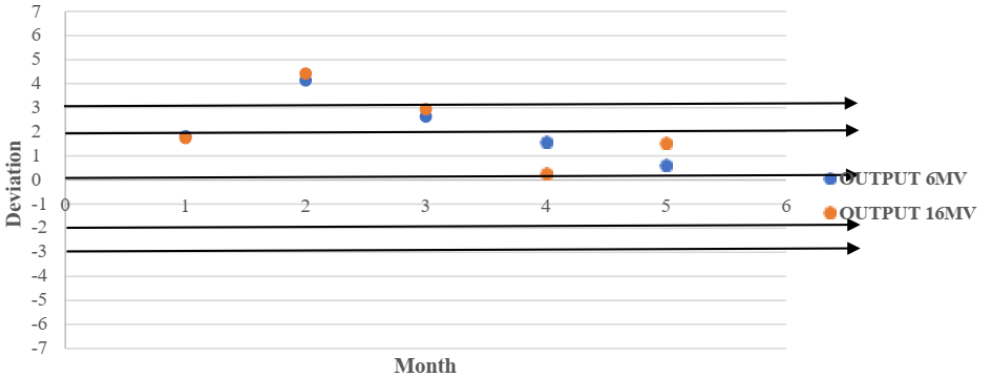

Fig.2 A graph of monthly photon output deviation

IV. DISCUSSION

The output value above the tolerance might be due to power fluctuations, procedural errors and concentrated charges at the effective point of measurement of the ionization chamber. These will be adjusted to meet the tolerance value for better treatment outcome. For daily QA tests, these parameters could seriously affect patient positioning and therefore the registration of the radiation field and target volume (collimator size indicators, lasers, ODI) and safety (Door interlock and console, video monitors, beam on light indicator, and audio intercom system) were carried out. From tables 4, 2, 3 and 8 all these parameters checked were within the acceptable limits and in good working condition.

The monthly mechanical tests which include laser localization, distance indicator (ODI), collimator size indicator, gantry/collimator angle indicators, couch walk, collimator walk and treatment couch position indictors were all within the tolerance values of ±2 mm, ±2 mm, 1°, ±1 mm, 1° and ±2 mm respectively.

The daily safety checks were done and were found to be within tolerance (functional). The audiovisual monitor functioning proves that patient can be monitored whiles treatment is in session and communicated to ensure safety and comfortability. The beam on indicator being functional keeps the staff or authorized people in the known of whether the radiation is on or not.

V. CONCLUSION

A comprehensive QA program is essential for the safe delivery of radiation and the quality of treatment received

by patients. It was essential that centers transitioning from Cirus Co-60 units to modern Linac treatment implemented a robust QA program and have a system of tracking to verify any out of tolerance data to improve the quality of radiotherapy care that patients receive in their clinics.

ACKNOWLEDGEMENT

Medical Physics QA team at the Komfo Anokye Teaching Hospital.

REFERENCES

1. Loi G., Pignoli E., Scorsetti M., et al, Design and characterization of a dynamic multileaf collimator. *Phys. Med. Biol.* 43, 3149-3155 (1998).
2. D. D Deshpande, R.A. Kinhikar, S.Shelv, S. et al, Quality assurance (QA) and implementation of intensity modulated radiotherapy (IMRT) with dynamic multileaf collimator (DMLC) on 2100 cd linear accelerator.
3. GJ Kutcher, L Coia, M Gillin, et al, "Comprehensive QA for radiation oncology: Report of AAPM Radiation Therapy Committee Task Group 40", *Med Phys*. vol.21, 1994, pp.581–618.
4. EE Klein, J Hanley, J Bayouth, et al, "Task group 142 report: quality assurance of medical accelerators", *Med Phys*. Vol. 36, 2009, pp. 41974212.
5. R Nath, PJ Biggs, FJ Bova, et al, "AAPM code of practice for radiotherapy accelerators: Report of AAPM Radiation Therapy Task Group 45", *Med Phys*. Vol. 21, 1994, pp. 1093-1121.
6. Aletti P et al., Recommendations for a quality assurance programme in external radiotherapy, *ESTRO*, Booklet No. 2, 1995.
7. George Felix Acquah, Bernhard Schiestl, Quality Assurance and Performance Evaluation of an Elekta Linear Accelerator: Results from Over a Year QA Experience in Ghana, *IJSBAR* (2014) Volume 14, No 1, pp 354-363.
8. "Determination of absorbed dose in a patient irradiated by beams of x- or gamma-rays in radiotherapy procedures," International Commission on Radiation Units and Measurement Bethesda Report 24, 1976.
9. BG Haffty and LD Wilson. Handbook of radiation oncology: basic principles and clinical protocols. Jones & Bartlett Learning, 2008.
10. Khan FM. The physics of radiation therapy 4th ed. Lippincott Williams & Wilkins, Philadelphia, 2010, pp. 375-404.

Contacts of the corresponding author:

Author:	Kingsley Akosah
Institute:	Oncology Directorate, Komfo Anokye Teaching Hospital
Street:	Bantama High Street
City:	Kumasi
Country:	Ghana
Email:	akosahkingsley@rocketmail.com

ENHANCING BREAST RADIOTHERAPY: EVALUATING THE INFLUENCE OF HEART LIMITATION ON TARGET COVERAGE AND DOSIMETRY FOR IMPROVED TREATMENT OUTCOMES

A.M. Baidoo[1], E.K. Sosu[2], S.N.A. Tagoe[1,3], R.B. Awotwe[1], S.B. Boateng[1], B. Djan[4], A. Mamoud[1], A.K. Arthur[5]

[1] Sweden Ghana Medical Centre/Department of Radiation Oncology, Medical Physicist, Accra, Ghana
[2] University of Ghana/Department of Medical Physics, Head of Department, Accra, Ghana
[3] University of Ghana/Department of Radiography, Exam Officer, Accra, Ghana
[4] Ghana Atomic Energy Commission/Radiation Protection Institute, Research Scientist, Accra, Ghana
[5] Tiwnikli International Senior High School/Department of Science, Physics Tutor, Accra, Ghana

Abstract— **An optimal radiotherapy plan must primarily ensure comprehensive target coverage in order to inhibit the possibility of recurrence. Complete coverage in breast radiotherapy has over the years remained a challenge due to its location. This work aims to determine the impact of a heart limitation on complete target coverage, and to look into how breast position affects its dosimetry in radiotherapy. Treatment plans for fifteen (15) each of left and right-sided breast cancer patients, with similar body thickness and breast sizes, that have completed intact breast radiotherapy were generated, and dose parameters regarding target coverage were assessed for both breast locations. Treatment plans for the left breast patients were regenerated, in which the heart d_{max} constraint was varied with five different values whilst recording the target dosimetry at each variation. It was easier to achieve complete coverage in right breasts than the left, in terms of 100% and 95% reference isodose. Treatment planning for right breasts likewise resulted in relatively preferred dose conformity. Meanwhile, the left breasts produced relatively higher mean doses and better homogeneity. Target coverage did not vary significantly with changing heart constraints in IMRT planning, with some parameters staying nearly constant throughout the variation. This implies that, using IMRT, heart constraints have negligible effect on target coverage for breast radiotherapy. There were highly significant changes in target dosimetry when heart constraints were varied in 3DCRT planning, suggesting that heart constraint imposes substantial effect on target coverage in 3DCRT breast radiotherapy. The value of the heart D_{max} constraints used in treatment planning may limit complete target coverage in breast radiotherapy. The degree of this limitation, however, depends on the treatment planning technique. The additional restriction imposed by the heart constraint in left breast radiotherapy results in relatively poor target coverage and lower dose conformity.**

Keywords— **Prescription, Coverage, Dosimetry, Conformity, Homogeneity.**

I. INTRODUCTION

The quality of every radiotherapy treatment is determined by complete target coverage, normal tissue sparing, dose conformity and homogeneity[1]. Additional variables such as Normal Tissue Complication Probability (NTCP) and Secondary Cancer Complication Probability (SCCP) depend on Conformity Index (CI) and Homogeneity Index (HI) of the treatment plan respectively[2]. To prevent recurrence of the disease, an optimal radiotherapy plan must essentially provide comprehensive target coverage. Concurrently, clinical evidence suggests that the extent to which total coverage may be achieved depends on the kind and number of adjacent organs at risk (OAR).

Complete coverage in breast radiotherapy has over the years remained a challenge due to its location, and this is frequently seen in treatment planning for left breasts. It is only important to investigate complete coverage between the left and right breasts, as well as the effect of some OARs on complete coverage for breast radiotherapy plans using similar patient thickness and breast sizes, since several factors, such as sizes and shapes of breasts, patient thickness, size of the planning target volume (PTV), beam energy and beam weighting, can all affect the complete coverage in breast radiotherapy[3].

The purpose of this work is to determine the impact of a heart limitation on complete target coverage, and to look into how breast position affects its dosimetry in radiotherapy.

II. METHODOLOGY

Radiotherapy planned image data from Siemens CT simulator (Somatom Emotion 16 slice scanner) for 15 each of left and right-sided breast cancer patients, with similar body thickness and breast sizes, that have completed intact

breast radiotherapy were selected for this study. The images were exported to a treatment planning system, where 3D reconstruction were digitally obtained for the sagittal, coronal and axial images of the patients.

All contours except the PTV were completed by a Radiation Oncologist using the Monaco® version 5.11.03 workstation. The PTV was created by a Medical Physicist by expanding the CTV using the auto margin contouring feature of the TPS by an isotropic margin of 10 mm in three dimensions and contracting laterally to 5 mm under the skin. The maximum and the minimum PTVs for all images involved in the study were 1285.43 cc and 1204.78 cc respectively. The prescribed dose was 50.0 Gy in 25 fractions for all patients, and the prescription was done according to the ICRU Report 50 recommendations[4], with 95% isodose line of the prescribed dose required to cover 95% of the PTV (V95%≥47.5Gy). The OAR constraints were defined according to our clinical protocol as expressed in Table 1.

Treatment plans for all 30 patients were generated in an Elekta TPS Monaco® version 5.11.03. The Monaco TPS works on a network of two main high-performance computers (Intel® Xeon® Gold 6132 2.60GHz processor, 128GB DDR3 RAM, 1TB Storage), with both connected to the center's central server.

In phase 1 of the study, 3DCRT Field-in-Field (FiF) and Intensity Modulated Radiotherapy (IMRT) techniques were used to complete the treatment plans for all patients by the same medical physicist, taking into consideration the OAR objectives of Table 1. In phase 2 of the study, the aforementioned treatment planning techniques were employed to generate plans for the fifteen (15) left sided breasts, using the same OAR objectives in Table 1 except the heart. The heart D_{max} constraint in phase 2 was varied between $D_{max} \leq 48$ Gy, $D_{max} \leq 44$ Gy, $D_{max} \leq 40$ Gy, $D_{max} \leq 36$ Gy and $D_{max} \leq 32$ Gy.

The Field-in-Field (FiF) technique used a 3D conformal forward planning technique that employs electron density calibration curve to determine homogeneous media and density in the body using Collapsed Cone Convolution dose calculation algorithm. It involved the use of two tangential open fields and multiple field-in-fields that were repeated until the desired dose homogeneity was achieved within the target.

The IMRT technique used an inverse planning method that relies on electron density calibration curve to define homogeneous media and body density using Monte Carlo dose calculation algorithm for a segmented treatment. The Monaco TPS combined Monte Carlo dose calculation accuracy with robust optimization tools to generate IMRT plans with fast calculation speed using calculation properties of 3mm grid spacing and 3% Statistical Uncertainty per control point. All IMRT plans were generated with only two tangential beams in constrained optimization mode to stimulate normal tissue priority. The biological and physical cost functions were rightfully employed to make treatment planning faster and less tedious. Dose volume histogram (DVH) statistics was used along with the IMRT constraints tab to identify conflicts that makes it difficult to meet the planning goal following the isoconstraint, isoeffect and the relative impact display. The multicriterial optimization tool were selected for some cost functions to spare OARs as much as possible while maintaining target coverage.

The global maximum dose accepted was 107% of the prescribed dose with the isodose distribution being symmetrical in all axial planes considering ICRU report 50 recommendations. The DVH for each plan was displayed for plan analysis.

Table 1: Phase 1 OAR Optimization Objective

Structure	**Optimization Goal**
Contralateral breast	$D_{max} \leq 3$ Gy, $V_{5Gy} \leq 15$ %
Ipsilateral lung	$V_{20Gy} \leq 45\%$, $V_{30Gy} \leq 35\%$
Lung (Total volume)	$V_{20Gy} \leq 30$ %, $V_{30Gy} \leq 20\%$
Heart	$D_{max} \leq 40$ Gy, $D_{average} \leq 26$ Gy, $V_{5Gy} \leq 45$ %, $V_{20Gy} \leq 20$ %

The dosimetry for both breasts were studied by examining the PTV dose coverage for all 30 plans generated by each technique, using as criteria, full prescribed dose coverage, 95 % prescribed dose, mean dose, conformity index (CI) and homogeneity index (HI).

The conformity index is expressed in equation 1 as the ratio of the reference isodose (95% isodose) volume to the PTV, where V_{RI} is the reference isodose volume and TV is the target volume. Using the ICRU recommendations[5], the ideal value was 1.

Conformity Index, $CI = \frac{V_{RI}}{TV}$ (1),

The homogeneity index is expressed in equation 2 as the ratio of the maximum PTV dose to the prescribed dose[6], where $PTV\ D_{max}$ is the maximum point dose and D_p is the prescription dose, with 1 as the ideal value .

Homogeneity Index, $HI = \frac{PTV\ D_{max}}{D_p}$ (2),

Microsoft Excel 2016 version was used to record and analyze all dosimetric information collected from the study, and one-way ANOVA test was used to compare the dose parameters between the two set of patients with a p-value of 0.05 being statistically significant.

Ethical clearance

Using the dataset of the selected previously treated patients, treatment plans were created using the treatment planning system only without any clinical application. This activity does not require ethical clearance according to our institution's policies.

III. RESULTS

Table 2 presents the dosimetric parameters for PTV coverage for the left and right breasts for both treatment techniques. It expresses the dose parameters for TPS calculations in both techniques recorded for the treatment plans produced for all patients in phase 1. The results of phase 2 of the treatment planning of the left breast recorded for each of the dosimetric objectives achieved with the variation of the heart D_{max} constraint are expressed in Table 3. Values in Table 2 and 3 are all expressed in mean ± standard deviations. In Figure 1, a sagittal view of the isodose distribution on the TPS interphase have been displayed for the designated heart D_{max} constraints in phase 2. Figure 2 provides an illustration of the limitation the heart imposes on target coverage through a graph of Heart Dmax constraint versus the designated PTV dose parameters for both 3DCRT FiF and IMRT techniques for treatment planning of the left breast.

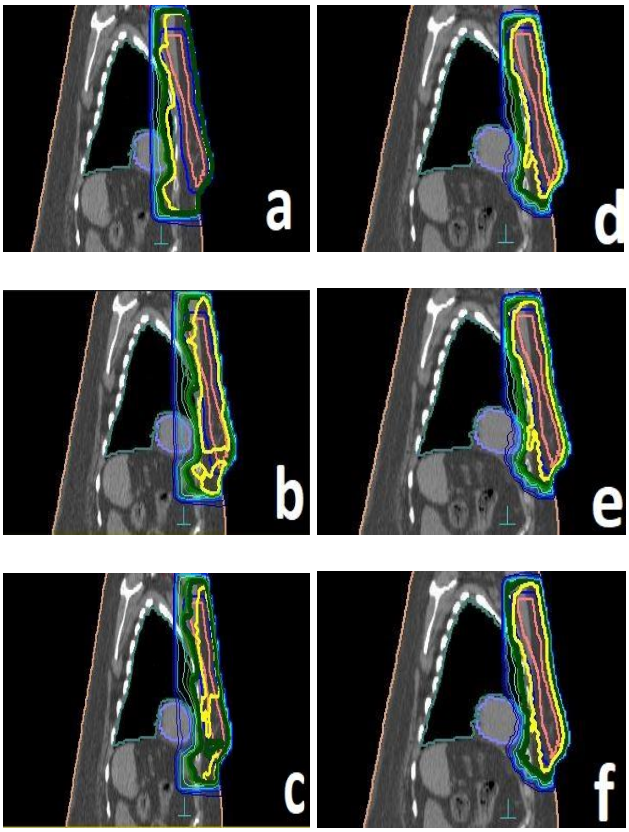

Figure 1: Dose display of variation in heart D_{max} constraint in a sagittal view: a) D_{max} = 48Gy in 3DCRT; b) D_{max} = 40Gy in 3DCRT; c) D_{max} = 32Gy in 3DCRT; d) D_{max} = 48Gy in IMRT; e) D_{max} = 40Gy in IMRT; f) D_{max} = 32Gy in IMRT

Table 2: Parameters for Target Coverage in Left and Right Sided Breasts in Phase 1 ($\bar{x}$±SD)

OBJECTIVE	3DCRT FIF		IMRT	
	Left Breast	Right Breast	Left Breast	Right Breast
V_{50GY} (%)	82.61 ± 9.07	83.83 ± 8.23	93.72 ± 2.31	94.38 ± 2.89
$V_{47.5GY}$ (%)	96.55 ± 1.33	97.33 ± 1.49	98.29 ± 0.73	99.24 ± 0.59
$D_{50\%}$ (GY)	50.84 ± 0.55	50.64 ± 0.42	50.78 ± 0.40	50.50 ± 0.30
CI	0.97 ± 0.01	0.97 ± 0.01	0.98 ± 0.01	0.99 ± 0.01
HI	1.06 ± 0.02	1.07 ± 0.02	1.04 ± 0.02	1.04 ± 0.02

Table 3: Changes in Target Coverage for Left Breasts over Varying Heart D_{max} in Phase 2 ($\bar{x}$±SD)

Parameter for Target Coverage	Heart D_{max}	3DCRT FiF	IMRT
V_{50Gy} (%)	D_{max} = 48 Gy	95.26 ± 2.64	93.91 ± 2.16
	D_{max} = 44 Gy	91.36 ± 2.13	93.79 ± 1.65
	D_{max} = 40 Gy	65.78 ± 1.35	93.56 ± 2.15
	D_{max} = 36 Gy	64.41 ± 2.06	93.47 ± 0.87
	D_{max} = 32 Gy	30.30 ± 3.63	93.45 ± 1.58
$V_{47.5Gy}$ (%)	D_{max} = 48 Gy	98.60 ± 1.04	98.70 ± 0.56
	D_{max} = 44 Gy	97.46 ± 2.07	98.68 ± 0.59
	D_{max} = 40 Gy	94.76 ± 1.16	98.67 ± 0.68
	D_{max} = 36 Gy	94.49 ± 3.01	98.64 ± 0.97
	D_{max} = 32 Gy	90.28 ± 1.45	98.59 ± 0.89
$D_{50\%}$ (Gy)	D_{max} = 48 Gy	53.12 ± 1.08	50.94 ± 0.60
	D_{max} = 44 Gy	52.21 ± 1.19	50.93 ± 0.34
	D_{max} = 40 Gy	50.43 ± 2.00	50.92 ± 0.68
	D_{max} = 36 Gy	50.39 ± 0.72	50.89 ± 0.24
	D_{max} = 32 Gy	49.48 ± 1.16	50.87 ± 0.71
CI	D_{max} = 48 Gy	0.99 ± 0.08	0.99 ± 0.00
	D_{max} = 44 Gy	0.97 ± 0.03	0.99 ± 0.01
	D_{max} = 40 Gy	0.95 ± 0.04	0.99 ± 0.01
	D_{max} = 36 Gy	0.94 ± 0.05	0.99 ± 0.01
	D_{max} = 32 Gy	0.90 ± 0.10	0.99 ± 0.02
HI	D_{max} = 48 Gy	1.09 ± 0.04	1.04 ± 0.01
	D_{max} = 44 Gy	1.07 ± 0.01	1.04 ± 0.01
	D_{max} = 40 Gy	1.05 ± 0.05	1.04 ± 0.01
	D_{max} = 36 Gy	1.05 ± 0.02	1.04 ± 0.00
	D_{max} = 32 Gy	1.03 ± 0.09	1.04 ± 0.01

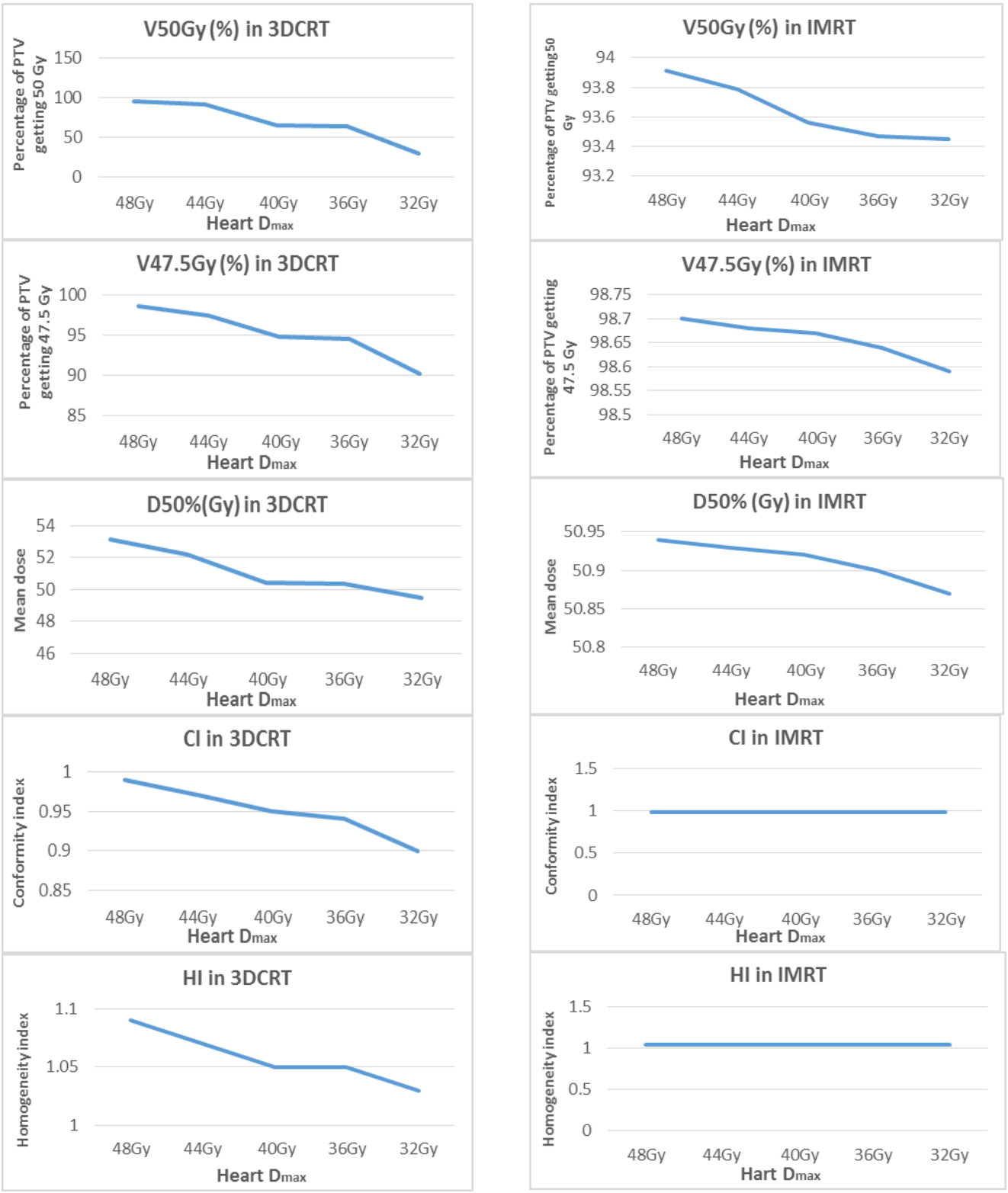

Figure 2: Graph of Heart Dmax constraint versus the designated PTV dose parameters for both 3DCRT FiF and IMRT techniques for treatment planning of the left breast

IV. DISCUSSIONS

Phase 1

In phase 1 of this study, PTV dose parameters were compared between the left and right-sided breasts to investigate the influence of breast position on PTV dosimetry for breast radiotherapy. This was realized by comparing the dosimetric parameters in terms of percentage of PTV covered by the full prescription dose (V_{50Gy}) as well as the 95% of the prescription ($V_{47.5Gy}$), the mean PTV dose ($D_{50\%}$), the Conformity Index (CI) and the Homogeneity Index (HI), taking into account the OAR objectives in Table 1.

The percentage of target volume that was covered by the full prescription dose was mostly higher in right breasts than in the left breasts, with all OARs passing the constraints, with a p-value of 0.00. This is seen in the results of V_{50Gy} (%) objective of Table 2 for both treatment planning techniques. The left breast recorded 82.61 ± 9.07 in 3DCRT and 93.72 ± 2.31 in IMRT whilst the right breast recorded 83.83 ± 8.23 in 3DCRT and 94.38 ± 2.89 in IMRT. Based on this, it is obvious that for similar breast sizes, achieving the full prescription in right breasts is easier than the left.

Following the ICRU recommendations where the 95% of the PTV is recommended to receive 95% of the prescription, both the left and right breasts in this study presented very good results, with a p-value of 0.00. However, the right breasts recorded a higher coverage of $V_{47.5Gy}$ (%) with 97.33 ± 1.49 in 3DCRT and 99.24 ± 0.59 in IMRT than the left breasts with 96.55 ± 1.33 in 3DCRT and 98.29 ± 0.73 in IMRT, with all OARs meeting their specified constraints in Table 1.

With a p-value of 0.01, the mean PTV doses were higher in left breasts than in right breasts for both planning techniques. The left breasts produced $D_{50\%}$ (Gy) values of 50.84 ± 0.55 in 3DCRT and 50.78 ± 0.40 in IMRT whilst the right breasts produced 50.64 ± 0.42 in 3DCRT and 50.50 ± 0.30 in IMRT. The outcomes of the mean dose values in both techniques are inconsistent with the V_{50Gy} (%) and $V_{47.5Gy}$ (%) outcomes, with a possible implication that mean dose values are generally higher in left breast radiotherapy plans than the right sided.

In the 3DCRT technique, both the left and the right breasts recorded seemingly equal CI values of 0.97 ± 0.01 and a p-value of 0.00. However, this is as result of a decimal approximation on the part of the left breast whose $V_{47.5Gy}$ (%) value was 96.55 ± 1.33. Due to the mathematical rule employed in the calculation of the CI values as stated in equation 1, the CI could be expressed as a mere fraction of the percentage value recorded in the $V_{47.5Gy}$ (%), thus a decimal approximation to two decimal places results in 0.97 rather than 0.9655. It becomes a bit clearer to understand that the CI value was ideally higher in right breasts than in left breasts for 3DCRT planning. In the IMRT technique also, the right breasts recorded a higher CI than the left breasts with 0.99 ± 0.01 for right breasts and 0.98 ± 0.01 for left breasts.

The dose homogeneity is the same for both left and right breasts in IMRT with an HI value of 1.04 ± 0.02. In 3DCRT technique, the left breasts produced a homogeneous value than the right breasts with a p-value of 0.01. The HI recorded 1.06 ± 0.02 and 1.07 ± 0.02 for left and right breasts respectively.

Based on the results of this study, it is quite deductible that it is easier to achieve complete coverage in right breasts than in left-sided ones in terms of 100% and 95% isodose in the target. Similarly, treatment planning for right breasts results in higher dose conformity than left breasts. Despite these results, it is ostensibly clear that left breasts result in higher mean doses and better dose homogeneity than right breasts.

Phase 2

In phase 2, the PTV dose parameters for the left breasts were recorded as the heart D_{max} constraints were varied to investigate the influence of the heart constraint on radiotherapy left breast target coverage. The percentage of PTV covered by the full prescription dose (V_{50Gy}), the 95% of the prescription ($V_{47.5Gy}$) dose coverage, the mean PTV dose ($D_{50\%}$), the CI and the HI, were investigated with each of the heart constraint variations, taking into account the other OAR objectives of Table 1.

Generally, PTV dosimetry did not vary significantly with the changing heart constraints in IMRT planning for V_{50Gy} (%), $V_{47.5Gy}$ (%) and $D_{50\%}$ (Gy) as displayed in Figure 2, with CI and HI values staying nearly constant throughout the variation. The V_{50Gy} (%) parameter recorded values ranging from 93.45 ± 1.58 to 93.91 ± 2.16, the $V_{47.5Gy}$ (%) recorded a range of PTV coverage between 98.59 ± 0.89 and 98.70 ± 0.56, whilst a dose range of 50.87 ± 0.71 to 50.94 ± 0.60 was recorded for $D_{50\%}$ (Gy) with the variation of the heart D_{max} in the IMRT planning. The CI and HI values remained approximately constant with 0.99 and 1.04 throughout the variation. The results of the present study suggest that heart constraints have minimal influence on target coverage for breast radiotherapy when using IMRT.
Conversely, the PTV dosimetry witnessed a highly significant change with variation of the heart constraints in 3DCRT planning as shown in Table 3. The V_{50Gy} (%) parameter recorded values ranging from 30.30 ± 3.63 to 95.26 ± 2.64, the $V_{47.5Gy}$ (%) recorded a range of PTV coverage between 90.28 ± 1.45 and 98.60 ± 1.04, with a dose range of 49.48 ± 1.16 to 53.12 ± 1.08 recorded for $D_{50\%}$ (Gy) in the course of varying the heart D_{max} constraint in the 3DCRT planning. The CI values were in the range of 0.90 ± 0.10 to 0.99 ± 0.08 whilst the HI values ranged from 1.03 ± 0.09 to 1.09 ± 0.04 throughout the variation study. It is evident that the heart constraint imposes substantial effect on target coverage in breast radiotherapy during 3DCRT planning, as presented by Figure 2.

V. CONCLUSIONS

The results obtained so far points to the fact that target coverage in breast radiotherapy can be limited by the value of the heart D_{max} constraint used in treatment planning. However, the extent of this limitation depends on the treatment planning technique. Heart constraints have minimal influence on target coverage for breast radiotherapy when using IMRT but imposes substantial effect on target coverage during 3DCRT planning. The results also reveals that the poor target coverage and lower dose conformity in left breast radiotherapy is due to the additional restriction imposed by the heart constraint in radiotherapy treatment planning of the left breast.

ACKNOWLEDGMENT

Our sincere gratitude to Mr. Joseph Kwadjo Lano for his support in terms of imaging setup on the CT machine.

REFERENCES

1. Hernandez V, Hansen CR, Widesott L. What is plan quality in radiotherapy? The importance of evaluating dose metrics, complexity, and robustness of treatment plans. *Radiother Oncol*. 2020;153:26-33. doi:10.1016/j.radonc.2020.09.038

2. Abo-Madyan Y, Aziz MH, Aly MMOM. Second cancer risk after 3D-CRT, IMRT and VMAT for breast cancer. *Radiother Oncol*. 2014;110(3):471-476. doi:10.1016/j.radonc.2013.12.002

3. Hansen CR, Hussein M, Bernchou U, Zukauskaite R, Thwaites D. Plan quality in radiotherapy treatment planning – Review of the factors and challenges. *J Med Imaging Radiat Oncol*. 2022;66(2):267-278. doi:10.1111/1754-9485.13374

4. Jones D. ICRU Report 50—Prescribing, Recording and Reporting Photon Beam Therapy. *Med Phys*. 1994;21(6):833-834. doi:10.1118/1.597396

5. Newhauser W. International Commission on Radiation Units and Measurements Report 78: Prescribing, Recording and Reporting Proton-beam Therapy. *Radiat Prot Dosimetry*. 2009;133(1):60-62. doi:10.1093/rpd/ncp005

6. Petrova D, Smickovska S, Lazarevska E. Conformity Index and Homogeneity Index of the Postoperative Whole Breast Radiotherapy. *Open Access Maced J Med Sci*. 2017;5(6):736-739. doi:10.3889/oamjms.2017.161

Contacts of the corresponding author:

Author: Alhassan Mohammed Baidoo
Institute: Sweden Ghana Medical Centre
Street: East Legon Hills
City: Accra
Country: Ghana
Email: ambaidoo1@gmail.com

A COMPREHENSIVE ANALYSIS OF THE BIOGRAPH VISION PET/CT SYSTEM USING NEMA-2-2012

S. Kheruka, N. Al-Maymani, N. Al-Makhmari, H. Al-Saidi, T. Raii, S. Al-Rashdi, A. Al-Balushi, V. Jayakrishnan, Anjali Jain, K. Al-Riyami, R. Al-Sukaiti

Department of Radiology and Nuclear Medicine, Sultan Qaboos Comprehensive Cancer Care and Research Centre, Muscat, Oman

Abstract— **This study examines the Biograph Vision 600 PET/CT system from Siemens Healthineers. Equipped with silicon photomultiplier-based detectors, this system focuses on enhancing imaging quality. By incorporating SiPM detectors and 3.2 mm LSO crystals, it maximizes scintillator coverage. The system comprises eight rings, each housing 38 detector blocks, which are further divided into 4x2 mini blocks. These mini blocks feature a 5x5 LSO array connected to a 16x16 mm SiPM array. Together, this configuration offers an axial FOV of 26.1 cm. The study evaluates the system's performance against the NEMA NU 2 2012 standard, assessing key metrics like spatial resolution, sensitivity, count rate dynamics, scatter correction efficiency, TOF performance, and overall image quality. Results show a NEMA sensitivity of 15 kcps/MBq, an axial spatial resolution of 3.2 mm (with a 1 cm offset from the FOV center), a peak NECR of 300 kcps at 32 kBq/mL concentration, and a TOF timing resolution of 213 ps. Image quality phantom tests based on NEMA standards indicate contrasts ranging from 77% to 92.5% and 80.8% to 90.9% for sphere-to-background ratios of 4:1 and 8:1, respectively. The Biograph Vision 600 PET/CT system conforms to NEMA standards, showing promise for clinical use and advanced diagnostics.**

Keywords— PET/CT, NEMA.

I. INTRODUCTION

Positron Emission Tomography (PET) is now a vital tool in the medical field, especially for the diagnosis and monitoring of various health conditions. The introduction of the first integrated PET/CT system in 1998 marked a significant advancement in medical imaging techniques [1]. Over time, PET technology has made impressive progress. The incorporation of lutetium oxyorthosilicate crystals has enhanced coincidence timing windows, allowing the development of time-of-flight (TOF) imaging methods [2-5]. Moreover, widening the axial field of view (FOV) has improved the capability to capture volumetric data [6].

The precision and efficiency of PET systems play a critical role in accurate clinical diagnoses. Standards like the NEMA NU 2-2012, set by the National Electrical Manufacturers Association (NEMA), outline comprehensive protocols for evaluating the technical performance of these systems. These standards ensure consistent assessments and provide a reliable foundation for comparing different PET systems [7].

In this dynamic landscape, different digital PET/CT systems have been engineered, including the Biograph Vision 600 by Siemens Healthineers, the Vereos by Philips Healthcare, and the Discovery MI by GE Healthcare [8-10]. These systems feature silicon photomultiplier (SiPM) detectors and lutetium oxyorthosilicate crystals to enable efficient interfacing and enhance imaging quality.

This study's primary goal is to evaluate the performance metrics of the Biograph Vision 600 PET/CT system, comparing it against the benchmarks set by both the NEMA NU 2-2012 and NEMA NU 2-2018 standards [7,11]. The evaluation will encompass spatial resolution, sensitivity metrics, scatter fraction, and noise-equivalent count rate (NECR). Additionally, we will focus on the accuracy of attenuation and scatter corrections to ensure a comprehensive performance analysis.

II. OVERVIEW OF THE BIOGRAPH VISION PET/CT SYSTEM

The Biograph using an integrated 128-slice CT scanner and lutetium oxyorthosilicate PET system. It features a spacious 78 cm bore accommodating various body types as well as a sturdy table rated for loads up to 227 kg.

The PET component consists of 8 detector rings, each with 19 detector electronics modules housing two detector blocks apiece for 38 blocks total. Every block contains a grid of smaller mini blocks arranged in a 4 by 2 formation. Each mini block has a 5 by 5 matrix of 3.2 by 3.2 by 20 mm lutetium oxyorthosilicate crystals paired with a segmented 16 by 16 mm silicon photomultiplier array.

The strategic placement of mini blocks extending axially two per block results in an axial field of view of 32 mm for each block. With 8 blocks oriented lengthwise, this configuration spans a 25.6 cm axial field of view. Accounting for the spaces between blocks makes the effective axial field of view 26.1 cm.

Central to this design is a square crystal array fully covered by silicon photomultiplier detector elements. The 3.2 mm crystals ensure high spatial resolution while extensive coverage enhances light absorption, improving timing resolution and signal-to-noise ratio as studies have confirmed [13].

III. METHODS OF EVALUATION

We assessed a range of performance indicators, such as the ones listed below:

- Spatial Resolution
- Scatter Fraction, Count Losses, and Randoms Measurement
- Sensitivity
- Accuracy of Count Losses and Randoms Corrections
- Image Quality, Accuracy of Attenuation, and Scatter Corrections
- Timing resolution

The NEMA NU 2-2012 and NEMA NU 2-2018 criteria were closely followed in our assessments. The system's manufacturer provided the tools for acquisition, reconstruction, and NEMA's particular analysis. Every outcome complied with the NEMA NU 2 definitions and criteria.

A. Spatial Resolution Using F-18

Adhering to the guidelines of NEMA NU 2-2012, it's recommended to employ a point source of ^{18}F with dimensions less than 1mm in all three axes. However, given the precise features of the Vision system, a smaller point source may yield better results. Following this, the 2018 upgrade recommends the use of a ^{22}Na point source. Accordingly, a minute ^{22}Na point source was acquired from Eckert and Ziegler Isotope Products for our use. To further comply with the 2012 NEMA guidelines, an ^{18}F point source was also employed.

- Source Preparation and Positioning: A capillary tube with an inner diameter of 1mm and an outer diameter of 2 mm, containing 370 MBq/ml of ^{18}F, was utilized. A capillary tube positioning device was employed to ensure precise placement provided by Siemens Healthcare. Three-point sources were meticulously positioned at coordinates: (0, 1), (0, 10), and (0, 20) cm using the capillary tube positioning device at the center and ¼th of FOV.
- PET/CT Acquisition: A PET/CT scan was performed to accumulate at least 10,000,000 counts at the center of the axial Field of View (FOV) and at ¼th of the axial FOV from the isocenter.
- Data Collection: A back-projection technique was deployed to reconstruct the data collected from various positions after undergoing Fourier rebinning.
- Spatial Resolution Analysis: The Full Width at Half Maximum (FWHM) of each point source at various positions was determined, encapsulating radial, tangential, and axial dimensions.

The Biograph Vision demonstrated a transverse spatial resolution at FWHM of 3.7 mm at a 1 cm offset from the center of the FOV. The findings from the spatial resolution analysis at 1, 10, and 20 cm are illustrated in the succeeding Table 1.

B. Spatial Resolution Using Na-22

Thus, a 74-kBq, 0.25-mm-diameter spheric ^{22}Na point source (Eckert and Ziegler Isotope Products) was used. Acquired and processed according to the NEMA NU 2-2018 standard [2]. The results are shown in Table 1.

Table 1: Spatial Resolution Findings

Spatial Resolution:

	Distance	FWHM (mm)		FWTM (mm)	
	(cm)	**Na-22**	**F-18**	**Na-22**	**F-18**
Radial	1	3.2	3.7	6.4	7.4
	10	4.4	4.5	8.32	8.2
	20	5.7	5.6	9.9	9.4
Tangential	1	3.4	3.7	6.7	7.2
	10	3.5	3.9	6.9	8.5
	20	3.5	4	7.3	8.8
Axial	1	3.2	3.7	6.4	7.6
	10	3.5	4.3	7	9.2
	20	3.48	4.6	7.08	10.2

C. Sensitivity Analysis

Positron Emission Tomography (PET) is a pivotal imaging modality in clinical and research settings. The sensitivity of a PET scanner, defined as its ability to detect

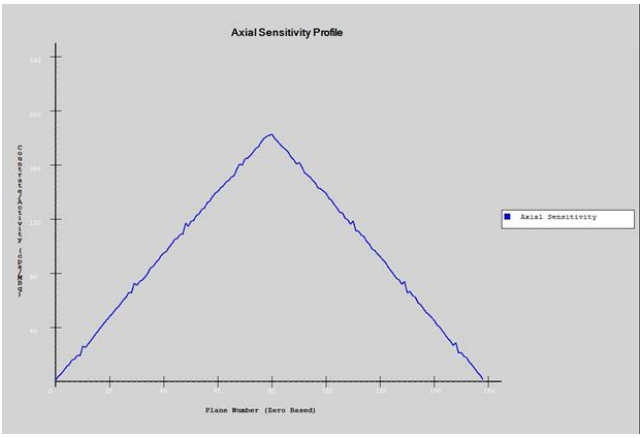

Fig 1: Axial sensitivity profiles for 0-cm off-center position

coincident photons emitted within its field of view (FOV), is a fundamental parameter affecting the quality of the imaging output. Accurate determination of scanner sensitivity is imperative for ensuring reliable and consistent imaging data. This study aims to meticulously evaluate the sensitivity of a PET scanner using a standardized NEMA PET Sensitivity Phantom.

The materials employed for this study comprised a NEMA PET Sensitivity Phantom, fillable plastic tubing of 700 mm length, (4.6 MBq) ^{18}F at the time of acquisition, various sleeves for increasing wall thickness, and low-density support materials to minimize scatter while positioning the phantom in air.

The tubing was filled with 4.6 MBq of ^{18}F and positioned centrally in the transaxial FOV with the help of low-density support materials to minimize scatter. Initially, data acquisition was performed at the isocenter. Starting with the smallest sleeve, an acquisition was carried out to collect a minimum of 10,000 true events per slice. The wall thickness was incrementally increased by adding the next smallest sleeve, with an acquisition performed at each stage, until all sleeves were utilized. Subsequently, the phantom and line sources were repositioned to a 10 cm offset from the central axis, and the acquisition procedure was reiterated for each sleeve at this offset position. The acquired data were then analyzed to ascertain the sensitivity at the isocenter and the 10 cm offset for each wall thickness, followed by an examination of the variation of sensitivity within the FOV.

The PET scanner's sensitivity was assessed at both the isocenter (0 cm offset) and a 10 cm offset from the central axis. At the isocenter, the sensitivity measured was 15.0 kcps/MBq and remained consistent at 15.0 kcps/MBq even at the 10 cm offset. The consistent sensitivity across the field of view (FOV) indicates the scanner maintains stable sensitivity critical for accurate clinical imaging data.

The vendor-stated sensitivity is 16.0 kcps/MBq, with an acceptable range of ±10% from this value. Hence, the acceptable sensitivity range is:

Lower bound: 15.0 kcps/MBq - 10% = 13.5 kcps/MBq

Upper bound: 15.0 kcps/MBq + 10% = 16.5 kcps/MBq

The measured sensitivity, although slightly below the vendor-declared value, falls within the acceptable range of 13.5 to 16.5 kcps/MBq. This confirms that the PET scanner satisfies the required sensitivity criteria. Findings are presented in Table 2 and Figure 1 and 2.

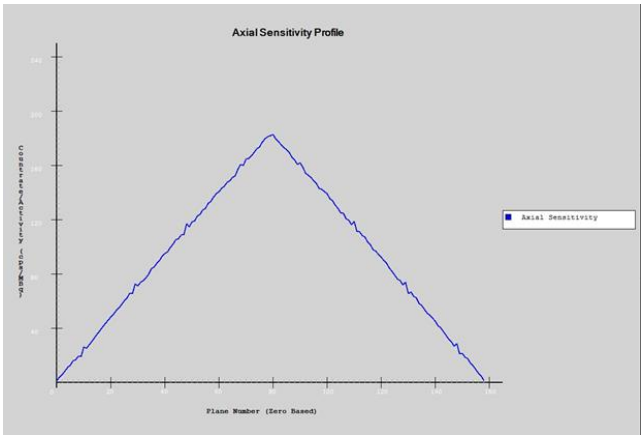

Fig 2. Axial sensitivity profiles for 10-cm off-center position.

Table 2 Sensitivity Findings

Distance (cm)	Sensitivity (kcps/MBq)
0	15
10	15

D. Scatter Fraction, Count Losses, and Randoms Measurement

The performance measurement of count rates in a Positron Emission Tomography (PET) scanner is crucial as it evaluates system count losses under various radioactivity quantities within the Field of View (FOV). Factors like scattering, count losses, and random counts significantly affect image quality and quantitation accuracy. This study employed a NEMA cylindrical polyethylene phantom and a line source of radioactivity to investigate these impacts.

The materials employed in this study included a NEMA cylindrical polyethylene phantom with a diameter of 203 mm and length of 700 mm and a line source of radioactivity containing 1.18 GBq of ^{18}F.

Multiple scans spanning over 6–7 half-lives were executed, each comprising a 15-minute scan followed by a 15-minute delay. Utilizing the PET sinogram and designated software, a meticulous analysis was conducted to evaluate true, scatter, random, and noise-equivalent count rates as a function of activity concentration.

The analysis revealed a NEMA peak Noise-Equivalent Count Rate (NECR) of 300 kcps at an activity concentration of 32 kBq/mL. Additionally, a scatter fraction of 39% was observed at the peak NECR and 37% at low activity. The vendor specification for the Peak NEC rate was also listed as 300 kcps, aligning with our findings. The results are shown in Table 3 and Figure 2.

Table 3: Scatter Fraction and Peak NECR Findings

Peak NECR (kcps at kBq/mL)	300 at 32.6
Scatter fraction (%)	
At peak NECR	39
At low activity	37

at each bed position. During scanning, coincidences along with the time of arrival were acquired and documented. A histogram depicting the differences in the time of arrival was generated from the acquired data. The timing Full Width at Half Maximum (FWHM) was then extracted from the histogram.

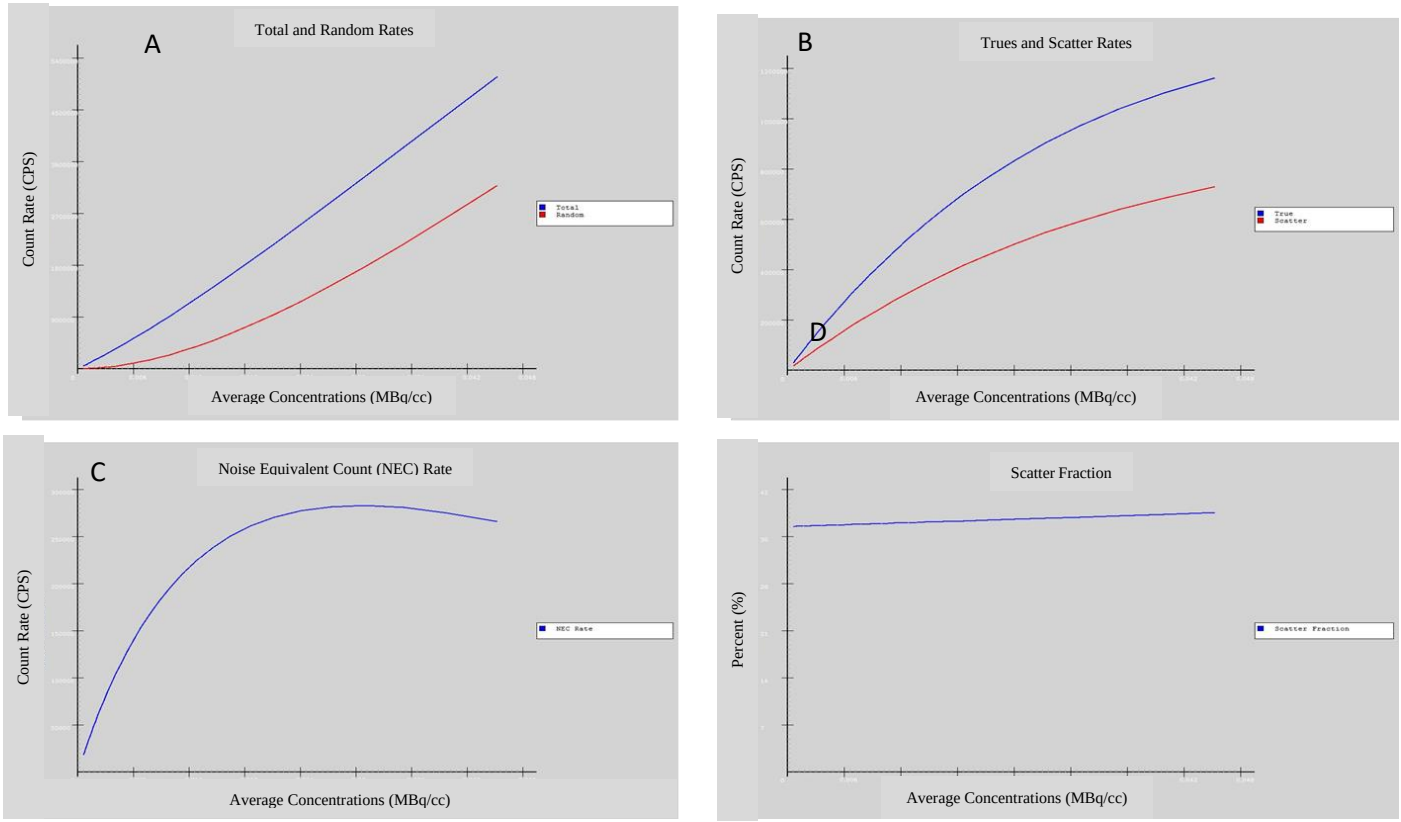

Fig 1. (A) Plots of Total and Randoms. (B) Plots of Trues and Scatter event rates. (C) Plot of NECR as a function of activity concentration. (D) The plot of Scatter fraction as a function of activity concentration.

E. Timing Resolution

Timing resolution in Time-of-Flight Positron Emission Tomography/Computed Tomography (TOF PET/CT) systems is a critical parameter as it determines the difference in the time of arrival of the two coincident photons. This difference in time is essential for obtaining information about the probable location of the annihilation event along the Line of Response (LOR). This study aims to evaluate the timing resolution of a TOF PET/CT system under varying conditions.

Line source filled with F-18 activity spanning between 27.75 MBq to 37 MBq to cover all rings. The thinnest Aluminum (Al) sleeve was used in the sensitivity test.

Initially, the line source was filled with F-18 and inserted into the thinnest Al sleeve used for the sensitivity test. A two-bed PET/CT scan was performed for 5 minutes

The evaluation yielded a detailed insight into how the TOF resolution varied with the change in count rate. The TOF resolution was observed to range from 210 to 215 and it was 213 ps as the count rate increased up to the peak NECR. This variation in TOF resolution underscores the impact of the count rate on the timing resolution of the system.

F. Image Quality Assessment

For evaluating image quality and verifying the precision of both *attenuation and scatter corrections*, we utilized the PET NEMA NU2 Image Quality (IQ) Phantom. Through gravimetric analysis, the volume of the phantom's background compartment was determined to be 9,742 mL.

The phantom also contained six spheres, each with varying internal diameters: 10 mm, 13 mm, 17 mm, 22

mm, 28 mm, and 37 mm. Central lung inserts, which was filled with polystyrene beads, remained devoid of any radioactivity.

At the onset of the image acquisition, the background activity concentration of ^{18}F stood at 5.3 kBq/mL, serving as our reference for low-activity concentration. The 4 smallest spheres were filled with a sphere-to-background ratio of 8:1 for the first set of scans and 4:1 for the second set of scans. The remaining 2 largest spheres were filled with non-radioactive water. The phantom was positioned with all spheres aligned in the axial and transaxial center of the FOV. For the simulation of a clinical situation with activity outside the FOV, the cylindric scatter phantom was placed axially next to the image quality phantom.

The line source inside the scatter phantom was filled with approximately 116 MBq of ^{18}F activity at the start of both data acquisitions. Two sequential measurements of 240 s each were acquired for a single bed position after a low-dose CT scan for attenuation correction. All data were corrected for random coincidences, normalization, decay, scatter, and attenuation. The data were reconstructed using an OP-OSEM 3D-iterative algorithm with 8 iterations and 5 subsets, applying PSF and TOF into a 440 × 440 matrix with a voxel size of 1.6 × 1.6 × 1.6 mm. The percentage contrast was obtained for hot and cold spheres, and the background count variability for each sphere was evaluated. Finally, we used the activity spillage into the non-radioactive lung insert to derive the average residual error.

The NEMA image quality phantom tests further emphasized an image contrast ranging from 77% to an impressive 92.5 % and background variability ranging from 5.2 % to 2.7 % for 4:1 and image contrast ranging from 80.79% to an impressive 90.86% background variability ranging from 3.96% to 1.43% for 8:1. The Average lung residual was 37 for 4:1 and 39% for 8:1. The results are shown in Table 4 and Table 5.

Table 4: Contrast, Background Variability, and Average Lung Residual for 8:1 Sphere-to-Background Ratio on Biograph Vision 600.

Sphere Size (mm)	Contrast (%)	Background Variability (%)
10	80.8	3.9
13	83.8	2.9
17	83.4	2.2
22	88.3	1.9
28	87.6	1.7
37	90.9	1.4
Average Lung Residual (%)	3.9	

Table 5: Contrast, Background Variability, and Average Lung Residual for 4:1 Sphere-to-Background Ratio on Biograph Vision 600.

Sphere Size (mm)	Contrast (%)	Background Variability (%)
10	77	5.2
13	85.65	4.6
17	83.1	3.9
22	86.42	3.45
28	89.4	3.1
37	92.5	2.7
Average Lung Residual (%)	3.1	

IV. DISCUSSION AND ANALYSIS

A. Spatial Resolution:

The Vision system's spatial resolution, measured in Full Width at Half Maximum (FWHM), was evaluated against the mCT Flow system using ^{18}F. The Vision system showcased transaxial spatial resolution values of 0.6 mm, 0.6 mm, and 1.2 mm at radial distances of 1 cm, 10 cm, and 20 cm, respectively. This enhancement can be attributed to the utilization of smaller 3.2-mm lutetium oxyorthosilicate crystals in the Vision system, as opposed to the 4-mm crystals in the mCT Flow system. Furthermore, the Vision system's superior axial resolution at peripheral regions might be a result of an advanced rebinning technique [12].

For precise resolution assessment, it is essential to generate a sufficiently small point source. Given that the mean positron ranges of ^{22}Na and ^{18}F are similar, any differences in spatial resolution observed are likely tied to the source dimensions [13]. Creating a small source with ^{18}F presents challenges; hence, the NEMA NU 2-2018 guidelines recommend using a ^{22}Na source for spatial resolution evaluation. Following these guidelines, our experiments incorporated a ^{22}Na point source.

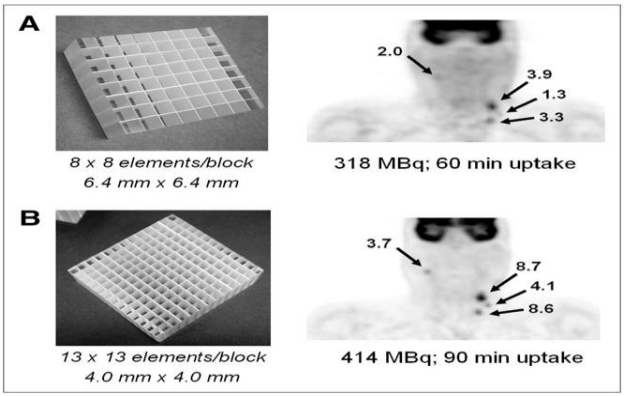

Fig.3: Comparative PET/CT scans Highlighting the Clinical Advantage of Increased Spatial Resolution in Detecting Bilateral Disease in Head and Neck Cancer. [14]

Figure 3 Comparative PET/CT scans illustrating the clinical advantage of increased spatial resolution in head and neck cancer. **(A)** The lower-resolution scan shows uptake in two left-sided lymph nodes, indicating primary disease on the left, leading to a scheduled left neck dissection. **(B)** The higher-resolution scan reveals additional uptake in a right-sided lymph node, suggesting bilateral disease. Consequently, the patient underwent a bilateral neck dissection, which confirmed the presence of disease on both sides [14].

B. Sensitivity Analysis:

The Vision 600 digital PET system has a sensitivity of 15.0 kcps/MBq, which, although slightly lower than the vendor's stated 16.0 kcps/MBq, still offers enhanced sensitivity that can significantly impact clinical PET imaging. This level of sensitivity ensures stable performance across the field of view, allowing for various benefits. These advantages include the potential for lower radiotracer doses, thereby reducing patient radiation exposure and costs, improving image quality for more precise diagnoses, decreasing scan times for patient comfort and increased efficiency, and enabling earlier disease detection. However, the deviation from the vendor's sensitivity specification underscores the necessity for ongoing performance validation in clinical settings. As shown in Figure 4. 2-D and 3-D PET images of a patient with a body mass index of 36, showing reduced noise level in the 3-D image compared to the 2-D image [15].

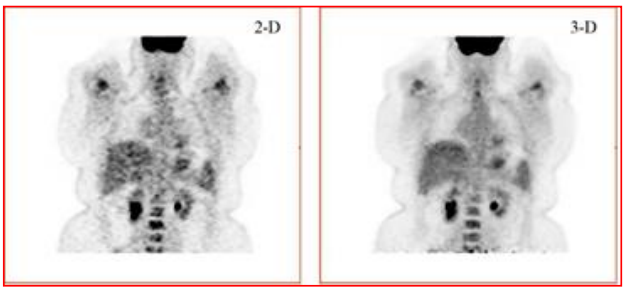

Fig 4: 2-D and 3-D PET images of a patient with a body mass index of 36, showing reduced noise level in the 3-D image compared to the 2-D image. (IAEA HUMAN HEALTH SERIES No. 27, IAEA 2014)

C. Scatter Fraction, Count Losses, and Randoms Measurement:

During the analysis of the Vision 600 digital Biograph, particular attention was given to examining the relationship between count rates and image quality, which is a pivotal aspect of PET imaging due to its direct influence on diagnostic precision.

The investigation revealed significant findings regarding the Noise-Equivalent Count Rate (NECR). At an activity concentration of 32 kBq/mL, the maximum NECR achieved was 300 kilocounts per second (kcps), aligning with the manufacturer's specified standards. NECR holds critical importance in PET imaging as it signifies the equilibrium between accurate signal detection and disruptive factors like scatter and random counts. It acts as an indicator of the system's capability to deliver high-quality images in clinical settings.

Furthermore, the study reported a scatter fraction of 37% at the peak NECR. The scatter fraction, representing the ratio of scattered gamma photons to the total count, is significant as scatter can diminish image quality by increasing background noise. A scatter fraction of this degree implies that the system can handle and maintain image clarity in the presence of substantial scatter.

The interplay between NECR and scatter fraction is crucial in determining the overall quality of images. The Vision 600's elevated NECR highlights its capacity to produce clear images even at high count rates, which is advantageous for swift scans and imaging with high activity concentration. Nevertheless, managing the scatter fraction remains vital to safeguard image sharpness and clarity.

These findings carry practical implications for clinical application. The digital PET demonstrates proficiency in managing high activity concentrations while skillfully balancing accurate and scattered counts. This competence is indispensable in clinical scenarios necessitating top-tier imaging for precise diagnosis and treatment.

D. Image Quality Evaluation

The assessment of digital PET systems (Vision 600) involved analyzing key factors such as attenuation and scatter correction accuracy, contrast, and background variability using the NEMA NU2 Image Quality (IQ) phantom. This evaluation is critical for determining the imaging performance of digital PET systems.

Tests with the NEMA IQ phantom indicated that digital PET systems could deliver high image contrast and minimal background noise. For a 4:1 contrast setting, image contrast typically fell between 77% and 92.5%, with background variability ranging from 5.2% to 2.7%. With an 8:1 contrast level, image contrast ranged from 80.79% to 90.86%, and background variability varied from 3.96% to 1.43%. These results demonstrate the capacity of digital PET systems to differentiate between areas of interest and adjacent tissue, crucial for accurate diagnosis.

Precise attenuation and scatter correction are vital in PET imaging as they ensure the accurate representation of tracer distribution in the body. Accurate correction guarantees dependable images, forming a solid basis for diagnosis. Figure 5 shows coronal whole-body FDG-PET images reconstructed with (a) and without (b) attenuation correction. The increased skin flare, hot lungs, and reduced activity in the central portion of the body in the uncorrected PET images should be noted. Figure 6 presents coronal images of whole-body FDG-PET reconstructed with (a) and without (b) scatter correction, highlighting the scatter artifacts in the uncorrected images [15].

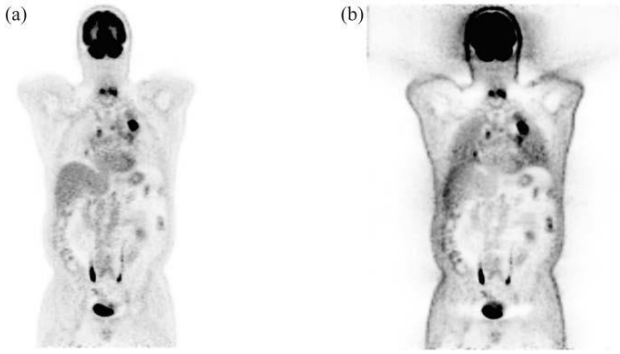

Fig.5: Coronal whole-body FDG-PET images reconstructed with (a) and without (b) attenuation correction. The increased skin flare, hot lungs, and reduced activity in the central portion of the body in the uncorrected PET images should be noted. (IAEA HUMAN HEALTH SERIES No. 27, IAEA 2014)

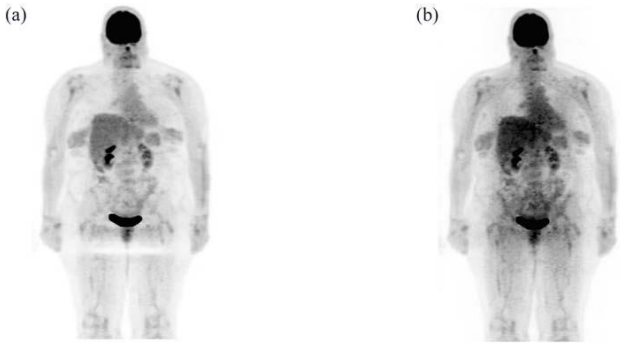

Fig. 6: Coronal images of whole body FDG-PET reconstructed with (a) and without (b) scatter correction. The scatter artifacts at the level of the hands should be noted (IAEA HUMAN HEALTH SERIES No. 27, IAEA 2014)

The research measured mean lung residual values around 37% for a 4:1 contrast ratio and 39% for an 8:1 ratio, highlighting the effectiveness of digital PET systems in visualizing regions with diverse densities, particularly in challenging lung imaging scenarios due to low density and high air content.

The implications of these outcomes are significant in clinical practice. The capability of digital PET systems to offer high contrast and low background variability is key for precise medical evaluations. Their efficiency in managing attenuation and scatter corrections further underscores their value in producing accurate diagnostic images.

E. Timing Resolution:

The assessment of the digital PET/CT (Vision 600) system primarily focused on its timing resolution, particularly the 213 picoseconds (ps) concerning Time-of-Flight (TOF) PET/CT imaging. The system's performance was evaluated against industry standards and requirements to ascertain its suitability for precise clinical diagnosis and research applications. This evaluation offers valuable insights into the capabilities of digital PET/CT systems, especially in TOF PET/CT imaging, assisting in informed decision-making for clinical purposes. Ultimately, the 213-picosecond timing resolution of the digital PET/CT system plays a critical role in determining its TOF PET/CT imaging capabilities, aiding healthcare practitioners in evaluating the system's consistency and dependability for both clinical and research uses.

V. CONCLUSION

The comprehensive assessment of the digital PET/CT system has emphasized its remarkable performance across a range of factors, including spatial resolution, sensitivity, scatter fraction, and overall image quality. The system exhibits strong adherence to established industry benchmarks and maintains uniform sensitivity throughout the entire field of view, emphasizing its reliability for both clinical and research applications. Our evaluation also highlights the importance of accounting for performance variations in different clinical scenarios. Continuous performance monitoring, quality assurance protocols, and ongoing research are vital to ensure the optimal utilization of the system in practical healthcare environments.

REFERENCES

1. Beyer T, Townsend DW, Brun T, et al. A combined PET/CT scanner for clinical oncology. J Nucl Med. 2000; 41:1369–1379.

2. Melcher CL. Scintillation crystals for PET. J Nucl Med. 2000;41:1051–1055.

3. Moses WW. Time of flight in PET revisited. IEEE Trans Nucl Sci. 2003;50:1325–1330.

4. Surti S, Kuhn A, Werner ME, Perkins AE, Kolthammer J, Karp JS. Performance of Philips Gemini TF PET/CT scanner with special consideration for its time-offlight imaging capabilities. J Nucl Med. 2007;48:471–480.

5. Jakoby BW, Bercier Y, Conti M, Casey ME, Bendriem B, Townsend DW. Physical and clinical performance of the mCT time-of-flight PET/CT scanner. Phys Med Biol. 2011;56:2375–2389.

6. Jakoby BW, Bercier Y, Watson CC, Bendriem B, Townsend DW. Performance characteristics of a new LSO PET/CT scanner with extended axial field-of-view and PSF reconstruction. IEEE Trans Nucl Sci. 2009;56:633–639.

7. National Electrical Manufacturers Association Performance Measurements of Positron Emission Tomographs. Rosslyn, VA: National Electrical Manufacturers Association; 2012. NEMA Standards Publication NU 2-2012.

8. Nguyen NC, Vercher-Conejero JL, Sattar A, et al. Image quality and diagnostic performance of a digital PET prototype in patients with oncologic diseases: initial experience and comparison with analog PET. J Nucl Med. 2015;56:1378–1385.

9. Rausch I, Ruiz A, Valverde-Pascual I, Cal-Gonzalez J, Beyer T, Carrio I. Performance evaluation of the Philips Vereos PET/CT system according to the NEMA NU2-2012 standard. J Nucl Med. October 25, 2018 [Epub ahead of print].

10. Hsu DFC, Ilan E, Peterson WT, Uribe J, Lubberink M, Levin CS. Studies of a next-generation silicon-photomultiplier–based time-of-flight PET/CT system. J Nucl Med. 2017;58:1511–1518.

11. National Electrical Manufacturers Association Performance Measurements of Positron Emission Tomographs. Rosslyn, VA: National Electrical Manufacturers Association; 2018. NEMA Standards Publication NU 2-2018.

12. Vandenberghe S, Daube-Witherspoon ME, Lewitt RM, Karp JS. Fast reconstruction of 3D time-of-flight PET data by axial rebinning and transverse mashing. Phys Med Biol. 2006;51:1603–1621.

13. Jødal L, Le Loirec C, Champion C. Positron range in PET imaging: non-conventional isotopes. Phys Med Biol. 2014; 59:7419–7434.

14. Dual-Modality Imaging: Combining Anatomy and Function David W. Townsend, Journal of Nuclear Medicine Jun 2008, 49 (6) 938-955; DOI: 10.2967/jnumed.108.051276

15. PET/CT ATLAS ON QUALITY CONTROL AND IMAGE ARTEFACTS: IAEA HUMAN HEALTH SERIES No. 27, IAEA 2014

Contacts of the corresponding author:

Author: Subhash Chand Kheruka
Institute: Sultan Qaboos Comprehensive Cancer Care and Research Center (SQCCCRC)
Street: SQU Street
City: Muscat
Country: Oman
Email: S.kheruka@gmail.com

DEPTH DOSE DISTRIBUTIONS OF THERAPEUTIC ELECTRON BEAM FROM VARIAN LINAC: MONTE CARLO STUDY AND EXPERIMENTAL MEASUREMENTS

Y. Ali[1], S. Rahman[2], F.N. Islam[1], T. Siddiqua[2], N. Rasel[3], I. Islam[4]

[1] Department of Physics, University of Rajshahi, Rajshahi-6205, Bangladesh
[2] Institute of Nuclear Science & Technology, Bangladesh Atomic Energy Commission Dhaka-1349, Bangladesh
[3] Department of Physics, Comilla University, Cumilla-3506, Bangladesh
[4] Department of Physics, Mohila College Chattogram, Enayet bazar, Chattogram-4000, Bangladesh

Abstract— **Linac-based electron beam therapies are used for the treatment of superficial cancer tumors. Central axis depth dose distributions for 6, 9, 12, and 15 MeV nominal electron energies delivered by Varian Clinac iX with 10 × 10 cm^2 applicator were computed by using the MCNPX (V. 2.6.0) Monte Carlo code. Percent Depth Dose (PDD) distributions computed by MC simulations were validated through comparison with the corresponding measured data. Discrepancies between MCNP and experimental data were found within 1.62% and 1.31 mm in the therapeutic range (90 to 80% of maximum dose values) of electron beam and these are within the recommended standard (±2%) used in the dose calculation. However, notable variations were found beneath the depth of 50% dose, especially towards the bremsstrahlung tail region which is not normally considered in the treatment planning system. The deviations at the high-dose gradient region might be due to scattering foils and collimator jaws during MC modelling, resulting in the lower production of bremsstrahlung photons. As the MC computed data were in good agreement with experimental values except for the high-dose gradient region, the developed Monte Carlo program can be used in the various dosimetric study of the therapeutic electron beam in a homogenous and inhomogeneous media as well as to investigate the contaminations of photons and neutrons during the treatment.**

Keywords— **Electron beam, Dose distributions, Monte Carlo simulation, MCNPX, Varian linac.**

I. INTRODUCTION

Electron beam therapy is an important modality for the treatment of superficial tumors (less than 5 cm deep). It is extensively used for chest wall irradiation of breast cancer, skin and lip cancers, head and neck cancers, etc. [1]. Modern external electron beam therapy is carried out using a medical linear accelerator. Treatment planning in radiotherapy is an important procedure to evaluate the dose in a patient before performing the actual treatment. Central axis depth dose distributions of the electron beam are evaluated during the treatment planning of superficial cancerous cells. In early methods, central axis dose distributions of electron beams were carried out experimentally using phantom which was time-consuming. Later on, various algorithms such as Pencil Beam, Pencil Beam Redefinition, Collapsed Cone Convolution algorithms, etc., were developed to calculate dose distributions theoretically and thus improved efficiency [2]. However, in radiation therapy, it is recommended that the accuracy of dose delivery to cancer cells should be within ±5% [3]. To obtain it, the accuracy in dose calculation must not exceed ±2%. But the complexity of electron-tissue interactions makes it very difficult to obtain such accuracy by using conventional treatment planning algorithms. Currently, the Monte Carlo algorithm is used as the most accurate method for calculating dose distribution in radiotherapy. The MC algorithm can reduce the uncertainty in the dose calculation within recommended values as it takes into account the multiple scattering and the creation of secondary particles or delta rays in electron dosimetry [4].

Various studies have been performed on central axis dose distributions of the electron beam in water phantom by Monte Carlo simulations and experimental techniques. Toossi *et al.* [5] simulated Siemens Primus linac by using MCNPX (version 2.4.0) MC code for 8, 12, and 14 MeV electron beams with various electron applicators (10 × 10 cm^2, 15 × 15 cm^2, 25 × 25 cm^2). The PDD data from their simulation were in good agreement with experimental ones. The maximum discrepancy between the simulated and measured values of R_{50} was 1.3 mm at 10 × 10 cm^2 applicator. Nedaie *et al.* [6] performed an MC simulation of ELEKTA Precise linac using MCNP4C code to investigate the effect of various components of linac head and efficacy of MC algorithm in producing dosimetric data. They used 8 & 15 MeV electron beams and a 10 × 10 cm^2 treatment field to get percent depth dose (PDD) data and beam profiles. A p-type diode detector was used in getting experimental data. The discrepancy between the simulated and experimental PDD was within 2% and they concluded that to get better results theoretically, all the main components of the linac head must be added in simulation geometry. Lalić *et al.* [7] investigated central axis depth dose distribution in water for 6, 9, and 12 MeV electron beams from a Varian 2100C medical linac. They utilized FOTELP MC code in their simulation. Due to the unavailability of a high-speed computer, they made some simplifications in the geometry of the linac head and used a lower number of electron histories. As a result, their simulation results have significantly differed from their experimental values. Aziz *et al.* [2] performed both the experimental and theoretical

calculations of depth dose distribution along the beam central axis in a homogenous 3-D water phantom for a 9 MeV electron beam from a Seimens Primus medical linac. They used both BEAMnrc and DOSXYZnrc source code in the EGSnrc MC package. Simulation results were in good agreement with the measured data obtained by an ion chamber and the maximum discrepancy was less than 2%.

This work aims to simulate the treatment head of Varian linac by using MCNPX code for 6, 9, 12, and 15 MeV electron beams and to compare the Monte Carlo calculated central axis depth dose data with the corresponding experimental values obtained by the PPC40 plane-parallel ion chamber.

II. METHODOLOGY

Monte Carlo Simulation

The treatment head of an electron mode Varian CLINAC (model IX) was simulated by using the MCNPX (version 2.6.0) Monte Carlo code [8]. The details of Varian linac head description are given elsewhere [9]. The Varian IX CLINAC has a two-photon mode (6, 10 MV) and several electron modes. Among them four electron beam energies 6, 9, 12, and 15 MeV were selected for simulation purposes. The major components of the accelerator head such as electron scattering foils (the primary foil made of tantalum, and the secondary foil made of aluminum), a 6.77 cm long primary conical collimator (made of tungsten), secondary collimator pairs with a thickness of 7.77 cm (made of tungsten) and 10×10 cm^2 electron applicator were simulated in this study. The materials compositions, shapes, and dimensions of these components were collected from the technical drawing manual of linac provided by the Varian medical system [10]. Moreover, a standard cubic water phantom ($40 \times 40 \times 40$ cm^3) was included as a part of head components. A monoenergetic and monodirectional beam with a radius of 1 mm was used as a primary electron source. Figure 1 shows the geometry of accelerator head components considered in this study.

To compute the absorbed dose values, a series of cylinders, with 1 mm height and 1 cm radius, were modeled on the central beam axis of the water phantom. The *F8 tally was used to calculate the depth dose distribution of the electron beam. PDD values were obtained by normalizing the MC calculated dose values to the maximum dose at arbitrary depth on the beam central axis and multiplied by 100. Several input files were run with at least 3E8 source particles and the average statistical uncertainty was within 3%. The whole simulation work was carried out with an Intel Core i9 processor desktop computer.

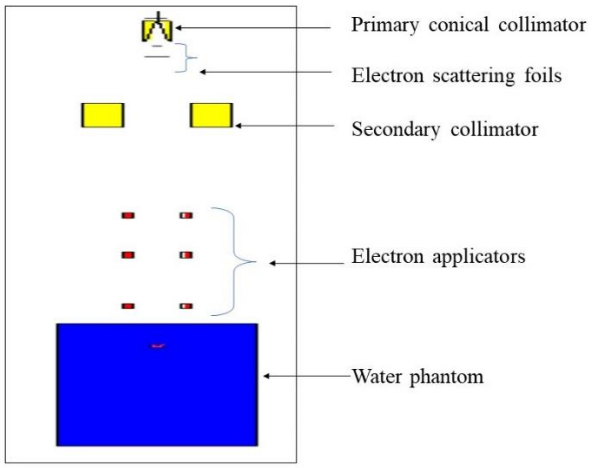

Figure 1. Simulated accelerator head components of electron mode Varian CLINAC

Experimental Techniques

Dose measurements were carried out in an IBA blue phantom 3D water phantom by using a PPC40 plane-parallel ion chamber (0.6 cc) at Nuclear Medical Physics Institute (NMPI), Savar, Bangladesh. The water phantom was set at 100 cm SSD (source to surface distance) and projected a 10×10 cm^2 treatment field vertically at the phantom surface. After readjusting the effective point of ion chamber to 100 cm SCD, the ion chamber charge readings were taken with a 1 mm step from the phantom surface towards its bottom along the beam central axis until a constant value was reached. These charge readings were then converted to dose values by using the appropriate stopping power ratio, water to air, according to the TRS-398 code of practice [11]. The experimental setup for depth dose determination is shown in Figure 2.

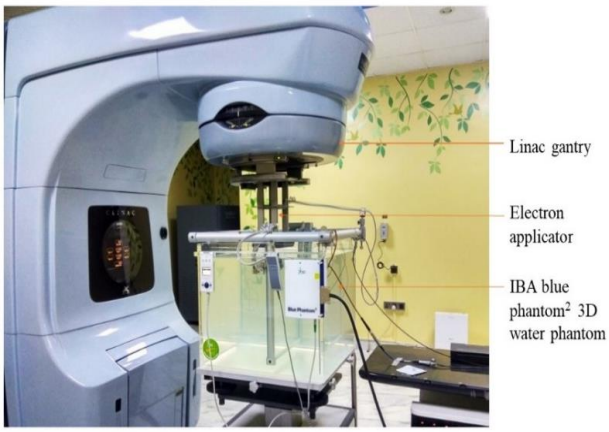

Figure 2. Experimental set-up for obtaining electron beam depth-dose distributions

III. RESULTS

The calculated and measured central axis depth dose distributions for 6, 9, 12, and 15 MeV electron beams with 10×10 cm^2 applicator are presented in Figure 3. Dose values at different depths were normalized to the maximum dose. From this figure, it was seen that the MC calculated absorbed dose values were in excellent agreement with the measured ones up to 50% of the maximum dose in 6, 12 and 15 MeV energies.

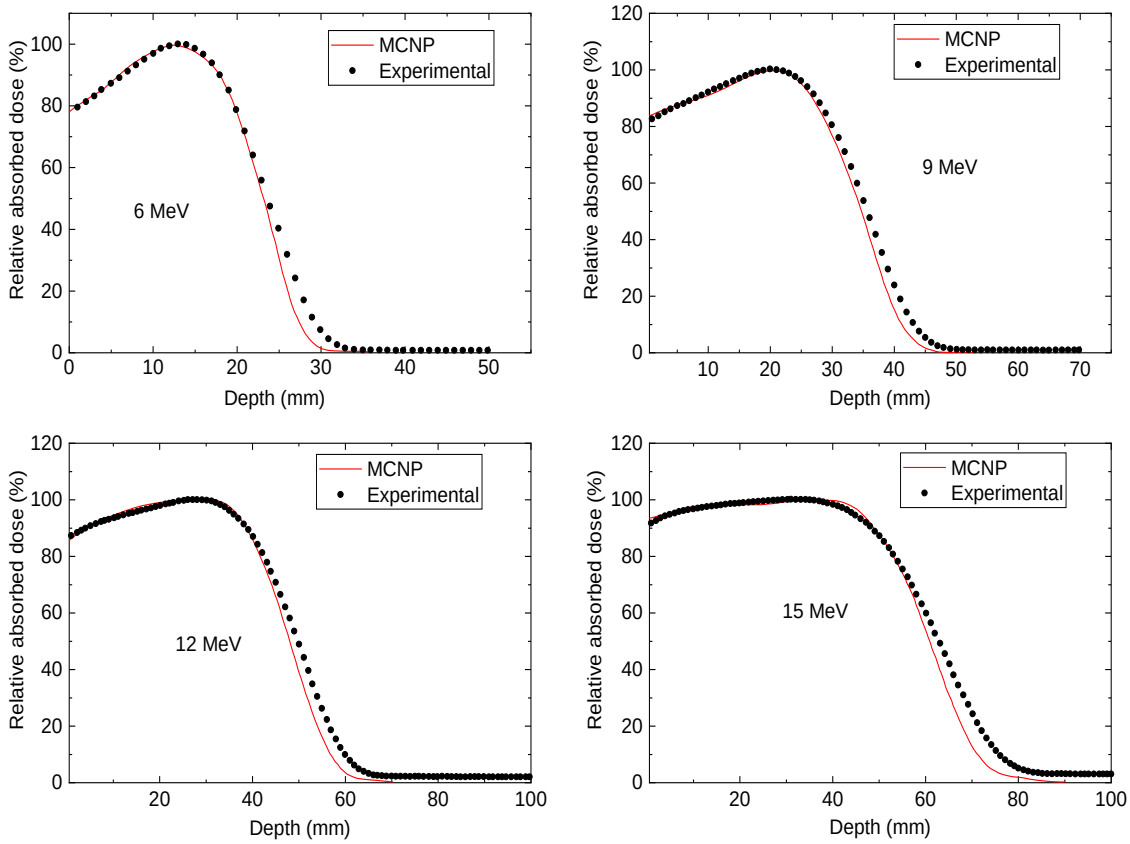

Figure 3. PDD distributions of 6, 9, 12, and 15 MeV electron beams for 10×10 cm^2 applicator

A point-to-point comparison between MCNP and measured doses up to D_{max} shows the differences within 1.27%, 1.44%, 1.62%, and 1.27% for 6, 9, 12, and 15 MeV nominal electron beams respectively. Dose differences at D_{max} position were found to be 0.53 mm, 0.29 mm, 0.85 mm, and 1.31 mm for these energies respectively. The maximum deviation in dose determination at the R_{50} position was 0.19 mm which was related to 12 MeV energy. Figure 3 also shows that the dose discrepancies were more pronounced in the high dose-gradient region. It could be due to the lower production of bremsstrahlung photons during MC simulation. As we know the most bremsstrahlung photons are mainly produced in the scattering foil and the collimator jaws, so the small differences in the declaration of these thicknesses can create an inappropriate prediction of the contaminated photons. However, these regions are not important in treatment planning with the electron beam. Most importantly, the discrepancy in the electron beams therapeutic range (90% - 80% of maximum dose values) was within 2% which is the acceptable standard for dose evaluation. From figure 3, we also evaluated some important electron depth dose parameters such as mean energy $\bar{E}_0$ on the phantom surface, depth of maximum dose (Z_{max}), depth of 90% dose level (R_{90}), and electron beam quality index (R_{50}). Among them $\bar{E}_0$ was calculated using the following expression [12]:

$$\bar{E}_0 = 2.33\ R_{50} \quad (1)$$

These parameters are shown in Table.

From this table, it was observed that the maximum difference of R_{90} values between these two sets of data was 1.9 mm which was related to 12 MeV energy. The maximum discrepancy of $\bar{E}_0$ and Z_{max} was 0.44 MeV and 4 mm corresponding to 9 and 15 MeV respectively.

Table. Typical depth dose parameters of clinical electron beams

Depth dose parameters	Nominal Electron Energy							
	6 MeV		9 MeV		12 MeV		15 MeV	
	MCNP	Measurement	MCNP	Measurement	MCNP	Measurement	MCNP	Measurement
R_{90}	17.99 mm	17.98 mm	26.6 mm	27.48 mm	38.59 mm	38.59 mm	48.59 mm	48.12 mm
R_{50}	23.2 mm	23.7 mm	34.7 mm	35.6 mm	47.9 mm	49.8 mm	61.1 mm	62.8 mm
Z_{max}	12 mm	13 mm	20 mm	20 mm	25 mm	28 mm	35 mm	31 mm
$\bar{E}_0$	5.41 MeV	5.52 MeV	8.08 MeV	8.29 MeV	11.16 MeV	11.60 MeV	14.24 MeV	14.63 MeV

IV. CONCLUSION

This study presented the MCNP simulation of electron mode of a Varian CLINAC for 6, 9, 12, and 15 MeV energies in a homogenous medium and it was validated by comparing the computed dose distributions with experimentally measured values. From the analysis of our findings, we observed that the discrepancies were within 1.62% and 1.31 mm in the treatment regions of the electron beam and it is fulfilled the criteria (2%/2mm) which is mainly used in the commissioning of Monte Carlo based dose calculation [13]. However, the maximum discrepancy was observed in the high-dose region especially in the tail part of the PDD curve. This might be due to scattering foils and collimator jaws during MC modelling, resulting in the lower production of bremsstrahlung photons at higher depth. But in fact, the target cells are not generally located in this region so that the large discrepancy in dose evaluation in this part does not affect the precession of dose delivery to the targeted tumors but a contribution to the normal cell. Thus, the good agreement between the calculated and measured results encourages the use of MCNP Monte Carlo code as a reliable dose predictor where experimental measurements may not be easily feasible. Moreover, the developed MC program could also be used to study the dose distribution in a heterogeneous medium and to investigate the contamination of other particles during the treatment by a high-energy electron beam.

ACKNOWLEDGEMENT

The authors would like to express their sincere thanks to the staffs and scientists of Secondary Standard Dosimetry Laboratory of Bangladesh Atomic Energy Commission for their strong support in performing this research work. This work was supported by ADP project “Establishment of Calibration and Quality Control Facilities for Radiotherapy, Diagnostic Radiology and Neutron” of Ministry of Science and Technology, Bangladesh and Department of Physics, Faculty of Science, University of Rajshahi, Bangladesh.

REFERENCES

1. K.R. Hogstrom, and P.R. Almond, “Review of Electron Beam Therapy Physics”, Phys. Med. Biol. **51**(13), R455-489 (2006). https://doi.org/10.1088/0031-9155/51/13/R25
2. M.Z.A. Aziz, M.S. Salikin, A.L. Yusoff, and R. Abdullah, “Monte Carlo Simulation of Electron Beam in 3-D Water Phantom”, World Acad. Sci. Eng. Technol, **3** (2011).
3. J.E. Cygler, C. Lochrin, G.M. Daskalov, M. Howard, R. Zohr, B. Esche B et al., Clinical Use of a Commercial Monte Carlo Treatment Planning System for Electron Beams, Phys. Med. Biol. **50**(5), 1029-1034 (2005). https://doi.org/10.1088/0031-9155/50/5/025
4. D.W.O. Rogers, and A.F. Bielajew, in: *The Dosimetry of Ionizing Radiation*, edited by K.R. Kase, B.E. Bjarngard, and F.H. Attix, (Academic Press, 1990), Chapter 5, Vol. III, https://people.physics.carleton.ca/~drogers/pubs/papers/RB90.pdf
5. M.T.B. Toossi, M. Ghorbani, F. Akbari, L.S. Sabet, and M. Mehrpouyan, Monte Carlo Simulation of Electron Modes of a Siemens Primus Linac (8, 12 and 14 MeV), J. Radio. Pract., 12(4), 352-359 (2013). https://doi.org/10.1017/S1460396912000593
6. H.A. Nedaie, M. Shariary, H. Gharaati, Monte Carlo Study of Electron Dose Distributions Produced by the Elekta Precise Linear Accelerator. Rep. Pract. Oncol Radio., 11(6):287–92 (2006). http://dx.doi.org/10.1016/S1507-1367(06)71074-4
7. D. Lalić, D.R. Ilić, and S. Stanković, “Comparison of Measured and Monte Carlo Calculated Electron Beam Central Axis Depth Dose in Water”, Arch. Oncol. **9**(2), 83–87 (2001). https://scindeks-clanci.ceon.rs/data/pdf/0354-7310/2001/0354-73100102083L.pdf
8. D. Pelowitz, MCNPX User’s Manual, version 2.6.0. Report LA-CP-07-1473 (2008). Los Alamos National Laboratory.
9. Varian [Internet]. [cited 2021 Jul 29]. Available from: https://www.varian.com/products/radiotherapy/treatment-delivery/truebeam
10. Varian Medical Systems Confidential (supplied by the company), Monte Carlo data package, DWG NO. 100040466-02 (REV2)
11. Technical Report Series No. 398. *Absorbed Dose Determination in External Beam Radiotherapy*, (Vienna: International Atomic Energy Agency, 2000).
12. R. Akbarpoor, N. Khaledi, X. Wang, and F. Samiei, Optimization of Low-Energy Electron Beam Production for Superficial Cancer Treatments by Monte Carlo Code. J. Cancer. Res. Ther. **15**(3), 475 (2019). https://doi.org/10.4103/jcrt.JCRT_203_18

13. C. Ma, E. Mok, A. Kapur, T. Pawlicki, D. Findley, S. Brain et al. Clinical Implementation of a Monte Carlo Treatment Planning System. Med. Phys. **26**(10), 2133-43(1999). https://doi.org/10.1118/1.598729

Contacts of the corresponding author:

Author: Shakilur Rahman
Institute: Institute of Nuclear Science & Technology, Bangladesh Atomic Energy Commission
City: Dhaka-1349
Country: Bangladesh
Email: shakilurssdl@baec.gov.bd

INFORMATION FOR AUTHORS

PUBLICATION OF DOCTORAL THESIS AND DISSERTATION ABSTRACTS

A special feature of Medical Physics International (on line at www.mpijournal.org) is the publication of thesis and dissertation abstracts for recent graduates, specifically those receiving doctoral degrees in medical physics or closely related fields in 2010 or later. This is an opportunity for recent graduates to inform the global medical physics community about their research and special interests.

Abstracts should be submitted by the author along with a letter/message requesting and giving permission for publication, stating the field of study, the degree that was received, and the date of graduation. The abstracts must be in English and no longer than 2 pages (using the MPI manuscript template) and can include color images and illustrations. The abstract document should contain the thesis title, author's name, and the institution granting the degree.

Complete information on manuscript preparation is available in the INSTRUCTIONS FOR AUTHORS section of the online journal: www.mpijournal.org.

INSTRUCTIONS FOR AUTHORS

The goal of the new IOMP Journal Medical Physics International (http://mpijournal.org) is to publish manuscripts that will enhance medical physics education and professional development on a global basis. There is a special emphasis on general review articles, reports on specific educational methods, programs, and resources. In general, this will be limited to resources that are available at no cost to medical physicists and related professionals in all countries of the world. Information on commercial educational products and services can be published as paid advertisements. Research reports are not published unless the subject is educational methodology or activities relating to professional development. High-quality review articles that are comprehensive and describe significant developments in medical physics and related technology are encouraged. These will become part of a series providing a record of the history and heritage of the medical physics profession.

A special feature of the IOMP MPI Journal will be the publication of thesis and dissertation abstracts for will be the publication of thesis and dissertation abstracts for recent doctoral graduates, specifically those receiving their doctoral degrees in medical physics (or closely related fields) in 2010 or later.

MANUSCRIPT STYLE

Manuscripts shall be in English and submitted in WORD. Either American or British spelling can be used but it must be the same throughout the manuscript. Authors for whom English is not their first language are encouraged to have their manuscripts edited and checked for appropriate grammar and spelling. Manuscripts can be up to 10 journal pages (approximately 8000 words reduced by the space occupied by tables and illustrations) and should include an unstructured abstract of no more than 100 words.

The style should follow the template that can be downloaded from the website at:

http://mpijournal.org/authors_submitapaper.aspx

ILLUSTRATIONS SPECIAL REQUIREMENTS

Illustrations can be inserted into the manuscript for the review process but must be submitted as individual files when a manuscript is accepted for publication.

The use of high-quality color visuals is encouraged. Any published visuals will be available to readers to use in their educational activities without additional approvals.

REFERENCE WEBSITES

Websites that relate to the manuscript topic and are sources for additional supporting information should be included and linked from within the article or as references.

EDITORIAL POLICIES, PERMISSIONS AND APPROVALS

AUTHORSHIP

Only persons who have made substantial contributions to the manuscript or the work described in the manuscript shall be listed as authors. All persons who have contributed to the preparation of the manuscript or the work through technical assistance, writing assistance, financial support shall be listed in an acknowledgements section.

CONFLICT OF INTEREST

When they submit a manuscript, whether an article or a letter, authors are responsible for recognizing and disclosing financial and other conflicts of interest that might bias their work. They should acknowledge in the manuscript all financial support for the work and other financial or personal connections to the work.

All submitted manuscripts must be supported by a document (form provided by MPI) that:

• Is signed by all co-authors verifying that they have participated in the project and approve the manuscript as submitted.

• Stating where the manuscript, or a substantially similar manuscript has been presented, published, or is being submitted for publication. Note: presentation of a paper at a conference or meeting does not prevent it from being published in MPI and where it was presented can be indicated in the published manuscript.

• Permission to publish any copyrighted material, or material created by other than the co-authors, has been obtained.

• Permission is granted to MPI to copyright, or use with permission copyrighted materials, the manuscripts to be published.

• Permission is granted for the free use of any published materials for non-commercial educational purposes.

MEDICAL PHYSICS INTERNATIONAL
INSTRUCTION FOR AUTHORS

A. FamilyName[1], B.C. CoauthorFamilyName[2], D. CoauthorFamilyName [1]

[1] Institution/Department, Affiliation, City, Country
[2] Institution/Department, Affiliation, City, Country

Abstract— **Paper abstract should not exceed 300 words. Detailed instructions for preparing the papers are available to guide the authors during the submission process. The official language is English.**

Keywords— **List maximum 5 keywords, separated by commas.**

I. Introduction

These are the instructions for preparing papers for the Medical Physics International Journal. English is the official language of the Journal. Read the instructions in this template paper carefully before proceeding with your paper.

II. Detailed Instructions

Paper Size: A4
Length: The maximum document size is usually 8 pages. For longer papers please contact the Editor(s).
Margins: The page margins to be set to: "mirror margins", top margin 4 cm, bottom margin 2,5 cm, inside margin 1.9 cm and outside margin 1.4 cm.
Page Layout: 2 columns layout.
Alignment: Justified.
Fonts: Times New Roman with single line spacing throughout the paper.
Title: Maximum length – 2 lines. Avoid unusual abbreviations. Font size - 14 point bold, uppercase. Authors' names and affiliations (Institution/Department, City, Country) shall span the entire page.
Indentation: 8 point after the title, 10 point after the authors' names and affiliations, 20 point between author's info and the beginning of the paper.
Abstract: Font - 9 point bold. Maximum length - 300 words.
Style: Use separate sections for introduction, materials and methods, results, discussion, conclusions, acknowledgments and references.
Headings: Enumerate Chapter Headings by Roman numbers (I., II., etc.). For Chapter Headings use ALL CAPS. First letter of Chapter Heading is font size 12, regular and other letters are font 8 regular style. Indents - 20 point before and 10 point after each Chapter Heading. *Subchapter Headings* are font 10, italic. Enumerate Subchapter Headings by capital letters (*A.*, *B.*, etc.). Indents - 15 point before and 7,5 point after each Subchapter Heading.
Body Text: Use Roman typeface (10 point regular) throughout. Only if you want to emphasize special parts of the text use *Italics*. Start a new paragraph by indenting it from the left margin by 4 mm (and not by inserting a blank line). Font sizes and styles to be used in the paper are summarized in Table 1.
Tables: Insert tables as close as possible to where they are mentioned in the text. If necessary, span them over both columns. Enumerate them consecutively using Arabic numbers and provide a caption for each table (e.g. Table 1, Table 2, ...). Use font 10 regular for Table caption, 1st letter, and font 8 regular for the rest of table caption and table legend. Place table captions and table legend above the table. Indents - 15 point before and 5 point after the captions.

Table 1 Font sizes and styles

Item	Font Size, pt	Font Style	Indent, points
Title	14	Bold	After: 8
Author	12	Regular	After: 10
Authors' info	9	Regular	After: 20
Abstract	9	Bold	
Keywords	9	Bold	
Chapters			
Heading - 1st letter	12	Regular	Before: 20
Heading - other letters	8	Regular	After: 10
Subchapter heading	10	Italic	Before: 15, After:7,5
Body text	10	Regular	First line left: 4mm
Acknowledgment	8	Regular	First line left: 4mm
References	8	Regular	First line left: 4mm
Author's address	8	Regular	
Tables			
Caption, 1st letter	10	Regular	Before: 15
Caption – other letters	8	Regular	After: 5
Legend	8	Regular	
Column titles	8	Regular	
Data	8	Regular	
Figures			
Caption - 1st letter	10	Regular	Before: 15
Caption – other letters	8	Regular	After: 5
Legend	8	Regular	

Submission of Manuscripts

Manuscripts to be considered for publication should be submitted as a WORD document to:

Francis Hasford, Co-editor: haspee@yahoo.co.uk
Sameer Tipnis, Co-editor: tipnis@musc.edu

Manuscript Proposals

Authors considering the development of a manuscript for a Review Article can first submit a brief proposal to the editors. This should include the title, list of authors, an abstract, and other supporting information that is appropriate. After review of the proposal the editors will consider issuing an invitation for a manuscript. When the manuscript is received it will go through the usual peer-review process.

Figures: Insert figures where appropriate as close as possible to where they are mentioned in the text. If necessary, span them over both columns. Enumerate them consecutively using Arabic numbers and provide a caption for each figure (e.g. Fig. 1, Fig. 2, ...). Use font 10 regular for Figure caption, 1st letter, and font 8 regular for the rest of figure caption and figure legend. Place figure legend beneath figures. Indents - 15 point before and 5 point after the captions. Figures are going to be reproduced in color in the electronic versions of the Journal, but may be printed in grayscale or black & white.

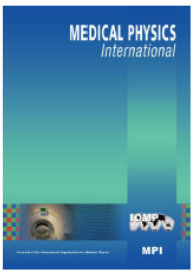

Fig. 1 Medical Physics International Journal

Equations: Write the equation in equation editor. Enumerate equations consecutively using Arabic numbers

$$A + B = C \quad (1)$$

$$X = A \times e^{at} + 2lkt \quad (2)$$

Items/Bullets: In case you need to itemize parts of your text, use either bullets or numbers, as shown below:

- First item
- Second item

1. Numbered first item
2. Numbered second item

References: Use Arabic numbers in square brackets to number references in such order as they appear in the text. List them in numerical order as presented under the heading 'References'. Examples of citations for Journal articles [1], books [2], the Digital Object Identifier (DOI) of the cited literature [3], Proceedings papers [4] and electronic publications [5].

III. Conclusions

Send your papers only in electronic form. Papers to be submitted prior the deadline. Check the on-line Editorial Process section for more information on Paper Submission and Review process.

Acknowledgment

Format the Acknowledgment headlines without numbering.

References

The list of References should only include papers that are cited in the text and that have been published or accepted for publication. Citations in the text should be identified by numbers in square brackets and the list of references at the end of the paper should be numbered according to the order of appearance in the text.

Cited papers that have been accepted for publication should be included in the list of references with the name of the journal and marked as ''in press''. The author is responsible for the accuracy of the references. Journal titles should be abbreviated according to Engineering Index Inc. References with correct punctuation.

1. LeadingAuthor A, CoAuthor B, CoAuthor C et al. (2012) Paper Title. Journal 111:220–230
2. LeadingAuthor D, CoAuthor E (2000) Title. Publisher, London
3. LeadingAuthor A, CoAuthor B, CoAuthor C (2012) Paper Title. Journal 111:330–340 DOI 123456789
4. LeadingAuthor F, CoAuthor G (2012) Title, IOMP Proceedings. vol. 4, World Congress on Med. Phys. & Biomed. Eng., City, Country, 2012, pp 300–304
5. MPI at http://www.mpijournal.org

Contacts of the corresponding author:

Author:
Institute:
Street:
City:
Country:
Email:

IUPESM 2025

World Congress on Medical Physics and Biomedical Engineering

29 September – 4 October 2025
Adelaide Convention Centre, Australia

ENGINEERS AUSTRALIA

ACPSEM
Australasian College of Physical Scientists & Engineers in Medicine

www.wc2025.org
#IUPESM2025

Host Organisations

IUPESM IOMP IFMBE

IFMBE

International Organization for Medical Physics
IOMP

Supported by

Business Events Adelaide

SOUTH AUSTRALIA

Government of South Australia
Department of the Premier and Cabinet

ADELAIDE CONVENTION CENTRE